Molecular Mechanisms of Autophagosome-Vacuole Fusion and Degradation of Peroxisomes by Autophagy

by

Xu Liu

A dissertation submitted in partial fulfillment
of the requirements for the degree of
Doctor of Philosophy
(Molecular, Cellular and Developmental Biology)
in the University of Michigan
2017

Doctoral Committee:

Professor Daniel J. Klionsky, Chair
Professor Robert S. Fuller
Professor Anuj Kumar
Professor Yanzhuang Wang

2017

Email: liuxu@umich.edu

ORCID iD: 0000-0002-3314-6511

To my parents and grandparents

ACKNOWLEDGEMENTS

First, I would like to thank my mentor Dr. Daniel Klionsky, for his continuous support and invaluable guidance throughout my graduate studies. His passion towards science and his expertise in science have inspired me a lot. Thanks to his support, I am always free to explore new ideas and projects. Thanks to his guidance and encouragement, I always feel assured and confident when I try to solve scientific problems. I am greatly thankful for having him as my mentor.

I would like to thank my thesis committee members, Dr. Robert Fuller, Dr. Anuj Kumar, and Dr. Yanzhuang Wang, for all their generous support. Their insightful suggestions and criticisms for my projects are indispensible. I am very grateful to all of them.

I am also thankful to all the members of the Klionsky lab. Thank you for your companionship, help and support during these years. I thank Dr. Ke Wang and Mantong Zhao for their patient guidance, and Dr. Usha Nair and Dr. Wei-Lien Yen for their help, during my rotation in the lab. I am also thankful to Ke for being a great friend. I greatly thank Dr. Kai Mao for being a patient teacher in the lab and a reliable friend. Working with Kai on two projects, I learned a lot from him. My great gratitude also goes to Dr. Meiyan Jin. I am lucky to have Meiyan as my colleague and dear friend. She is like a

sister to me. I would also like to thank Yuchen Feng, Zhiyuan Yao, Ding He, Xin Wen Zhangyuan Yin, and Ziheng Xu for all your support in the lab and in life. I thank Dr. Amélie Bernard and Damián Gatica for their thoughtful discussions. I also received a lot of help from Dr. Hana Popelka, Dr. Aileen Ariosa, Dr. Elizabeth Delorme-Axford, Katie Parzych and Clarence Pascual.

Last but not least, I am extremely grateful to my family for their love and support. Thanks to my parents who are there for me whenever I need them. They have supported me unconditionally. I could not have become who I am without their support.

PREFACE

This thesis summarizes the research I conducted while working in Dr. Daniel J. Klionsky's laboratory since September 2011. Through my thesis research, we obtained a better understanding of how peroxisomal fission promotes pexophagy and how autophagosome-vacuole fusion is specifically regulated.

Chapter 1 consists of part of chapter 1 in the book *Autophagy, Infection, and the Immune Response* (doi: 10.1002/9781118677551.ch1), and part of a Snapshot published in *Cell* (doi: 10.1016/j.cell.2013.01.004), with some modifications. I wrote the text for the snapshot in *Cell* and Meiyan Jin did the primary work on the poster.

Chapter 2 characterizes of the molecular machinery of how peroxisomal fission facilitates engulfment of peroxisomes by autophagy, which is published in the journal *Autophagy* (doi.org/10.4161/auto.27852). Kai Mao and I contributed equally to this work. Kai Mao initiated the project and co-designed all the experiments with me, and Kai Mao and I generated most of the data. Yuchen Feng helped with the yeast-two-hybrid analysis in Figure 5A.

Chapter 3 describes the observation that the Atg17-Atg31-Atg29 complex and Atg11 recruit Vam7 to the phagophore assembly site to facilitate autophagosome-vacuole fusion. This study is published in *Current Biology* (doi.org/10.1016/j.cub.2015.11.054).

Kai Mao and I contribute equally to this work. Kai Mao and I co-designed most of the experiments and generated most of the data. Angela Y.H. Yu and Dr. Calvin K. Yip did the GST isolation assay in Figure 3G and Figure 4F,G; Amin Omairi-Nasser, Jotham Austin II and Dr. Benjamin S. Glick did the correlative fluorescence microscopy and electron tomography for Figure 6E.

Chapter 4 summarizes the major implications of my thesis research and future directions. The second part of this chapter is part of an autophagic punctum published in *Autophagy* (doi.org/10.1080/15548627.2016.1162364).

TABLE OF CONTENTS

DEDICATION....ii

ACKNOWLEDGEMENTS....iii

PREFACE....v

LIST OF TABLES....ix

LIST OF FIGURES....x

ABSTRACT....xii

CHAPTER 1. Introduction....1

1.1 Types of autophagy....1

1.2 Morphology....2

1.3 Molecular machinery....3

1.4 Physiological roles....10

1.5 References....12

CHAPTER 2. The progression of peroxisomal degradation through autophagy requires peroxisomal division....18

2.1 Abstract....18

2.2 Introduction....19

2.3 Results....21

2.4 Discussion....31

2.5 Experimental procedures....34

2.6 References....36

CHAPTER 3. The Atg17-Atg31-Atg29 complex coordinates with Atg11 to recruit the Vam7 SNARE and mediate autophagosome-vacuole fusion 54

3.1 Abstract....54

3.2 Introduction.....55
3.3 Results.....57
3.4 Discussion.....70
3.5 Experimental procedures.....74
3.6 References.....78
CHAPTER 4. Summary.....101
4.1 Atg11 and Atg36 coordinate with peroxisome fission machinery to facilitate degradation of peroxisomes through autophagy.....101
4.2 The Atg17-Atg31-Atg29 complex and Atg11 regulate autophagosome-vacuole fusion.....103

LIST OF TABLES

Table 2.1 Strains used in this study.....39

Table 3.1 Yeast strains used in this study.....83

LIST OF FIGURES

Figure 1.1 Schematic model of autophagy process in yeast.....16

Figure 1.2 A cargo-ligand-receptor-scaffold model of selective autophagy pathways.....17

Figure 2.1 Peroxisomal fission is required for pexophagy 40

Figure 2.2 Atg11 recruits the Dnm1 fission complex to peroxisomes.....42

Figure 2.3 Atg11 recruits Vps1 to peroxisomes that are targeted for degradation.....44

Figure 2.4 Atg36 interacts with both Dnm1 and Vps1 on the degrading peroxisomes.....46

Figure 2.5 Overexpression of Vps1 induced pexophagy.....48

Figure 2.S1 Peroxisomal fission is required for pexophagy.....50

Figure 2.S2 Atg11 recruits the Dnm1 fission complex to peroxisomes.....51

Figure 2.S3 Atg11 recruits Vps1 to peroxisomes that are targeted for degradation.....52

Figure 3.1 The Atg17-Atg31-Atg29 Complex Recruits Vam7 to the PAS upon Autophagy Induction.....85

Figure 3.2 Cytosolic Vam7 Is Recruited to the PAS at an Early Stage of Autophagy.....87

Figure 3.3 Atg17 Directly Interacts with the SNARE Domain of Vam7.....88

Figure 3.4 Hydrophobic Residues in Helix 1 and Helix 4 of Atg17 Mediate its Interaction with Vam7.....90

Figure 3.5 Atg11 Recruits Vam7 to the PAS Independent of the Atg17-Atg31-Atg29 Complex.....92

Figure 3.6 Impaired Recruitment of Vam7 to the PAS Leads to Defects in Autophagosome-Vacuole Fusion and Autophagy Activity.....93

Figure 3.S1 The Atg17-Atg31-Atg29 Complex Recruits Vam7 to the PAS upon Autophagy Induction.....95

Figure 3.S2 Cytosolic Vam7 Is Recruited to the PAS at an Early Stage of Autophagy...97
Figure 3.S3 Hydrophobic Residues in Helix 1 and Helix 4 of Atg17 Mediate its Interaction with Vam7.....98
Figure 3.S4 Impaired Recruitment of Vam7 to the PAS Leads to Defects in Autophagosome-Vacuole Fusion and Autophagy Activity.....100

ABSTRACT

Macroautophagy, hereafter referred to as autophagy, is a well-conserved cellular process among eukaryotes, through which portions of cytoplasm are degraded and recycled. Malfunction of autophagy has been related to many human diseases, including cancer, liver, heart and lung diseases and neurodegeneration. Therefore, it is important to study the molecular mechanisms of autophagy and how autophagy activity is regulated.

Autophagy can be non selective or selective. Selective engulfment of peroxisomes by autophagy is termed pexophagy. Collaborating with Kai Mao, a previous Ph.D student in the lab, we determined that in mutants where peroxisome fission is compromised, pexophay is defective. The selective autophagy scaffold Atg11 and the pexophagy specific receptor Atg36 are able to interact with the fission machinery components including Dnm1 and Vps1 on peroxisomes being degraded. These findings imply that the autophagy machinery recruits peroxisome fission machinery to drive pexophay specific fission, facilitating efficient engulfment of the organelle.

The later steps of the autophagy process involve fusion of the outer membrane of autophagosomes with the vacuole membrane. Working with Kai Mao, we confirmed an interaction between Atg17, a scaffold protein required for autophagy induction, and a vacuolar SNARE Vam7. The SNARE domain of Vam7 and several hydrophobic residues

in helix1 and helix4 of Atg17 mediate the interaction. Specifically diminishing the interaction leads to defects in autophagosome-vacuole fusion and autophagic flux. This study provides new insights into the role of the Atg17-Atg31-Atg29 complex in the late stage of autophagy and how auophagosome-vacuole fusion is specifically regulated.

CHAPTER 1. Introduction[1]

Autophagy is an evolutionarily conserved process through which cells degrade and recycle cellular components, including protein aggregates, damaged organelles and invading pathogens. Basal autophagy functions to modulate cellular and tissue homeostasis, but the process can also be induced under stress conditions to facilitate cellular adaptation or survival. Dysfunction of autophagy is linked with many pathologies, including cancer, diabetes, myopathies, heart, liver and lung diseases and certain types of neurodegenerative disease [1-6].

1.1 Types of autophagy

There are three main types of autophagy: chaperone-mediated autophagy (CMA), microautophagy, and macroautophagy. CMA is a process where a cytosolic chaperone protein, HSPA8/HSC70, specifically recognizes its cargo proteins through a KFERQ-like motif and facilitates their translocation directly across the lysosomal membrane for degradation [7, 8]. Microautophagy involves the uptake of portions of cytoplasm by the

[1] This chapter is reprinted partly from Liu, X. and Klionsky, DJ. (2014) Autophagy and Immunity, in Autophagy, Infection, and the Immune Response (eds W. T. Jackson and M. S. Swanson), John Wiley & Sons, Inc, Hoboken, NJ, USA (doi:10.1002/9781118677551.ch1), and partly from Jin M., Liu X., Klionsky D.J. (2013) Snapshot: Selective autophagy. *Cell* 152 (doi: 10.1016/j.cell.2013.01.004), with some modifications.

direct invagination or protrusion of the lysosomal or vacuolar membrane [9]. The third process, macroautophagy, hereafter referred to as autophagy, is the best characterized and will be the focus of this chapter.

1.2 Morphology

The morphological hallmark of autophagy involves the *de novo* formation of a double-membrane organelle named the autophagosome (Figure 1.1); however, this structure is essentially an end product of the sequestration process and as such is not really the primary functional unit of autophagy. Rather, the precursor to the autophagosome, the phagophore, is the dynamic membrane structure that is responsible for sequestering the cargos such as damaged organelles and invading pathogens. The phagophore expands with the addition of membrane, the sources of which are suggested to include almost every intracellular organelle. Upon completion, the phagophore seals and becomes a completed autophagosome. In yeasts, the autophagosome fuses with the vacuole. In mammals, the autophagosome may fuse directly with a lysosome, or first with a late endosome to form an intermediate amphisome. The subsequent fusion of the outer membrane of the autophagosome or the amphisome limiting membrane with a lysosome generates an autolysosome and exposes the cargoes to the degradative lysosomal enzymes. The degradation products, especially amino acids, are subsequently released back into the cytosol and are used in generating energy or as substrates for biosynthetic pathways.

1.3 Molecular machinery

Even though autophagosomes have been observed by electron microscopy as early as the 1950s, the molecular mechanisms of autophagy have been poorly studied until the past two decades [10]. The molecular machinery was first identified through studies in budding yeast, *Saccharomyces cerevisiae*, and to date more than 40 autophagy-related (*ATG*) genes have been identified as being involved in this process [11-14]. Subsequent work with mammalian cells has revealed homologs of the core autophagy machinery [15], supporting the notion that autophagy is evolutionarily conserved. At the same time, there are also increasing numbers of Atg proteins being identified in mammals and other model systems such as *C. elegans* that lack yeast homologs, suggesting an increased complexity and diversity of function in more complex eukaryotes [3]. For ease of discussion, the core protein machinery of autophagy is subdivided into four major complexes in the following sections and I will focus on the yeast autophagy molecular machinery. I will also discuss a group of proteins that function in the selective autophagy pathways either as scaffold or as receptor proteins.

1.3.1 Atg1 complex

Autophagy occurs at a basal level in cells under normal conditions. Upon stress or other stimuli, autophagy can be induced, and defects in regulation that prevent proper induction can lead to aberrant cell physiology; however, too much autophagy activity can also be detrimental to the cell. Thus, the level of autophagy must be tightly controlled.

Accordingly, there are various factors that regulate autophagy induction, and studies have shown that the Atg1 complex functions in part in an early stage of autophagy regulation.

Atg1 is the kinase and the other components of the complex include Atg13, Atg17, Atg29 and Atg31 [16-18]. Atg13 directly interacts with Atg1 regardless of the nutrient availability; however, the phosphorylation status of these proteins changes under different conditions. In nutrient-rich conditions, a key upstream negative regulator of autophagy, the target of rapamycin complex 1 (TORC1) interacts with the complex and phosphorylates Atg1 and Atg13, inhibiting Atg1 kinase activity. Upon starvation, TORC1 gets released from the complex. Atg1 and Atg13 are then partially dephosphorylated, leading to activation of Atg1 kinase activity, which in turn leads to phosphorylation of Atg13 (presumably on distinct sites from those used by TORC1) to induce autophagy [18].

Atg17, Atg29 and Atg31 form a stable ternary complex in the cells. The Atg17-Atg31-Atg29 complex is among the very first Atg proteins recruited to the phagophore assembly site (PAS), where an autophagosome forms in yeast. The complex interacts with Atg1-Atg13 and may be involved in targeting of the latter to the PAS. Structural analysis reveals that this ternary complex forms a dimer with two crescents [19]. This complex, together with Atg1 and Atg13, may function to tether Atg9 vesicles, which will be discussed in more detail, to facilitate phagophore expansion [19].

1.3.2 Class III phosphatidylinositol 3-kinase (PtdIns3K) complexes

The class III PtdIns3K is generally thought to act downstream of the Atg1 complex, mediating formation of phosphatidylinositol-3-phosphate (PtdIns3P) on the phagophore membrane, an event essential for autophagy. PtdIns3P serves to recruit downstream factors such as Atg18 and Atg2, which are involved in the trafficking of Atg9, and promote autophagosome maturation. In yeast, the only known PtdIns3K, Vps34, is able to form two distinct complexes [20]. PtdIns3K complex I is specific to the autophagy pathway and is composed of Atg14, Vps34, Vps15 and Vps30/Atg6 [20]. Vps15 regulates the kinase activity of Vps34 via modulating its membrane association [21]. Atg14 is specific for autophagy and targets the PtdIns3K complex I to the PAS [22]. Atg14 also bridges Vps30/Atg6 with Vps34-Vps15 in the complex. Recently, a study shows that Atg38, though is not essential for autophagy, stabilizes the Vps34 PtdIns3K complex I via interacting with Atg14 and Vps34. Vps34, Vps15 and Vps30/Atg6 can also form a complex with Vps38, which is part of the PtdIns3K complex II. This complex functions in the endosomal/Vps pathway [20].

1.3.3 Atg9 trafficking system

The Atg9 trafficking system is best characterized in yeast, although even in this model organism there are many questions that remain to be answered. The current model is that the transmembrane protein Atg9 cycles between the phagophore assembly site and peripheral (i.e., non-PAS) sites, and that this process is needed for the proper delivery of

membrane from various donor organelles to the expanding phagophore [23, 24]. Atg23 and Atg27 interact with Atg9 and facilitate its anterograde traffic from the peripheral sites to the PAS, whereas Atg2-Atg18 and the Atg1-Atg13 complex are required for its retrograde transport from the PAS back to the peripheral sites [25-28].

In mammals, ATG9 localizes to the *trans*-Golgi network and endosomes in nutrient-rich conditions. A pool of ATG9 translocates to LC3 (homolog of Atg8 in yeast)-positive compartments upon starvation. This translocation is dependent on ULK1 (homolog of Atg1 in yeast) and PIK3C3/VPS34 kinase activity [29]. The dynamic movement between ATG9 and the phagophore membrane during autophagy suggests a conserved role for ATG9 in membrane movement during phagophore expansion. Similar to yeast, ATG9 retrieval from the phagophore membrane is dependent on WIPI2, a homolog of yeast Atg18, but movement in this direction is ULK1 kinase independent [30].

1.3.4 Ubiquitin-like conjugation systems

There are two ubiquitin-like (Ubl) conjugation systems, which involve the Ubl proteins Atg12 and Atg8. These systems are quite well studied, playing important roles in phagophore expansion [31-33]. Atg12 is conjugated with Atg5 in a manner that is similar to canonical ubiquitination [32]. The E1-like enzyme, Atg7, activates Atg12 via a thioester bond [34]. Atg12 is then transferred to an E2-like enzyme, Atg10, before it is finally conjugated to an internal lysine of Atg5. Atg5 then noncovalently binds Atg16,

which subsequently dimerizes. During autophagy, Atg5 directs the Atg12–Atg5-Atg16 complex to the phagophore [35].

Atg8 is conjugated to the lipid phosphatidylethanolamine (PE), and this modification is required for association with the phagophore membrane [36, 37]. Initially, the cysteine protease Atg4, removes the C-terminal amino acids of Atg8 to reveal a glycine residue, generating a cytosolic form of Atg8. This soluble Atg8 is then sequentially activated by Atg7 and conjugated via the E2-like enzyme Atg3, resulting in the membrane-associated form, Atg8–PE [34, 38]. The PE group can ultimately be cleaved by Atg4 in a deconjugation step, which is important for maintaining the proper level of autophagy activity [39].

1.3.5 Selective autophagy pathways and molecular machinery

Autophagy can be categorized as nonselective or selective. Nonselective autophagy randomly engulfs a portion of the cytoplasm into autophagosomes and then delivers them to the vacuole or the lysosome for degradation. Selective autophagy, however, specifically recognizes and degrades a particular cargo, either a protein complex, an organelle, or an invading microbe.

Selective autophagy utilizes the same core machinery used for nonselective autophagy. A small number of additional proteins suffice to make the process selective; A cargo-ligand-receptor-scaffold model is proposed to describe how cells achieve selectivity (Figure 1.2). The ligand is the recognition component on the cargo that binds a

receptor. In some cases, the receptor is a resident protein on the cargo (e.g., Atg32 or BNIP3L/NIX, which are located in the mitochondria outer membrane, in mitophagy). The interaction between the receptor and scaffold is vital for cargo recruitment to the PAS, where an autophagosome forms. In yeast, Atg11 is the most commonly used scaffold protein, mediating several types of selective autophagy including the cytoplasm-to-vacuole targeting (Cvt) pathway, mitophagy, pexophagy and reticulophagy [40-45]; however, in mammals a functional counterpart of Atg11 is yet to be discovered. In many cases, the receptor proteins subsequently bind Atg8 in yeast, or in mammalian cells one of the LC3 family proteins, through a particular sequence referred to as AIM (Atg8-family interacting motif) or LIR (LC3-interacting region). This interaction may connect the cargo directly with the macroautophagy machinery. In the following sections, the Cvt pathway, mitophagy and pexophagy will be discussed in more details as examples of the selective autophagy pathways.

The Cvt pathway

The yeast Cvt pathway is the best-characterized example of a biosynthetic process that utilizes the macroautophagy machinery [43]. It is a transport route through which vacuolar resident enzymes are targeted from the cytosol to the vacuole, their final site of action. Enzymes that utilize the Cvt pathway include Ape1, Ape4 and Ams1. Atg19 is the primary receptor for these cargos, binding each through a different domain. Atg34 is another receptor similar to Atg19 that appears to bind only Ams1 under starvation conditions. The interaction of Atg11 with either Atg19 or Atg34 mediates the transport of

prApe1 oligomers in the form of a large complex to the PAS [43]. Atg19 and Atg34 also interact with Atg8 via a C-terminal WXXL motif that functions as an AIM to connect the cargo with the sequestration machinery.

Mitophagy

Selective degradation of surplus or dysfunctional organelles by autophagy has been observed both in yeast and mammals. Mitophagy, selective removal of mitochondria by autophagy, is one of the most studied types of "organelle autophagy" in part due to the connection between dysfunction of this process and certain diseases [42, 46, 47]. In yeast, mitophagy is associated with the cellular remodeling that occurs upon the transition to a preferred carbon source. For example, when yeast cells are shifted from respiratory substrates such as lactate to glucose, excess mitochondria are degraded. The mitochondria outer membrane protein Atg32 functions as the receptor for mitophagy, by interacting sequentially with Atg11 and Atg8 [42, 46, 47]. These interactions are critical for mitochondria delivery to, and subsequent degradation within, the vacuole.

In mammals, the functional counterpart of Atg32 is yet to be determined. BNIP3L, FUNDC1 and SQSTM1/p62 have been implied to function as receptors to link mitochondria with the autophagy machinery, depending on the cell type [47]. During erythrocyte maturation, BNIP3L is essential for mitochondrial clearance where mitophagy plays a developmental role [48]. Another such example is allophagy, a process observed in *Caenorhabditis elegans* embryos, where sperm-derived paternal mitochondria and their mtDNA are degraded by autophagy [49]. SQSTM1 may function

as a receptor for depolarization-induced mitophagy. According to one model, PINK1 accumulates on the outer membrane of depolarized or damaged mitochondria, where it recruits PARK2/Parkin, an E3 ubiquitin ligase. PARK2 mediates the ubiquitination of numerous outer mitochondrial membrane proteins including MFN1 and MFN2. SQSTM1 contains a LIR motif, allowing it to bridge the ligand on the mitochondrial membrane with the autophagy machinery. However, SQSTM1 is not essential for mitophagy, suggesting that other factors may be able to function in its place.

Pexophagy

Pexophagy, the selective autophagic degradation of peroxisomes, shares certain features with mitophagy in that it can also occur by both macro- and microautophagic mechanisms, and is primarily a response to changing nutrients [50]. When fungi are grown on oleic acid or methanol, the peroxisomes proliferate, as this organelle contains the enzymes necessary to utilize these carbon sources. When subsequently shifted to glucose or ethanol, the peroxisomes are rapidly and selectively degraded through autophagy. PpAtg30 and Atg36 function as receptors for pexophagy in *Pichia pastoris* and *Saccharoymces cerevisiae*, respectively [41, 44].

1.4 Physiological roles

Autophagy has many physiological roles. First, autophagy is a protective mechanism against cellular stress [6, 51]. For example, autophagy's role in supplying essential building blocks or metabolic substrates such as amino acids under conditions of nutrient

deprivation is critical for maintaining cell viability under adverse conditions; autophagic degradation and recycling enable cells to maintain the synthesis of essential proteins and to generate ATP.

Recent studies indicate that autophagy is also indispensible during development. One example of such a role is seen after oocyte fertilization in *C. elegans* where autophagy is involved in the elimination of maternal mitochondria [52, 53]; however, this does not appear to be the case in mammals [54]. In addition, during embryonic development, clearance of apoptotic cells is achieved through autophagy [55]. Autophagy is also implicated in life span extension; induction of autophagy increases longevity in several model organisms [56], and its role in clearing aggregate-prone proteins and damaged mitochondria might be relevant to its anti-aging effects.

As autophagy acts to eliminate many harmful components in a cell, malfunction of autophagy has also been suggested to correlate with or be the cause of a variety of diseases, such as cancer, neurodegeneration, cardiovascular myopathies, and lysosomal storage disorders [3]. For example, the selective degradation of damaged mitochondria is suggested to underlie the tumor suppressive effects of autophagy, possibly through reducing oxidative stress and preventing DNA damage [57]. Several lines of evidence suggest that the role of autophagy in clearing toxic aggregate-prone proteins is critical to prevent certain types of neurodegeneration, including those associated with Huntington, Alzheimer and Parkinson diseases [58, 59].

1.5 References

1. Castets, P., Lin, S., Rion, N., Di Fulvio, S., Romanino, K., Guridi, M., Frank, S., Tintignac, L.A., Sinnreich, M., and Ruegg, M.A. (2013). Sustained activation of mTORC1 in skeletal muscle inhibits constitutive and starvation-induced autophagy and causes a severe, late-onset myopathy. Cell Metab *17*, 731-744.
2. Gonzalez, C.D., Lee, M.-S., Marchetti, P., Pietropaolo, M., Towns, R., Vaccaro, M.I., Watada, H., and Wiley, J.W. (2011). The emerging role of autophagy in the pathophysiology of diabetes mellitus. Autophagy *7*, 2-11.
3. Klionsky, D.J., and Codogno, P. (2013). The mechanism and physiological function of macroautophagy. J Innate Immun *5*, 427-433.
4. Murrow, L., and Debnath, J. (2013). Autophagy as a stress-response and quality-control mechanism: implications for cell injury and human disease. Annu Rev Pathol *8*, 105-137.
5. Rubinsztein, D.C., Codogno, P., and Levine, B. (2012). Autophagy modulation as a potential therapeutic target for diverse diseases. Nat Rev Drug Discov *11*, 709-730.
6. Yang, Z., and Klionsky, D.J. (2010). Mammalian autophagy: core molecular machinery and signaling regulation. Curr Opin Cell Biol *22*, 124-131.
7. Dice, J.F. (2007). Chaperone-mediated autophagy. Autophagy *3*, 295-299.
8. Kaushik, S., and Cuervo, A.M. (2012). Chaperone-mediated autophagy: a unique way to enter the lysosome world. Trends Cell Biol *22*, 407-417.
9. Mijaljica, D., Prescott, M., and Devenish, R.J. (2011). Microautophagy in mammalian cells: Revisiting a 40-year-old conundrum. Autophagy *7*, 673-682.
10. Stromhaug, P.E., and Klionsky, D.J. (2001). Approaching the molecular mechanism of autophagy. Traffic *2*, 524-531.
11. Harding, T.M., Morano, K.A., Scott, S.V., and Klionsky, D.J. (1995). Isolation and characterization of yeast mutants in the cytoplasm to vacuole protein targeting pathway. J Cell Biol *131*, 591-602.
12. Klionsky, D.J., Cregg, J.M., Dunn, W.A., Jr., Emr, S.D., Sakai, Y., Sandoval, I.V., Sibirny, A., Subramani, S., Thumm, M., Veenhuis, M., et al. (2003). A unified nomenclature for yeast autophagy-related genes. Dev Cell *5*, 539-545.
13. Thumm, M., Egner, R., Koch, B., Schlumpberger, M., Straub, M., Veenhuis, M., and Wolf, D.H. (1994). Isolation of autophagocytosis mutants of *Saccharomyces cerevisiae*. FEBS Lett *349*, 275-280.
14. Tsukada, M., and Ohsumi, Y. (1993). Isolation and characterization of autophagy-defective mutants of *Saccharomyces cerevisiae*. FEBS Lett *333*, 169-174.
15. Xie, Z., and Klionsky, D.J. (2007). Autophagosome formation: core machinery and adaptations. Nat Cell Biol *9*, 1102-1109.
16. Kabeya, Y., Kamada, Y., Baba, M., Takikawa, H., Sasaki, M., and Ohsumi, Y. (2005). Atg17 functions in cooperation with Atg1 and Atg13 in yeast autophagy. Mol Biol Cell *16*, 2544-2553.

17. Kabeya, Y., Kawamata, T., Suzuki, K., and Ohsumi, Y. (2007). Cis1/Atg31 is required for autophagosome formation in *Saccharomyces cerevisiae*. Biochem Biophys Res Commun *356*, 405-410.
18. Mizushima, N. (2010). The role of the Atg1/ULK1 complex in autophagy regulation. Curr Opin Cell Biol *22*, 132-139.
19. Ragusa, M.J., Stanley, R.E., and Hurley, J.H. (2012). Architecture of the Atg17 complex as a scaffold for autophagosome biogenesis. Cell *151*, 1501-1512.
20. Kihara, A., Noda, T., Ishihara, N., and Ohsumi, Y. (2001). Two distinct Vps34 phosphatidylinositol 3-kinase complexes function in autophagy and carboxypeptidase Y sorting in *Saccharomyces cerevisiae*. J Cell Biol *152*, 519-530.
21. Stack, J.H., Herman, P.K., Schu, P.V., and Emr, S.D. (1993). A membrane-associated complex containing the Vps15 protein kinase and the Vps34 PI 3-kinase is essential for protein sorting to the yeast lysosome-like vacuole. EMBO J *12*, 2195-2204.
22. Kametaka, S., Okano, T., Ohsumi, M., and Ohsumi, Y. (1998). Apg14p and Apg6/Vps30p form a protein complex essential for autophagy in the yeast, *Saccharomyces cerevisiae*. J Biol Chem *273*, 22284-22291.
23. Noda, T., Kim, J., Huang, W.P., Baba, M., Tokunaga, C., Ohsumi, Y., and Klionsky, D.J. (2000). Apg9p/Cvt7p is an integral membrane protein required for transport vesicle formation in the Cvt and autophagy pathways. J Cell Biol *148*, 465-480.
24. Reggiori, F., Shintani, T., Nair, U., and Klionsky, D.J. (2005). Atg9 cycles between mitochondria and the pre-autophagosomal structure in yeasts. Autophagy *1*, 101-109.
25. Guan, J., Stromhaug, P.E., George, M.D., Habibzadegah-Tari, P., Bevan, A., Dunn, W.A., and Klionsky, D.J. (2001). Cvt18/Gsa12 is required for cytoplasm-to-vacuole transport, pexophagy, and autophagy in *Saccharomyces cerevisiae* and *Pichia pastoris*. Mol Biol Cell *12*, 3821-3838.
26. Reggiori, F., Tucker, K.A., Stromhaug, P.E., and Klionsky, D.J. (2004). The Atg1-Atg13 complex regulates Atg9 and Atg23 retrieval transport from the pre-autophagosomal structure. Dev Cell *6*, 79-90.
27. Wang, C.W., Kim, J., Huang, W.P., Abeliovich, H., Stromhaug, P.E., Dunn, W.A., Jr., and Klionsky, D.J. (2001). Apg2 is a novel protein required for the cytoplasm to vacuole targeting, autophagy, and pexophagy pathways. J Biol Chem *276*, 30442-30451.
28. Yen, W.-L., Legakis, J.E., Nair, U., and Klionsky, D.J. (2007). Atg27 is required for autophagy-dependent cycling of Atg9. Mol Biol Cell *18*, 581-593.
29. Young, A.R.J., Chan, E.Y.W., Hu, X.W., Kochl, R., Crawshaw, S.G., High, S., Hailey, D.W., Lippincott-Schwartz, J., and Tooze, S.A. (2006). Starvation and ULK1-dependent cycling of mammalian Atg9 between the TGN and endosomes. J Cell Sci *119*, 3888-3900.
30. Orsi, A., Razi, M., Dooley, H.C., Robinson, D., Weston, A.E., Collinson, L.M., and Tooze, S.A. (2012). Dynamic and transient interactions of Atg9 with autophagosomes, but not membrane integration, are required for autophagy. Mol Biol Cell *23*, 1860-1873.

31. Ichimura, Y., Kirisako, T., Takao, T., Satomi, Y., Shimonishi, Y., Ishihara, N., Mizushima, N., Tanida, I., Kominami, E., Ohsumi, M., et al. (2000). A ubiquitin-like system mediates protein lipidation. Nature *408*, 488-492.
32. Mizushima, N., Noda, T., Yoshimori, T., Tanaka, Y., Ishii, T., George, M.D., Klionsky, D.J., Ohsumi, M., and Ohsumi, Y. (1998). A protein conjugation system essential for autophagy. Nature *395*, 395-398.
33. Mizushima, N., Yamamoto, A., Hatano, M., Kobayashi, Y., Kabeya, Y., Suzuki, K., Tokuhisa, T., Ohsumi, Y., and Yoshimori, T. (2001). Dissection of autophagosome formation using Apg5-deficient mouse embryonic stem cells. Journal of Cell Biology *152*, 657-667.
34. Tanida, I., Tanida-Miyake, E., Ueno, T., and Kominami, E. (2001). The human homolog of *Saccharomyces cerevisiae* Apg7p is a Protein-activating enzyme for multiple substrates including human Apg12p, GATE-16, GABARAP, and MAP-LC3. J Biol Chem *276*, 1701-1706.
35. Mizushima, N. (2003). Mouse Apg16L, a novel WD-repeat protein, targets to the autophagic isolation membrane with the Apg12-Apg5 conjugate. J Cell Sci *116*, 1679-1688.
36. Kabeya, Y., Mizushima, N., Yamamoto, A., Oshitani-Okamoto, S., Ohsumi, Y., and Yoshimori, T. (2004). LC3, GABARAP and GATE16 localize to autophagosomal membrane depending on form-II formation. J Cell Sci *117*, 2805-2812.
37. Tanida, I., Komatsu, M., Ueno, T., and Kominami, E. (2003). GATE-16 and GABARAP are authentic modifiers mediated by Apg7 and Apg3. Biochem Biophys Res Commun *300*, 637-644.
38. Tanida, I., Tanida-Miyake, E., Komatsu, M., Ueno, T., and Kominami, E. (2002). Human Apg3p/Aut1p homologue is an authentic E2 enzyme for multiple substrates, GATE-16, GABARAP, and MAP-LC3, and facilitates the conjugation of hApg12p to hApg5p. J Biol Chem *277*, 13739-13744.
39. Tanida, I., Sou, Y.S., Minematsu-Ikeguchi, N., Ueno, T., and Kominami, E. (2006). Atg8L/Apg8L is the fourth mammalian modifier of mammalian Atg8 conjugation mediated by human Atg4B, Atg7 and Atg3. Febs J *273*, 2553-2562.
40. Cebollero, E., Reggiori, F., and Kraft, C. (2012). Reticulophagy and ribophagy: regulated degradation of protein production factories. Int J Cell Biol *2012*, 182834.
41. Farre, J.C., Manjithaya, R., Mathewson, R.D., and Subramani, S. (2008). PpAtg30 tags peroxisomes for turnover by selective autophagy. Dev Cell *14*, 365-376.
42. Kanki, T., Wang, K., Cao, Y., Baba, M., and Klionsky, D.J. (2009). Atg32 is a mitochondrial protein that confers selectivity during mitophagy. Dev Cell *17*, 98-109.
43. Lynch-Day, M.A., and Klionsky, D.J. (2010). The Cvt pathway as a model for selective autophagy. FEBS Lett *584*, 1359-1366.
44. Motley, A.M., Nuttall, J.M., and Hettema, E.H. (2012). Pex3-anchored Atg36 tags peroxisomes for degradation in *Saccharomyces cerevisiae*. Embo J *31*, 2852-2868.
45. Yorimitsu, T., and Klionsky, D.J. (2005). Atg11 links cargo to the vesicle-forming

machinery in the cytoplasm to vacuole targeting pathway. Mol Biol Cell *16*, 1593-1605.
46. Okamoto, K., Kondo-Okamoto, N., and Ohsumi, Y. (2009). Mitochondria-anchored receptor Atg32 mediates degradation of mitochondria via selective autophagy. Dev Cell *17*, 87-97.
47. Youle, R.J., and Narendra, D.P. (2011). Mechanisms of mitophagy. Nat Rev Mol Cell Biol *12*, 9-14.
48. Sandoval, H., Thiagarajan, P., Dasgupta, S.K., Schumacher, A., Prchal, J.T., Chen, M., and Wang, J. (2008). Essential role for Nix in autophagic maturation of erythroid cells. Nature *454*, 232-235.
49. Sato, M., and Sato, K. (2012). Maternal inheritance of mitochondrial DNA: Degradation of paternal mitochondria by allogeneic organelle autophagy, allophagy. Autophagy *8*, 424-425.
50. Till, A., Lakhani, R., Burnett, S.F., and Subramani, S. (2012). Pexophagy: the selective degradation of peroxisomes. Int J Cell Biol *2012*, 512721.
51. Kuma, A., Hatano, M., Matsui, M., Yamamoto, A., Nakaya, H., Yoshimori, T., Ohsumi, Y., Tokuhisa, T., and Mizushima, N. (2004). The role of autophagy during the early neonatal starvation period. Nature *432*, 1032-1036.
52. Al Rawi, S., Louvet-Vallee, S., Djeddi, A., Sachse, M., Culetto, E., Hajjar, C., Boyd, L., Legouis, R., and Galy, V. (2011). Postfertilization autophagy of sperm organelles prevents paternal mitochondrial DNA transmission. Science *334*, 1144-1147.
53. Sato, M., and Sato, K. (2011). Degradation of paternal mitochondria by fertilization-triggered autophagy in *C. elegans* embryos. Science *334*, 1141-1144.
54. Luo, S.M., Ge, Z.J., Wang, Z.W., Jiang, Z.Z., Wang, Z.B., Ouyang, Y.C., Hou, Y., Schatten, H., and Sun, Q.Y. (2013). Unique insights into maternal mitochondrial inheritance in mice. Proc Natl Acad Sci U S A *110*, 13038-13043.
55. Qu, X., Zou, Z., Sun, Q., Luby-Phelps, K., Cheng, P., Hogan, R.N., Gilpin, C., and Levine, B. (2007). Autophagy gene-dependent clearance of apoptotic cells during embryonic development. Cell *128*, 931-946.
56. Rubinsztein, D.C., Marino, G., and Kroemer, G. (2011). Autophagy and aging. Cell *146*, 682-695.
57. Narendra, D., Tanaka, A., Suen, D.F., and Youle, R.J. (2008). Parkin is recruited selectively to impaired mitochondria and promotes their autophagy. J Cell Biol *183*, 795-803.
58. Bjorkoy, G., Lamark, T., Brech, A., Outzen, H., Perander, M., Overvatn, A., Stenmark, H., and Johansen, T. (2005). p62/SQSTM1 forms protein aggregates degraded by autophagy and has a protective effect on huntingtin-induced cell death. J Cell Biol *171*, 603-614.
59. Ravikumar, B., Duden, R., and Rubinsztein, D.C. (2002). Aggregate-prone proteins with polyglutamine and polyalanine expansions are degraded by autophagy. Hum Mol Genet *11*, 1107-1117.

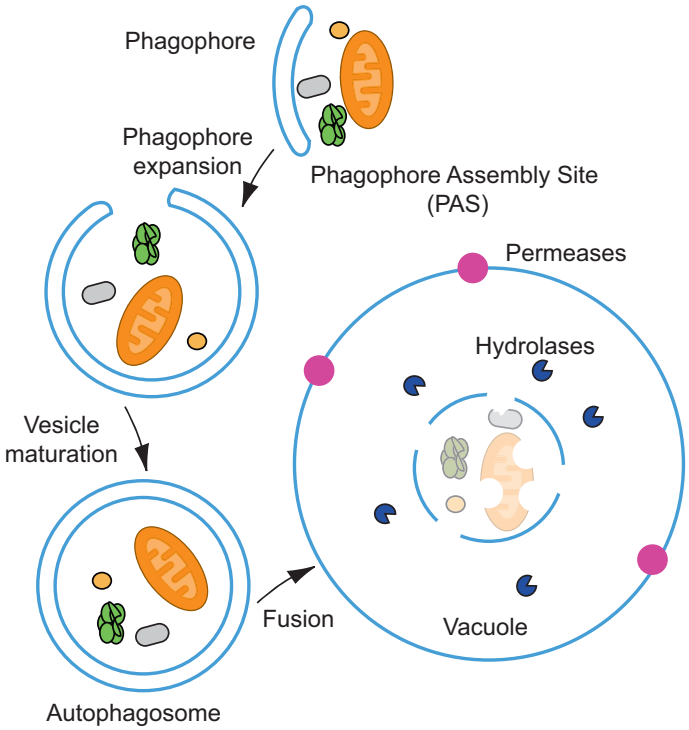

Figure 1.1 Schematic model of autophagy process in yeast. Cargoes including cytosolic proteins, protein aggregates, and damaged organelles are sequestered by a phagophore, which will expand and mature to form a complete autophagosome. The outer membrane of the autophagosome fuses with the vacuole membrane, releasing the inner membrane together with cargoes into the vacuole lumen, which are then degraded by the resident hydrolases. The breakdown products are released back into the cytosol for reuse.

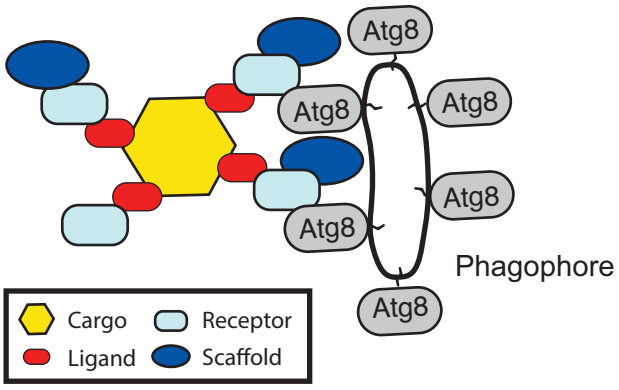

Figure 1.2 A cargo-ligand-receptor-scaffold model of selective autophagy pathways. In yeast, during selective autophagy processes, the cargo or ligand on the cargo recruits specific receptor, which can interact with Atg8 and the scaffold protein Atg11. These interactions mediate the recruitment of core autophagy molecular machinery to form an autophagosome encapsulating the cargo.

CHAPTER 2. The progression of peroxisomal degradation through autophagy requires peroxisomal division[2]

2.1 Abstract

Peroxisomes are highly dynamic organelles that have multiple functions in cellular metabolism. To adapt the intracellular conditions to the changing extracellular environment, peroxisomes undergo constitutive segregation and degradation. The segregation of peroxisomes are mediated by two dynamin-related GTPases, Dnm1 and Vps1, whereas, the degradation of peroxsisomes is accomplished through pexophagy, a selective type of autophagy. During pexophagy, the size of the organelle is always a challenging factor for the efficiency of engulfment by the sequestering compartment, the phagophore, which implies a potential role for peroxisomal fission in the degradation process, similar to the situation with selective mitochondria degradation. In this study, we report that peroxisomal fission is indeed critical for the efficient elimination of the organelle. When pexophagy is induced, both Dnm1 and Vps1 are recruited to the degrading peroxisomes through interactions with Atg11 and Atg36. In addition, we find that specific peroxisomal fission, which is only needed for pexophagy, occurs at

[2] This chapter is reprinted from Mao K*, Liu X*, Feng Y, Klionsky DJ. (2014) The progression of peroxisomal degradation through autophagy requires peroxisomal division. *Autophagy* 10(4):652-661 (doi.org/10.4161/auto.27852).

mitochondria-peroxisome contact sites.

2.2 Introduction

In most eukaryotic cells, mitochondria and peroxisomes drive the catabolism of long chain fatty acids through β-oxidation, and convert the hydrogen peroxide into water and oxygen; in yeasts, this process is restricted to peroxisomes. One byproduct of β-oxidation is the production of reactive oxygen species that have the potential to damage cellular components. Therefore, it is essential that proper peroxisomal function is maintained, and that these organelles are removed if damaged or no longer needed. To adapt to the changing extracellular environment, peroxisomes undergo a remarkable remolding of their cellular pattern of expression, morphology, and abundance. Peroxisomes achieve this dynamic property through biogenesis, division, and degradation. Budding from the endoplasmic reticulum (ER) appears to be one source of the peroxisome membrane, which is generated in a Pex3- and Pex19-dependent manner; however, the organelle may be primarily generated through fission of a preexisting peroxisome followed by import of additional membrane and proteins [1]. The proliferation and replication of peroxisomes that is achieved by division is under the control of two dynamin-related GTPases, Dnm1 and Vps1[1, 2]. Superfluous, or extensively damaged peroxisomes are targeted for vacuole-dependent degradation through selective autophagy, which is termed pexophagy [3, 4].

Autophagy is a conserved lysosome/vacuole-dependent catabolic pathway degrading

cytosol, protein aggregates, and organelles. Depending on the extracellular stresses and the degrading targets, autophagy can occur in either nonselective or selective modes. Nonselective autophagy mediates bulk degradation and recycling of cytoplasm to support cell survival during nutrient deprivation [5, 6]. Selective autophagy recognizes and targets specific cargos or organelles, such as peroxisomes (pexophagy) and mitochondria (mitophagy) [7].

After a decade of study, a general model has been established for selective autophagy. A ligand on the degrading target binds to a specific receptor; the receptor in turn recruits a scaffold protein, which links the cargo-receptor complex with the autophagy machinery [8]. In yeast, Atg11 is the scaffold and its binding receptor varies depending on the degrading cargos. In the case of pexophagy, Atg36 serves as the receptor in *Saccharomyces cerevisiae*, and PpAtg30 in *Pichia pastoris*; Pex3 functions as the ligand, binding to either Atg36 or ppAtg30 [9, 10]. The receptor Atg36 binds to Atg11, a scaffold, which will promote the attachment of the degrading peroxisomes with Atg8–PE, and subsequent engulfment of the organelles by the phagophore, the initial sequestering compartment. We recently showed that when mitophagy is induced, the Atg11 scaffold is recruited by the mitophagy receptor Atg32, and in turn links the fission complex containing Dnm1 to those mitochondria that are destined for degradation to drive their division [11]. Similar to mitochondria, the size of peroxisomes also makes it problematic to sequester this organelle by the phagophore, leading us to hypothesize that peroxisomal fission is necessary for pexophagy.

Here, we show that the two dynamin-related GTPases Dnm1 and Vps1 are important for pexophagy. The scaffold protein Atg11 interacts with both Dnm1 and Vps1 with the Atg11-Dnm1 interaction occurring on both mitochondria and peroxisomes, whereas the Atg11-Vps1 interaction takes place exclusively on peroxisomes. Unlike the mitophagy receptor Atg32, the pexophagy receptor Atg36 is able to interact directly with Dnm1 and Vps1, and these interactions occur on the peroxisomes. Importantly, these interactions represent the process of pexophagy-specific fission, which always occurs at mitochondria-peroxisome contact sites.

2.3 Results

2.3.1 Peroxisomal fission is a significant step during pexophagy.

In *Saccharomyces cerevisiae*, peroxisomes proliferate with increasing number and size when cells are cultured in growth medium containing oleic acid as the sole carbon source. When these cells are subjected to conditions of nitrogen starvation in the presence of glucose, this elevated population of peroxisomes is no longer necessary, and pexophagy is dramatically induced to degrade the excess organelles [3]. To track the state and morphology of peroxisomes during pexophagy, we transformed a plasmid expressing the blue fluorescent protein (BFP) fused with a C-terminal type I peroxisomal targeting signal, serine-lysine-leucine (BFP-SKL) [12]. When yeast cells were cultured in nutrient rich medium with oleic acid (YTO), punctate peroxisomes appeared in the cytosol (Fig. 2.1A, left). After we shifted the cells to nitrogen starvation medium with glucose (SD-N)

for 2 h, which we have previously shown induces pexophagy [3], the morphology of some peroxisomes changed and displayed an elongated pattern (Fig. 2.1A, right). The elongation of peroxisomal membrane precedes the division of these organelles, which is significant for their replication and proliferation [2]. The occurrence of peroxisomal elongation under pexophagy-inducing conditions implied that the fission event also happened during the degradation of peroxisomes. Accordingly, we asked whether fission plays an important role for the progression of pexophagy.

The division of peroxisomes in budding yeast is mediated by two dynamin-related GTPases, Dnm1 and Vps1. Dnm1 is able to constrict membrane, and its proper function and localization on the peroxisomes requires a fission complex, which also includes Fis1, Mdv1, and Caf4 [13]. Fis1 is a tail-anchored membrane receptor that interacts with the partially redundant proteins Mdv1 and Caf4, which in turn bind to Dnm1, to recruit the latter to the peroxisome. This fission complex is shared with mitochondria, and promotes mitochondrial fission through the same mechanism of Dnm1 recruitment [2, 14]. Vps1 also controls the segregation of peroxisomes, and is recruited to the peroxisomes through interaction with Pex19 [15].

In order to detect and quantify the number of peroxisomes during pexophagy, we used a plasmid containing a green fluorescent protein with the C-terminal type I peroxisomal targeting signal (GFP-SKL) and CellTracker Blue CMAC dye to mark the peroxisomes and vacuole lumen, respectively. The *atg1*Δ mutant served as a control, since autophagy induction and peroxisomal degradation are completely absent in the

*atg1*Δ mutant. When the yeast cells were grown in YTO medium, wild-type and *atg1*Δ mutant cells had approximately 11.5 and 12.3 peroxisomes on average per cell, respectively (Fig. 2.1C); however, there were fewer peroxisomes in *fis1*Δ (9.2/cell) and *dnm1*Δ (8.3/cell) mutants (Fig. 2.1B and C), which is consistent with the previous report that the replication of peroxisomes is compromised in these mutants [16]. In *vps1*Δ and *dnm1*Δ *vps1*Δ mutants, peroxisomes are highly clustered making it difficult to differentiate and quantify individual peroxisomes (Fig. 2.1B). After the wild-type cells were starved in SD-N medium for 7 h, peroxisomes were degraded in the vacuole, however, the fluorescent signal from GFP-SKL was relatively stable and was diffuse in the vacuolar lumen; at the same time, the number of peroxisomes in the cytosol was largely decreased (corresponding to 56.4% turnover). In *fis1*Δ and *dnm1* mutants, a vacuolar GFP signal was also detected, but a reduced number of peroxisomes (39.1% and 35.3%, respectively) were degraded (Fig. 2.1B and 2.1C), which indicated that pexophagy was partially blocked in these two mutants. In *atg1*Δ, *vps1*Δ and *dnm1*Δ *vps1*Δ mutants, no vacuolar GFP was detected, which implied that pexophagy was largely defective in these mutants (Fig. 2.1B). However, as noted above, peroxisomes were largely clustered in the *vps1*Δ and *dnm1*Δ *vps1*Δ mutants (Fig. 2.1B), making the quantification of peroxisomal degradation difficult.

To confirm the pexophagy defects in fission mutants, and to more precisely evaluate the pexophagy activities in *vps1*Δ and *dnm1*Δ *vps1*Δ mutants, we took advantage of a second method for monitoring pexophagy, the Pex14-GFP processing assay. *PEX14*

encodes a peroxisomal integral membrane protein, and a chromosomally tagged version with GFP at the C terminus is correctly localized on this organelle. When pexophagy is induced, peroxisomes, along with Pex14-GFP, are delivered into the vacuole for degradation. Pex14 is proteolytically degraded, whereas the GFP moiety is relatively stable and accumulates in the vacuolar lumen. Thus, pexophagy can be monitored based on the amount of free GFP by immunoblot [17]. After 1 or 2 h of nitrogen starvation with glucose, a considerable amount of free GFP was detected in wild-type cells, however, free GFP was hardly detectable in *atg1*Δ (Fig. 2.S1). The amount of free GFP was reduced in *fis1*Δ, and *dnm1*Δ mutants, and dramatically reduced in *vps1*Δ, and *dnm1*Δ *vps1*Δ mutants (Fig. 2.1D). These results were consistent with the previous report and suggested that both Dnm1-dependent and Vps1-dependent peroxisomal fission are important for pexophagy, with Vps1 playing a more significant role [18].

2.3.2 Atg11 interacts with Dnm1 and Fis1 on the degrading peroxisomes.

In growing yeast cells, Atg11 is mostly diffuse in the cytosol; its translocation to various organelles depends on the presence of different receptor proteins. Our recent studies showed that upon translocation to mitochondria through binding to Atg32, Atg11 recruits the Dnm1-containing fission complex to these mitochondria that are being targeted for degradation by mitophagy[11]. The Atg11-bound population of Dnm1, which is specific for fission associated with mitophagy, is different from the previously characterized Atg11-free Dnm1, which controls homeostatic mitochondrial division. Pexophagy and

mitophagy share the use of the Atg11 scaffold and the Dnm1-containing fission complex. Accordingly, we speculate that Atg11 is also able to recruit the Dnm1-containing fission complex to peroxisomes to facilitate their division prior to pexophagy.

To test this hypothesis, we used the bimolecular fluorescence complementation (BiFC) assay to determine where the Atg11-Dnm1 interaction occurs. Briefly, in the BiFC assay, the Venus yellow fluorescent protein (vYFP) is split into two fragments, VN (N terminus of vYFP) and VC (C terminus of vYFP) [19]. We fused VN to Atg11 on the genome and transformed cells with a plasmid containing Dnm1-VC. Fluorescence from these two chimeras can only be detected when the two proteins interact and bring the two fragments of vYFP proximal to each other. Thus, for example, when mitophagy is induced, VN-Atg11 and Dnm1-VC form vYFP puncta on the mitochondrial network [11]. We carried out the same strategy and also introduced a C-terminal mCherry at the *PEX14* locus on the chromosome to be able to monitor peroxisomes. When we starved the yeast cells to induce pexophagy, the Atg11-Dnm1 interacting puncta colocalized with Pex14-mCherry (Fig. 2.2A, arrowhead), which indicated that Atg11 recruited Dnm1 to the degrading peroxisomes when pexophagy was induced. To exclude the possibility that the YFP signal detected was due to the overexpression of VN-Atg11 under the control of ribosomal protein promoter (RPL7Bp), we generated an RPL7Bp driven VN strain and transformed cells with a plasmid containing Dnm1-VC. No YFP fluorescence was detected in this control experiment, which suggested the YFP puncta represented Atg11-Dnm1 interaction (Fig. 2.S2A).

Atg11 and the Dnm1-containing fission complex are shared by peroxisomes and mitochondria. To carefully analyze the location of Atg11-Dnm1 interaction, we transformed a plasmid harboring BFP-SKL to display peroxisomes and stained the mitochondria with MitoTracker Red dye. After pexophagy was induced by nitrogen starvation with glucose, the localization of Atg11-Dnm1 interacting puncta could be classified into three major different classes. The class I puncta appeared on the mitochondrial network (Fig. 2.2B, arrow; Fig. 2.2C), and thus correspond to complexes that are involved in mitophagy-specific fission [11]. Mitophagy is highly induced when yeast are grown solely in the presence of a non-fermentable carbon source and then switched to nitrogen starvation medium containing a fermentable carbon source [20]. Because oleic acid is a non-fermentable carbon source, these culture conditions (i.e., switching from YTO to SD-N) likely induce mitophagy. Class II puncta were localized on peroxisomes (Fig. 2.2B, arrowhead; Fig. 2.2C), and are presumed to represent the fission complexes that mediate pexophagy-specific fission. Unexpectedly, these puncta were found to be proximal to mitochondria. The class III puncta colocalized with both peroxisomes and mitochondria (Fig. 2.2B, asterisk; Fig. 2.2C). At the same time, we also found very few puncta localized in the cytosol or on the peroxisomes which were not adjacent to mitochondria (Fig. 2.2C**)**. The cellular pattern of both class II and class III puncta implied the Dnm1-mediated peroxisomal fission might occur at the mitochondria-peroxisome contact sites.

To test this hypothesis, we also examined the sites of the Atg11-Fis1 interaction.

Based on our previous work, Atg11 interacts with Fis1 in addition to Dnm1 on the targeted mitochondria [11]. We chromosomally tagged *ATG11* and *FIS1* with VN and VC, respectively, and used BFP-SKL and MitoTracker Red to track peroxisomes and mitochondria, respectively. The distribution of Atg11-Fis1 puncta was extremely similar to that of Atg11-Dnm1 puncta, with the existence of distinct populations localized to mitochondria (Fig. 2.2D, arrow; Fig. 2.2E), peroxisomes that were proximal to mitochondria (Fig. 2.2D, arrowhead; Fig. 2.2E), and puncta localized on both organelles (Fig. 2.2D, asterisks; Fig. 2.2E). Of note, the peroxisomes marked by the Atg11-Fis1 interaction were always close to or associated with mitochondria. We also generated the control experiment to make sure that the YFP signal detected was due to Atg11-Fis1 interaction (Fig. 2.S2B). After the analysis of both Atg11-Dnm1 and Atg11-Fis1 puncta, we concluded that Atg11 recruited Dnm1-containing fission complexes to peroxisomes being targeted for degradation, and this fission event happened at mitochondria-peroxisome contact sites. We propose that this distinct localization might be due to the fact that mitochondria and peroxisomes share the Dnm1-containing fission complex.

2.3.3 Atg11 interacts with Vps1 on peroxisomes

We noticed that compared to Dnm1 inhibition of the Vps1-mediated peroxisomal fission had a stronger effect on pexophagy (Fig. 2.1B and D). Therefore, we wondered if there is also an Atg11-bound form of Vps1, which localizes on the peroxisomes that will become

targeted for sequestration and regulates pexophagy-specific division. We chromosomally tagged *ATG11* with VN and *PEX14* with mCherry, and transformed the cells with a plasmid expressing Vps1-VC. VN-Atg11 and Vps1-VC formed puncta in pexophagy-inducing conditions, and these puncta localized on the peroxisomes marked by Pex14-mCherry (Fig. 2.3A, arrowhead). At the same time these puncta were not due to the overexpression of VN-Atg11 (Fig. 2.S3A).

To verify the interaction between Atg11 and Vps1, we carried out protein A affinity isolation with IgG-Sepharose. In our previous work, we showed that the Dnm1 mutant lacking the last 30 amino acids [Dnm1 (30Δ)] is unable to interact with Atg11. The C terminus of Vps1 has a high similarity at the amino acid sequence level compared to Dnm1 (Fig. 2.S3B). We suspected that the Vps1 mutant lacking the last 30 amino acids [Vps1 (30Δ)] would also lose interaction with Atg11. Protein A (PA)-tagged wild-type Vps1 and Dnm1 co-precipitated a substantial amount of the available HA-Atg11, whereas Dnm1 (30Δ) precipitated a very small amount of this protein (Fig. 2.3B; Fig. 2.S3C). In contrast to our expectation, Vps1 (30Δ) precipitated a similar level of HA-Atg11 relative to that affinity isolated by wild-type (i.e., full length) Vps1 (Fig. 2.3B). Therefore, Vps1 interacts with Atg11 through a different mechanism from the one used by Dnm1.

We showed that the Dnm1-regulated peroxisomal division occurred extremely close to mitochondria (Fig. 2.2B), which we propose may be due to the fact that the Dnm1-containing fission complex is shared by mitochondria and peroxisomes. Up until now, there have not been any published data indicating a role for Vps1 in mitochondria

segregation. Accordingly, we decided to determine whether Vps1-mediated peroxisomal fission, in contrast to that driven by Dnm1, occurred at a site that was distal from mitochondria. We transformed cells with the BFP-SKL plasmid and used MitoTracker Red to allow us to monitor both peroxisomes and mitochondria, respectively. Puncta corresponding to the sites of Atg11-Vps1 interaction did not appear to localize directly on the mitochondrial network; however, the majority of peroxisomes marked by these puncta were still closely associated with mitochondria (Fig. 2.3C, arrowhead; Fig. 2.3D). This result suggested that pexophagy-specific fission, whether mediated by Dnm1 or Vps1, might require the participation of mitochondria.

2.3.4 Atg36 interacts with Dnm1 and Vps1

Atg32 and Atg36 are receptors that bind to Atg11 during mitophagy and pexophagy, respectively; however, their properties vary in several respects. For example, overexpression of Atg36 results in a high level of basal pexophagy independent of nitrogen starvation, whereas overexpression of Atg32 does not induce mitophagy in nutrient-rich conditions [10, 21]. Atg32 is localized on the mitochondrial outer membrane and interacts with the Dnm1-containing fission complex through Atg11. In contrast, Atg36 is a cytosolic protein and is targeted to peroxisomes through binding to Pex3 [10, 21], which raises the possibility that Atg36 is also able to interact with Dnm1 or Vps1, which are also cytosolic proteins, to recruit the fission complex to peroxisomes; this would be in contrast to Atg32, which binds Dnm1 indirectly through Atg11.

To test this hypothesis, and to gain further insight into the mechanism of Vps1-mediated pexophagy, we generated a series of strains expressing VN-Atg36 combined with Dnm1-VC, VC-Fis1, Mdv1-VC, Caf4-VC, or Vps1-VC, and carried out the BiFC assay to search for the possible interactions of these chimeric pairs. VN-Atg36 formed vYFP puncta with Dnm1-VC, or Vps1-VC, but not with the other fusion proteins (Fig. 2.4A). Therefore, unlike Atg32, Atg36 interacts with the two dynamin-related GTPases Dnm1 and Vps1.

To determine where Atg36 interacts with Dnm1 and Vps1, we used BFP-SKL and MitoTracker Red to track peroxisomes and mitochondria, respectively. Both Atg36-Dnm1 and Atg36-Vps1 interacting puncta were largely localized on peroxisomes extremely close to mitochondria (Fig. 2.4B and D, arrowheads; Fig. 2.4C and E). This location was similar to that seen for Atg11-Dnm1, Atg11-Fis1, and Atg11-Vps1, which reinforced our finding that the pexophagy-specific fission happened at the mitochondrial periphery.

It was reported that the phosphorylation of Atg36 is significant for its interaction with Atg11 and Atg8. Specifically, phosphorylation of serine 31 is required for interaction with Atg8, and phosphorylation of serine 97 is required for interaction with Atg11 [22]. Therefore, we tested whether phosphorylation of Atg36 is required for interaction with Dnm1 and Vps1 by yeast two hybrid. BD-Atg36 was able to interact with both AD-Dnm1 and AD-Vps1. BD-Atg36 (S31A), which was reported to lose interaction with Atg8, was still interacting with both AD-Dnm1 and AD-Vps1. At the meantime,

BD-Atg36 (S97A), which was reported to lose interaction with Atg11, interacted with both AD-Dnm1 and AD-Vps1 (Fig. 2.5A). These results suggested that Atg36-Atg11 interaction is not required for Atg36-Dnm1 and Atg36-Vps1 interactions. Therefore, Atg36 might be able to recruit Dnm1 and Vps1 to the peroxisomes independent of Atg11.

Overexpression of Atg36 enhanced pexophagy without nitrogen starvation [10]. We showed that Atg36 interacted with Vps1, which raised a possibility that overexpression of Atg36 increased the level of Vps1 recruitment to the peroxisomes. If this is the case, we should expect that overexpression of Vps1 also enhanced pexophagy independent of nitrogen starvation. We constructed two yeast strains containing either HA-Atg36 or HA-Vps1 under the control of GAL promoter, and used Pex14-GFP processing to detect pexophagy. Yeast cells were cultured in YTO, and shifted to nutrient rich medium with galactose (YPG). We observed robust increase of protein level of HA-Atg36 and HA-Vps1 (Fig. 2.5C). When we detected pexophagy, a clear increase of free GFP appeared after 9h culturing in YPG when Atg36 was overexpressed, which agreed with previous report [10]; surprisingly, pexophagy level was even higher when Vps1 was overexpressed (Fig. 2.5B). These results suggested overexpression of Atg36 might accelerate peroxisomal fission due to its interaction with Vps1.

2.4 Discussion

The degradation of organelles is an energy and time consuming process in eukaryotic cells. In addition, the size of the organelle can present steric challenges, and smaller

fragments of organelles are presumably easier for sequestering. Autophagy is the primary mechanism responsible for the bulk degradation of cytoplasmic components and the selective removal of organelles. In nonselective autophagy, the protein level of Atg8 controls the size of the autophagosomes [23]. In contrast, during selective types of autophagy the phagophore membrane is closely apposed to the cargo, excluding bulk cytoplasm. Therefore, the factors that determine the curvature of the phagophore and the ultimate size of the autophagsomes might be more somewhat distinct between these two modes of sequestration. The cytoplasm-to-vacuole targeting (Cvt) pathway is a biosynthetic route that delivers resident hydrolases to the vacuole. Overexpression of the primary cargo of the Cvt pathway, precursor aminopeptidase I, results in the formation of larger complexes, which are sequestered less efficiently [24]. Mitochondria exist as a highly extended, reticular structure, which is even more difficult for sequestering within phagophores. Our recent work suggested that during mitophagy a selective and specific fission event occurs on the mitochondria that will become substrates for degradation [11]. Although the peroxisomes may be dispersed in the cytosol as individual compartments, the size of this organelle appears to be close to the limit for sequestration by smaller phagophores, such as those generated in the absence of Atg17 [25]. This may be a particular problem after these organelles proliferate following growth in an oleic acid-containing medium. Therefore, we hypothesized that peroxisomes have to divide prior to degradation, and that only the small fragments of the peroxisomes would be targeted by autophagy.

Here, we showed that deletion of the *DNM1* and *VPS1* genes, which encode two dynamin-related GTPases, resulted in substantially lower efficiency of peroxisomal degradation. Previous work indicated that even though the amino acid sequences of Dnm1 and Vps1 are quite similar, deletion of either individual gene has different effects on peroxisomal division. Deletion of *VPS1* dramatically abolishes peroxisomal fission when yeast cells are cultured in both glucose and oleic acid media. However, deletion of *DNM1* affects the division of peroxisomes only in oleic acid, and the defect is not as strong as that of the *vps1*Δ mutant [16]. Consistent with these results, pexophagy is significantly blocked in a *vps1*Δ strain, whereas there was only an intermediate affect in the *dnm1*Δ mutant (Fig. 2.1B and D). Overall, it is clear that peroxisomal fission, whether mediated by Dnm1 or Fis1, is important for pexophagy, which is in agreement with our hypothesis. When we were preparing our manuscript, Manivannan et al published their work showing that Dnm1 and Vps1 are important for the removal of the intra-peroxisomal protein aggregates and pexophagy in yeast *Hansenula polymorpha* and *Saccharomyces cerevisiae* [18]. We also provided evidences indicating how the fission machinery was recruited to the peroxisomes and facilitated peoxphagy.

As a scaffold protein, Atg11 binds to a variety of cargo receptors to mediate different types of selective autophagy. For example, Atg11 binds to Atg19, to Atg32 and to Atg36 for cargo selection during the Cvt pathway, mitophagy and pexophagy, respectively [10, 12, 21, 26, 27]. Atg11 also interacts with Atg1 and Atg17, which connects the step of cargo selection to the initiation of autophagosome formation [27]. Here, and with our

previous work, we add a new piece to the puzzle: during pexophagy and mitophagy, Atg11 recruits the fission machineries to the organelles and promotes their specific segregation, resulting in smaller fragments of these compartments that can be easily degraded.

It is surprising that the pexophagy-specific fission, mediated either by Dnm1 or Vps1, is always occurring in proximity to mitochondria. The division of mitochondria requires the participation of the ER [28], and the fission of peroxisomes apparently involves mitochondria. The crosstalk that occurs between organelles is attracting increasing attention. The peroxisome represents an interesting organelle to study in this regard, having connections with the ER, the mitochondria, and the vacuole.

2.5 Experimental Procedures

2.5.1 Strains, media, and growth conditions.

Yeast strains are listed in Table 2.1. Yeast cells were grown in rich (YPD; 1% yeast extract, 2% peptone, and 2% glucose) or synthetic minimal (SMD; 0.67% yeast nitrogen base, 2% glucose, and auxotrophic amino acids and vitamins as needed) media. For peroxisomal proliferation, cells were grown in YPD to approximately 0.5 OD_{600} and shifted to glycerol medium (SGd; 0.67% yeast nitrogen base, 0.1% glucose, and 3% glycerol) for 16 h. The cells were then incubated for 4 h with the addition of yeast extract and peptone into the SGd medium. The cells were ultimately shifted to oleic acid medium (YTO; 0.67% yeast nitrogen base, 0.1% oleic acid, 0.1% Tween 40 and auxotrophic

amino acids as needed) for 20 h. Pexophagy was induced by shifting the cells to nitrogen starvation medium containing glucose (SD-N; 0.17% yeast nitrogen base without ammonium sulfate or amino acids, and 2% glucose). For GAL promoter driven overexpression, the cells were culture in galactose medium (YPG; 1% yeast extract, 2% peptone, and 2% galactose)

2.5.2 Plasmids

pBFP-SKL(405), pCuGFP-SKL(416), pCuHA-Atg11(416) and pDnm1-VC(416) have been reported previously [11, 12, 21]. For constructing pVps1-VC(416), the *DNM1* promoter and ORF were removed by XbaI and XmaI from pDnm1-VC(416), the resulting linearized vector was ligated in the presence of the DNA fragment containing the *VPS1* promoter and ORF, which was amplified by PCR from the genome of the yeast strain SEY6210 and digested with XbaI and XmaI. For constructing pAD-Dnm1, pAD-Vps1, and pBDU-Atg36, the *DNM1*, *VPS1* and *ATG36* ORF were amplified by PCR from the genome of SEY6210 yeast strain. XmaI and BamHI were used to digest *DNM1* and *ATG36*, and EcoRI and PstI to digest *VPS1*. The digested *DNM1* and *VPS1* fragments were inserted into pAD-C1, and *ATG36* into pBDU-C1 [29]. pBDU-Atg36 (S31A) and pBDU-Atg36 (S97A) were generated by site-directed mutagenesis from pBDU-Atg36.

2.5.3 Fluorescence microscopy.

For fluorescence microscopy, yeast cells were grown as described above to induce peroxisome proliferation and shifted to SD-N for nitrogen starvation. Samples were then examined by microscopy (Delta Vision, Applied Precision) using a 100x objective and pictures were captured with a CCD camera (CoolSnap HQ; Photometrics). For each microscopy picture, 12 Z-section images were captured with a 0.3-µm distance between two neighboring sections. MitoTracker Red CMXRos (Molecular Probes/Invitrogen, M7512) was used to stain the mitochondria.

2.5.4 Additional assay and reagents.

Immunoprecipitation was performed as described previously [21]. Immunoprecipitation was carried out with monoclonal anti-YFP antibody clone JL-8 (Clontech, 632381), monoclonal anti-HA antibody clone-HA7 (Sigma-Aldrich, H3663), and an antibody that binds to protein A with high affinity (no longer commercially available).

2.6 References

1. Motley, A.M., and Hettema, E.H. (2007). Yeast peroxisomes multiply by growth and division. J Cell Biol *178*, 399-410.
2. Schrader, M., Bonekamp, N.A., and Islinger, M. (2012). Fission and proliferation of peroxisomes. Biochim Biophys Acta *1822*, 1343-1357.
3. Hutchins, M.U., Veenhuis, M., and Klionsky, D.J. (1999). Peroxisome degradation in *Saccharomyces cerevisiae* is dependent on machinery of macroautophagy and the Cvt pathway. J Cell Science *112*, 4079-4087.
4. Sakai, Y., Oku, M., van der Klei, I.J., and Kiel, J.A. K.W. (2006). Pexophagy: autophagic degradation of peroxisomes. Biochim Biophys Acta *1763*, 1767-1775.
5. Xie, Z., and Klionsky, D.J. (2007). Autophagosome formation: core machinery and

adaptations. Nat. Cell Biol. *9*, 1102-1109.
6. Mizushima, N., Levine, B., Cuervo, A.M., and Klionsky, D.J. (2008). Autophagy fights disease through cellular self-digestion. Nature *451*, 1069-1075.
7. Reggiori, F., and Klionsky, D.J. (2013). Autophagic processes in yeast: mechanism, machinery and regulation. Genetics *194*, 341-361.
8. Mijaljica, D., Nazarko, T.Y., Brumell, J.H., Huang, W.P., Komatsu, M., Prescott, M., Simonsen, A., Yamamoto, A., Zhang, H., Klionsky, D.J., et al. (2012). Receptor protein complexes are in control of autophagy. Autophagy *8*, 1701-1705.
9. Farre, J.C., Manjithaya, R., Mathewson, R.D., and Subramani, S. (2008). PpAtg30 tags peroxisomes for turnover by selective autophagy. Dev Cell *14*, 365-376.
10. Motley, A.M., Nuttall, J.M., and Hettema, E.H. (2012). Pex3-anchored Atg36 tags peroxisomes for degradation in *Saccharomyces cerevisiae*. EMBO J *31*, 2852-2868.
11. Mao, K., Wang, K., Liu, X., and Klionsky, D.J. (2013). The scaffold protein atg11 recruits fission machinery to drive selective mitochondria degradation by autophagy. Dev Cell *26*, 9-18.
12. Kim, J., Kamada, Y., Stromhaug, P.E., Guan, J., Hefner-Gravink, A., Baba, M., Scott, S.V., Ohsumi, Y., Dunn, W.A., Jr., and Klionsky, D.J. (2001). Cvt9/Gsa9 functions in sequestering selective cytosolic cargo destined for the vacuole. J Cell Biol *153*, 381-396.
13. Motley, A.M., Ward, G.P., and Hettema, E.H. (2008). Dnm1p-dependent peroxisome fission requires Caf4p, Mdv1p and Fis1p. J. Cell Sci *121*, 1633-1640.
14. Okamoto, K., and Shaw, J.M. (2005). Mitochondrial morphology and dynamics in yeast and multicellular eukaryotes. Annu. Rev. Genet *39*, 503-536.
15. Vizeacoumar, F.J., Vreden, W.N., Fagarasanu, M., Eitzen, G.A., Aitchison, J.D., and Rachubinski, R.A. (2006). The dynamin-like protein Vps1p of the yeast *Saccharomyces cerevisiae* associates with peroxisomes in a Pex19p-dependent manner. J. Biol. Chem. *281*, 12817-12823.
16. Kuravi, K., Nagotu, S., Krikken, A.M., Sjollema, K., Deckers, M., Erdmann, R., Veenhuis, M., and van der Klei, I.J. (2006). Dynamin-related proteins Vps1p and Dnm1p control peroxisome abundance in *Saccharomyces cerevisiae.* J. Cell Sci *119*, 3994-4001.
17. Mao, K., Wang, K., Zhao, M., Xu, T., and Klionsky, D.J. (2011). Two MAPK-signaling pathways are required for mitophagy in *Saccharomyces cerevisiae*. J Cell Biol *193*, 755-767.
18. Manivannan, S., de Boer, R., Veenhuis, M., and van der Klei, I.J. (2013). Lumenal peroxisomal protein aggregates are removed by concerted fission and autophagy events. Autophagy *9*, 1044-1056.
19. Sung, M.K., and Huh, W.K. (2007). Bimolecular fluorescence complementation analysis system for in vivo detection of protein-protein interaction in *Saccharomyces cerevisiae*. Yeast *24*, 767-775.
20. Kanki, T., and Klionsky, D.J. (2008). Mitophagy in yeast occurs through a selective mechanism. J. Biol. Chem. *283*, 32386-32393.
21. Kanki, T., Wang, K., Cao, Y., Baba, M., and Klionsky, D.J. (2009). Atg32 is a

mitochondrial protein that confers selectivity during mitophagy. Dev Cell *17*, 98-109.
22. Farre, J.C., Burkenroad, A., Burnett, S.F., and Subramani, S. (2013). Phosphorylation of mitophagy and pexophagy receptors coordinates their interaction with Atg8 and Atg11. EMBO Rep *14*, 441-449.
23. Xie, Z., Nair, U., and Klionsky, D.J. (2008). Atg8 controls phagophore expansion during autophagosome formation. Mol Biol Cell *19*, 3290-3298.
24. Baba, M., Osumi, M., Scott, S.V., Klionsky, D.J., and Ohsumi, Y. (1997). Two distinct pathways for targeting proteins from the cytoplasm to the vacuole/lysosome. J Cell Biol *139*, 1687-1695.
25. Cheong, H., Yorimitsu, T., Reggiori, F., Legakis, J.E., Wang, C.W., and Klionsky, D.J. (2005). Atg17 regulates the magnitude of the autophagic response. Mol Biol Cell *16*, 3438-3453.
26. Shintani, T., Huang, W.P., Stromhaug, P.E., and Klionsky, D.J. (2002). Mechanism of cargo selection in the cytoplasm to vacuole targeting pathway. Dev Cell *3*, 825-837.
27. Yorimitsu, T., and Klionsky, D.J. (2005). Atg11 links cargo to the vesicle-forming machinery in the cytoplasm to vacuole targeting pathway. Mol Biol Cell *16*, 1593-1605.
28. Friedman, J.R., Lackner, L.L., West, M., DiBenedetto, J.R., Nunnari, J., and Voeltz, G.K. (2011). ER tubules mark sites of mitochondrial division. Science *334*, 358-362.
29. James, P., Halladay, J., and Craig, E.A. (1996). Genomic libraries and a host strain designed for highly efficient two-hybrid selection in yeast. Genetics *144*, 1425-1436.
30. Robinson, J.S., Klionsky, D.J., Banta, L.M., and Emr, S.D. (1988). Protein sorting in *Saccharomyces cerevisiae*: isolation of mutants defective in the delivery and processing of multiple vacuolar hydrolases. Mol. Cell. Biol *8*, 4936-4948.
31. Mao, K., Chew, L.H., Inoue-Aono, Y., Cheong, H., Nair, U., Popelka, H., Yip, C.K., and Klionsky, D.J. (2013). Atg29 phosphorylation regulates coordination of the Atg17-Atg31-Atg29 complex with the Atg11 scaffold during autophagy initiation. Proc Natl Acad Sci U S A *110*, E2875-2884.

Table 2.1. List of strains used in this study.

Name	Genotype	Reference
KDM1103	SEY6210 *PEX14-GFP::KAN dnm1Δ::LEU2*	This paper
KDM1104	SEY6210 *PEX14-GFP::KAN fis1Δ::LEU2*	This paper
KDM1105	SEY6210 *PEX14-GFP::KAN vps1Δ::HIS5*	This paper
KDM1247	SEY6210 *atg11Δ::LEU2 DNM1-PA::HIS3*	[11]
KDM1249	SEY6210 *atg11Δ::LEU2 DNM1(C30Δ)-PA::HIS3*	[11]
KDM1252	SEY6210 *dnm1Δ::LEU2*	[11]
KDM1269	SEY6210 *atg11Δ::LEU2 VPS1-PA::HIS3*	This paper
KDM1545	SEY6210 *RPL7Bp-VN-ATG11::TRP1 RPL7Bp-VC-FIS1::HIS3*	[11]
KDM1535	SEY6210 *RPL7Bp-VN-ATG11::TRP1*	[11]
SEY6210	MATα *leu2-3,112 ura3-52 his3-Δ200 trp1-Δ901 suc2-Δ9 lys2-801; GAL*	[30]
TKYM67	SEY6210 *PEX14-GFP::KAN*	[17]
TKYM72	SEY6210 *PEX14-GFP::KAN atg1Δ::HIS5*	[17]
WHY1	SEY6210 *atg1Δ::HIS5*	[31]
XLY049	SEY6210 *pRS405-BFP-SKL::LEU2*	This paper
XLY059	SEY6210 *PEX14-GFP::KAN dnm1Δ::LEU2 vps1Δ::HIS5*	This paper
XLY060	SEY6210 *fis1Δ::LEU2*	This paper
XLY061	SEY6210 *vps1Δ::LEU2*	This paper
XLY062	SEY6210 *dnm1Δ::LEU2 vps1Δ::HIS5*	This paper
XLY063	SEY6210 *RPL7Bp-VN-ATG36::TRP1*	This paper
XLY064	SEY6210 *RPL7Bp-VN-ATG36::TRP1 RPL7Bp-VC-FIS1::KAN*	This paper
XLY065	SEY6210 *RPL7Bp-VN-ATG36::TRP1 CAF4-VC::KAN*	This paper
XLY066	SEY6210 *RPL7Bp-VN-ATG36::TRP1 MDV1-VC::KAN*	This paper
XLY067	SEY6210 *RPL7Bp-VN-ATG11::TRP1 pRS405-BFP-SKL::LEU2*	This paper
XLY068	SEY6210 *RPL7Bp-VN-ATG11::TRP1 RPL7Bp-VC-FIS1::KAN pRS405-BFP-SKL::LEU2*	This paper
XLY069	SEY6210 *RPL7Bp-VN-ATG36::TRP1 pRS405-BFP-SKL::LEU2*	This paper
XLY070	SEY6210 *RPL7Bp-VN-ATG11::TRP1 PEX14-mCherry::KAN*	This paper
XLY072	SEY6210 *ATG36-VN::HIS3 pRS405-BFP-SKL::LEU2*	This paper
XLY073	SEY6210 *atg11Δ::LEU2 VPS1(C30Δ)-PA::HIS3*	This paper
XLY085	SEY6210 *RPL7Bp-VN::TRP1*	This paper
XLY086	SEY6210 *RPL7Bp-VN::TRP1 RPL7Bp-VC-FIS1::KAN*	This paper
XLY087	SEY6210 RPL7Bp-VN-ATG11::HIS3 RPL7Bp-VC::TRP1	This paper
XLY088	SEY6210 *PEX14-GFP::KAN GAL1p-3HA-ATG36:TRP1*	This paper
XLY089	SEY6210 *PEX14-GFP::KAN GAL1p-3HA-VPS1::TRP1*	This paper
YTS147	SEY6210 *atg11Δ::LEU2*	[20]

A

B

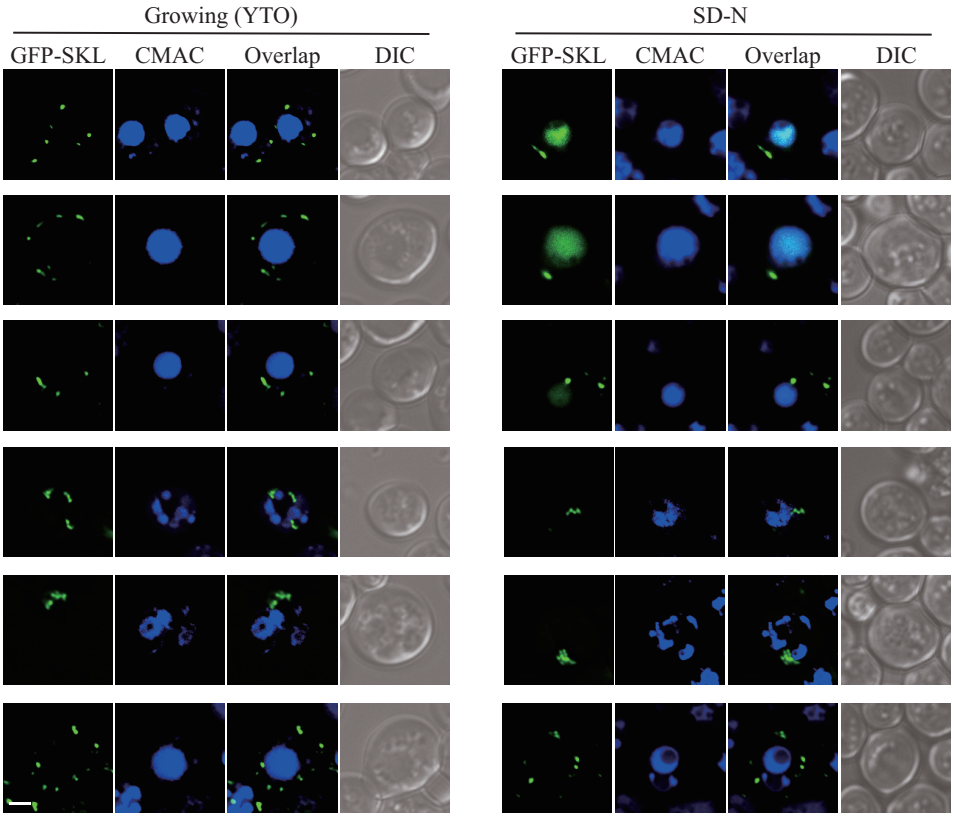

C

Strain	WT	*fis1*Δ	*dnm1*Δ	*atg1*Δ
$N_{growing}$	11.52±3.46 (n=106)	9.23±2.66 (n=108)	8.32±3.04 (n=95)	12.29±3.78 (n=116)
$N_{starvation}$	5.02±2.16 (n=123)	5.63±2.10 (n=104)	5.38±2.20 (n=112)	12.08±3.50 (n=101)
Percentage of degraded peroxisome	56.38%	39.07%	35.26%	1.73%

D

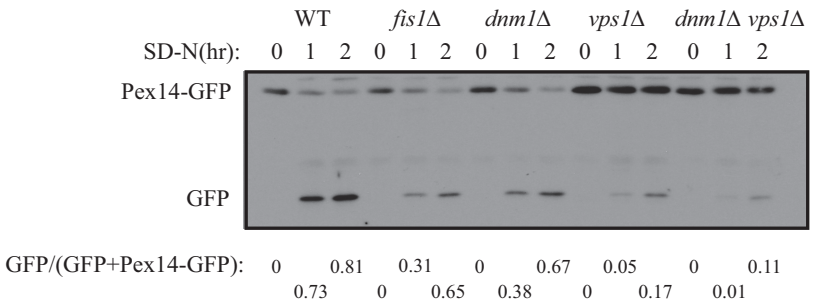

Figure 2.1 Peroxisomal fission is required for pexophagy. (A) Wild-type yeast cells, transformed with pBFP-SKL (XLY049), were cultured in YTO as described in Materials

and Methods to induce peroxisome proliferation, and shifted to SD-N for 2 h. (B) Wild-type (SEY6210), *atg1*Δ (WHY1), *dnm1*Δ (KDM1252), *fis1*Δ (XLY060), *vps1*Δ (XLY061), and *dnm1*Δ *vps1*Δ (XLY062) cells, transformed with pGFP-SKL, were cultured in YTO to induce peroxisome proliferation and shifted to SD-N for 7 h. CellTracker Blue CMAC was used to stain the vacuolar lumen. (C) Quantification of the numbers of peroxisomes in (B). 12 Z-section images were projected and the number of peroxisomes per cell was determined. Standard deviation was calculated from 3 independent experiments. In (A) and (C), all of the images are representative pictures from single Z-sections. DIC, differential interference contrast. Scale bar, 2 μm. (D) GFP was tagged at the C terminus of *PEX14* gene on the genome of wild-type (TKYM67), *dnm1*Δ (KDM1103), *fis1*Δ (KDM1104), *vps1*Δ (KDM1105), and *dnm1*Δ *vps1*Δ (XLY059) cells. These cells were cultured in YTO to induce peroxisome proliferation and shifted to SD-N for 1 and 2 h. Immunoblotting was done with anti-YFP antibody. Pexophagy level was estimated by calculating the amount of free GFP compared to the total amount of intact Pex14-GFP and free GFP.

A

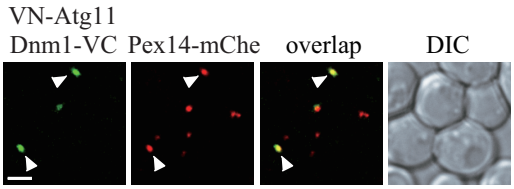

B

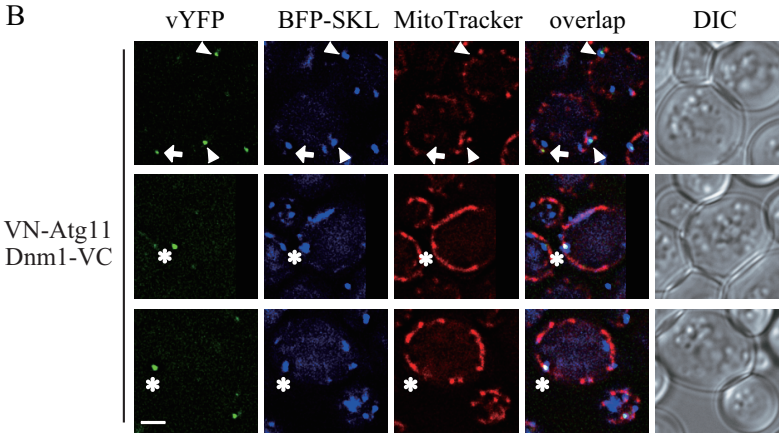

C

	cytosol	mitochondria	pero adjacent to mito	pero not adjacent to mito	pero and mito
VN-Atg11 Dnm1-VC	2.30±0.76%	16.67±1.28%	51.28±10.26%	1.80±0.26%	26.67±6.67%

D

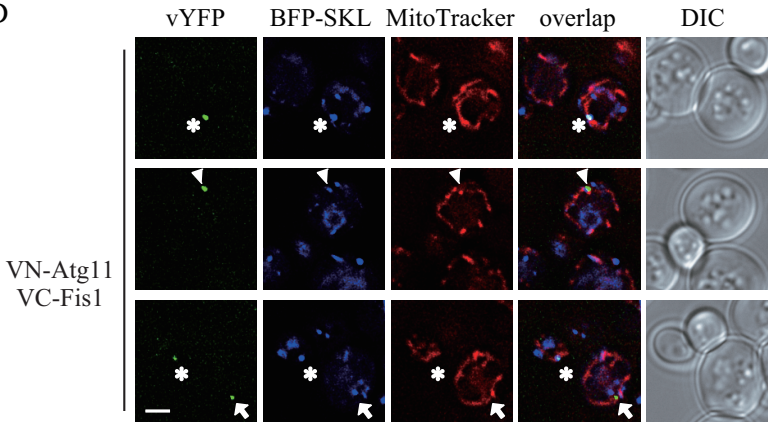

E

	cytosol	mitochondria	pero adjacent to mito	pero not adjacent to mito	pero and mito
VN-Atg11 VC-Fis1	6.78±1.02%	24.62±0.54%	38.98±9.16%	4.02±1.39%	25.61±6.21%

Figure 2.2. Atg11 recruits the Dnm1 fission complex to peroxisomes. (A) *VN-ATG11 PEX14-mCherry* (Pex14-mChe; XLY070) cells, transformed with pDnm1-VC, were cultured in YTO to induce peroxisome proliferation and then shifted to SD-N for 1 h. The

arrowheads mark colocalizing BiFC and mCherry puncta. (B, D) The plasmids pBFP-SKL and pDnm1-VC were transformed into the *VN-ATG11* (KDM1535) cells used in (B). pBFP-SKL was transformed into *VN-ATG11 VC-FIS1* (KDM1545) cells in (D). The arrows mark BIFC puncta colocalizing with MitoTracker Red; arrowheads denote BiFC puncta colocalizing with peroxisomes that are proximal to mitochondria; asterisks indicate BiFC puncta colocalizing with both peroxisomes and mitochondria. Cells were cultured as described in the Materials and Methods to induce peroxisome proliferation and shifted to SD-N for 1 h. MitoTracker Red was used to stain mitochondria. (C, E) Quantification of the localization of Atg11-Dnm1 interacting puncta in (B) and Atg11-Fis1 interacting puncta in (D); percentage was calculated based on the number of puncta at a specific location compared to the total number of puncta. In (A), (B) and (D), all of the images are representative pictures from single Z-sections. DIC, differential interference contrast. Scale bar, 2 μm.

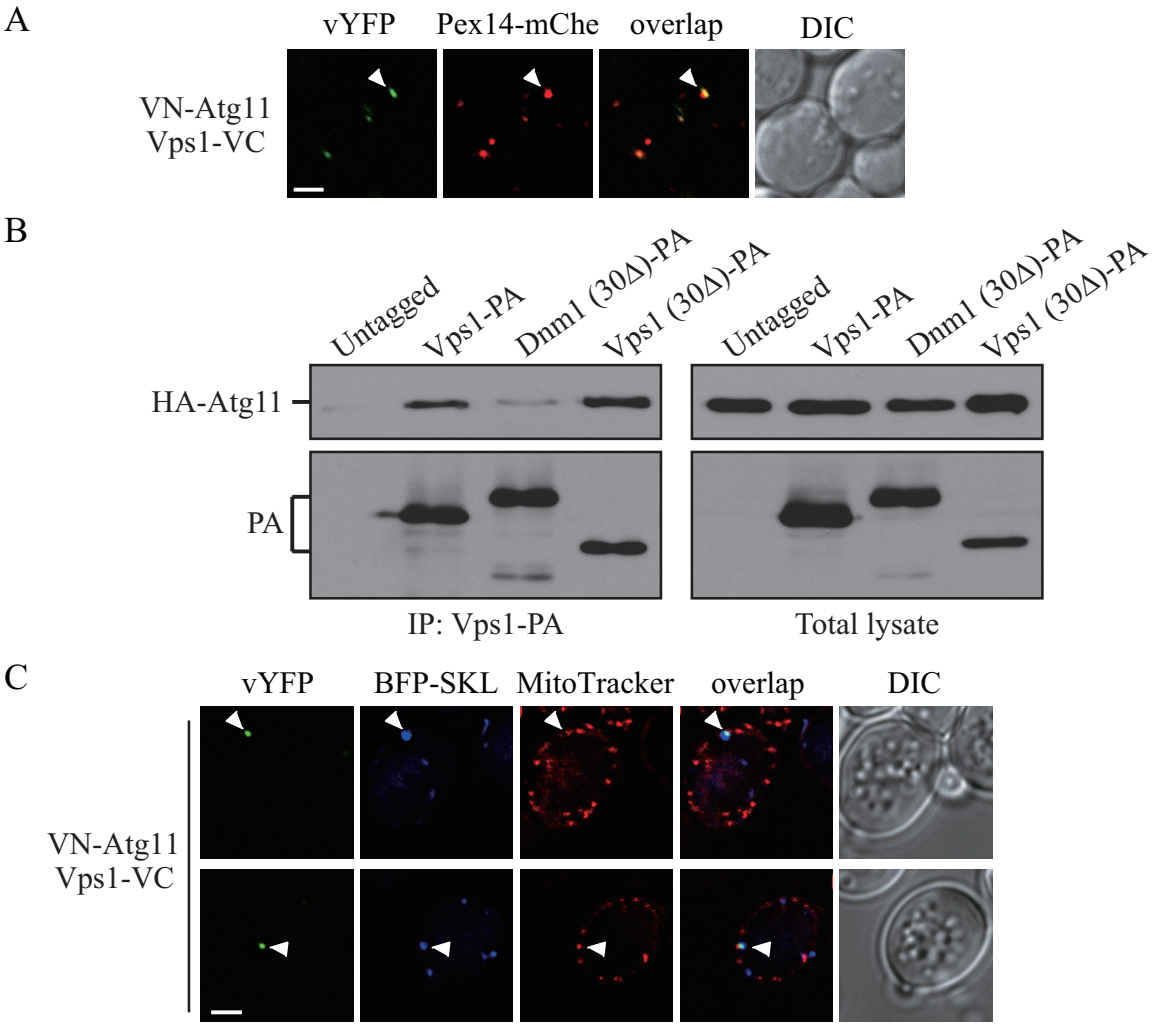

D

	cytosol	pero adjacent to mito	pero not adjacent to mito
VN-Atg11 Vps1-VC	25.36±3.84%	61.90±3.18%	12.74±0.66%

Figure 2.3. Atg11 recruits Vps1 to peroxisomes that are targeted for degradation. (A) *VN-ATG11 PEX14-mCherry* (Pex14-mChe; XLY070) cells, transformed with pVps1-VC, were cultured in YTO to induce peroxisome proliferation and subsequently shifted to SD-N for 1 h. (B) The plasmid pCuHA-Atg11 was transformed into *atg11*Δ (YTS147), *atg11*Δ *VPS1-PA* (KDM1269), *atg11*Δ *DNM1(C30*Δ*)* (KDM1249) cells, and *atg11*Δ *VPS1(C30*Δ*)* (XLY073). Cells were cultured in YTO to induce peroxisome proliferation and then shifted to SD-N for 2 h. Cell lysates were prepared and incubated with IgG-Sepharose for affinity isolation. The eluted proteins were separated by SDS-PAGE

and detected with monoclonal anti-HA antibody and an antibody that binds to PA. (C) The plasmids pBFP-SKL and pVps1-VC were transformed into *VN-ATG11* (KDM1535) cells. Cells were cultured in YTO to induce peroxisome proliferation and then shifted to SD-N for 1 h. MitoTracker Red was used to stain mitochondria. (D) Quantification of the localization of Atg11-Vps1 interacting puncta in (C); percentage was calculated based on the number of puncta at a specific location compared to the total number of puncta. In (A) and (C) all of the images are representative pictures from single Z-sections. DIC, differential interference contrast. Scale bar, 2 μm.

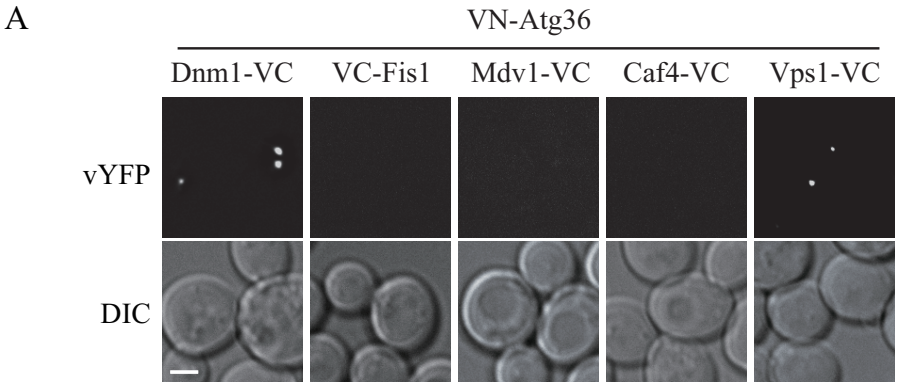

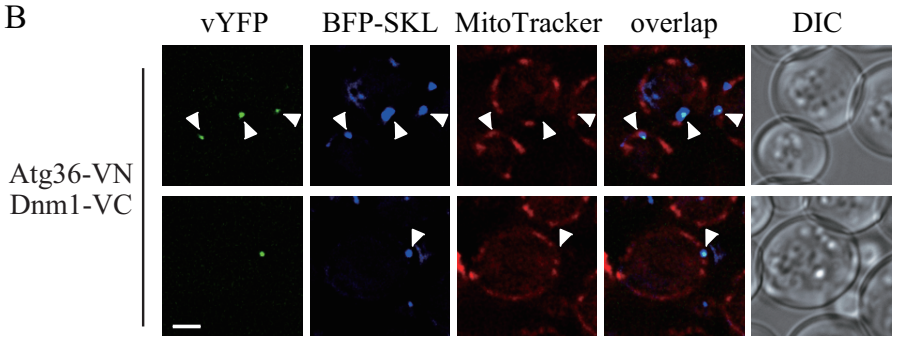

C

	cytosol	pero adjacent to mito	pero not adjacent to mito
Atg36-VN Dnm1-VC	4.83±0.62%	75.96±4.23%	19.22±4.85%

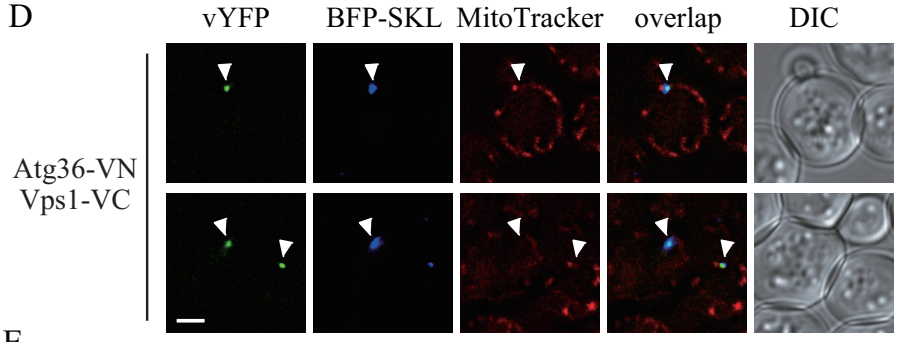

E

	cytosol	pero adjacent to mito	pero not adjacent to mito
Atg36-VN Vps1-VC	6.43±1.49%	86.77±3.50%	6.80±2.01%

Figure 2.4. Atg36 interacts with both Dnm1 and Vps1 on the degrading peroxisomes. (A) The plasmid pDnm1-VC or pVps1-VC was transformed into *VN-ATG36* (XLY063) cells. These cells together with cells from strains *VN-ATG36 VC-FIS1* (XLY064),

VN-ATG36 CAF4-VC (XLY065), and *VN-ATG36 MDV1-VC* (XLY066) were cultured in YTO to induce peroxisome proliferation and then shifted to SD-N for 1 h. (B, D) The plasmid pBFP-SKL and pDnm1-VC were transformed into *VN-ATG36* (XLY063) cells in (B), and pBFP-SKL and pVps1-VC were transformed into *VN-ATG36* (XLY063) cells in (D). Cells were cultured in YTO to induce peroxisome proliferation and then shifted to SD-N for 1 h. MitoTracker Red was used to stain mitochondria. (C, E) Quantification of the localization of Atg36-Dnm1 interacting puncta in (B) and Atg36-Vps1 interacting puncta in (D); percentage was calculated based on the number of puncta at a specific location compared to the total number of puncta. In (A), (B), and (D), all of the images are representative pictures from single Z-sections. DIC, differential interference contrast. Scale bar, 2 μm.

A

BD / AD	-	Atg36	Atg36 S31A	Atg36 S97A
-	-	-	-	-
Dnm1	-	+	+	+
Vps1	-	+	+	+

B

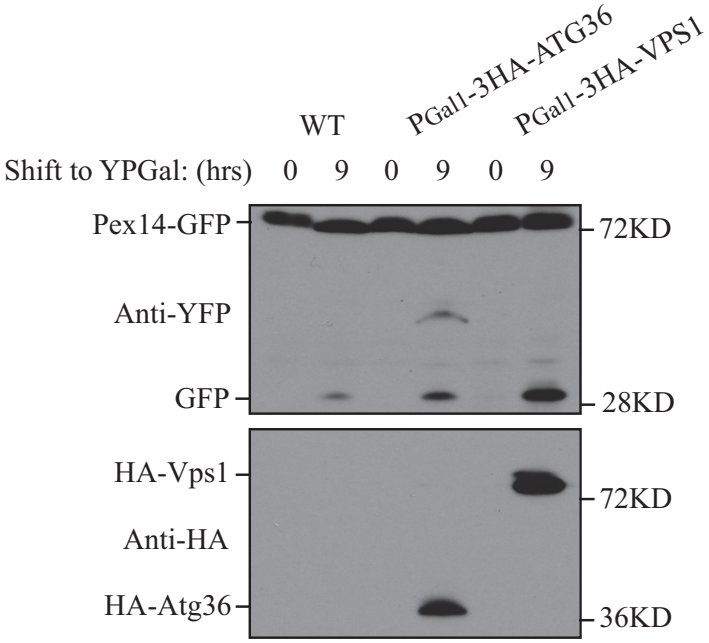

C

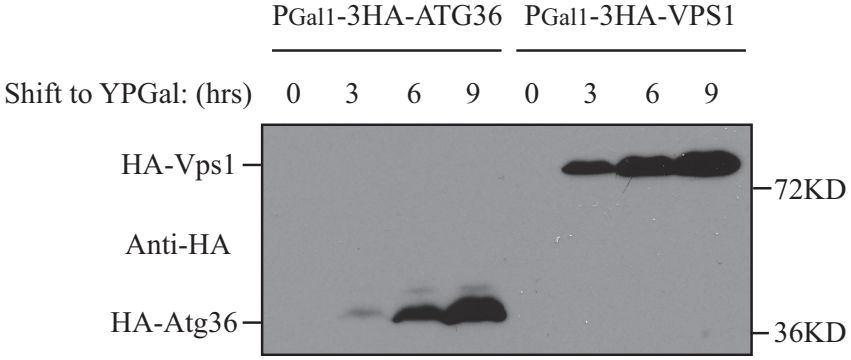

Figure 2.5. Overexpression of Vps1 induced pexophagy. (A) Yeast two hybrid analysis of Atg36 mutants interacting with Dnm1 and Vps1. (B, C) GFP was tagged at the C terminus of *PEX14* gene on the genome of wild-type (TKYM67), *GAL1p-3HA-ATG36* (XLY088), and *GAL1p-3HA-VPS1* (XLY089) cells. These cells were cultured in YTO to

induce peroxisome proliferation and shifted to YPG for 3h, 6h, and 9h. Immunoblotting was done with anti-YFP antibody in (B), and with anti-HA antibody in (C).

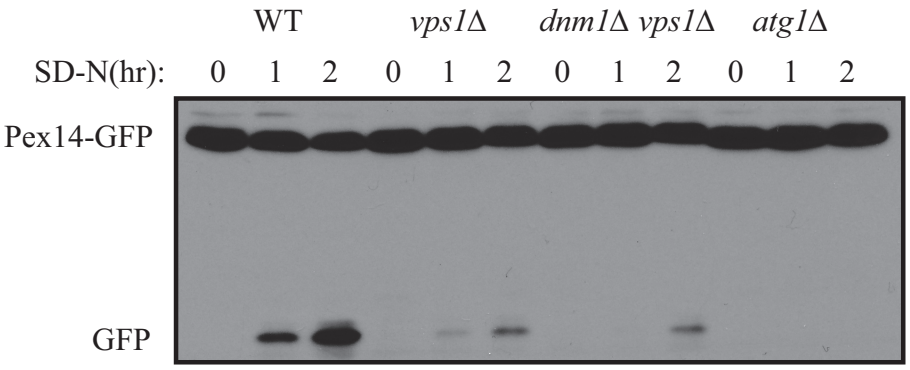

Figure 2.S1. Peroxisomal fission is required for pexophagy.

GFP was tagged at the C terminus of PEX14 gene on the genome of wild-type (TKYM67), vps1Δ (KDM1105), dnm1Δ vps1Δ (XLY059), and *atg1*Δ (TKYM72) cells. These cells were cultured in YTO to induce peroxisome proliferation and shifted to SD-N for 1 and 2 h. Immunoblotting was done with anti-YFP antibody.

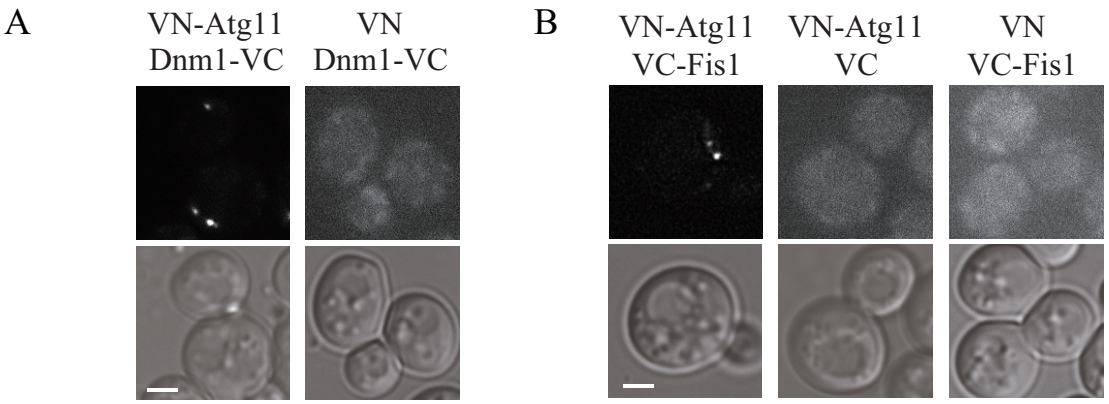

Figure 2.S2. Atg11 recruits the Dnm1 fission complex to peroxisomes. pDnm1-VC was transformed into *VN-ATG11* (KDM1535) and *VN* (XLY085) control cells in (A). These cells together with *VN-ATG11 VC-FIS1* (KDM1545), *VN-ATG11 VC* (XLY087) control, and *VN VC-FIS1* (XLY086) control cells in (B) were cultured in YTO to induce peroxisome proliferation and then shifted to SD-N for 1 h. All of the images are representative pictures from single Z-sections. DIC, differential interference contrast. Scale bar, 2 μm.

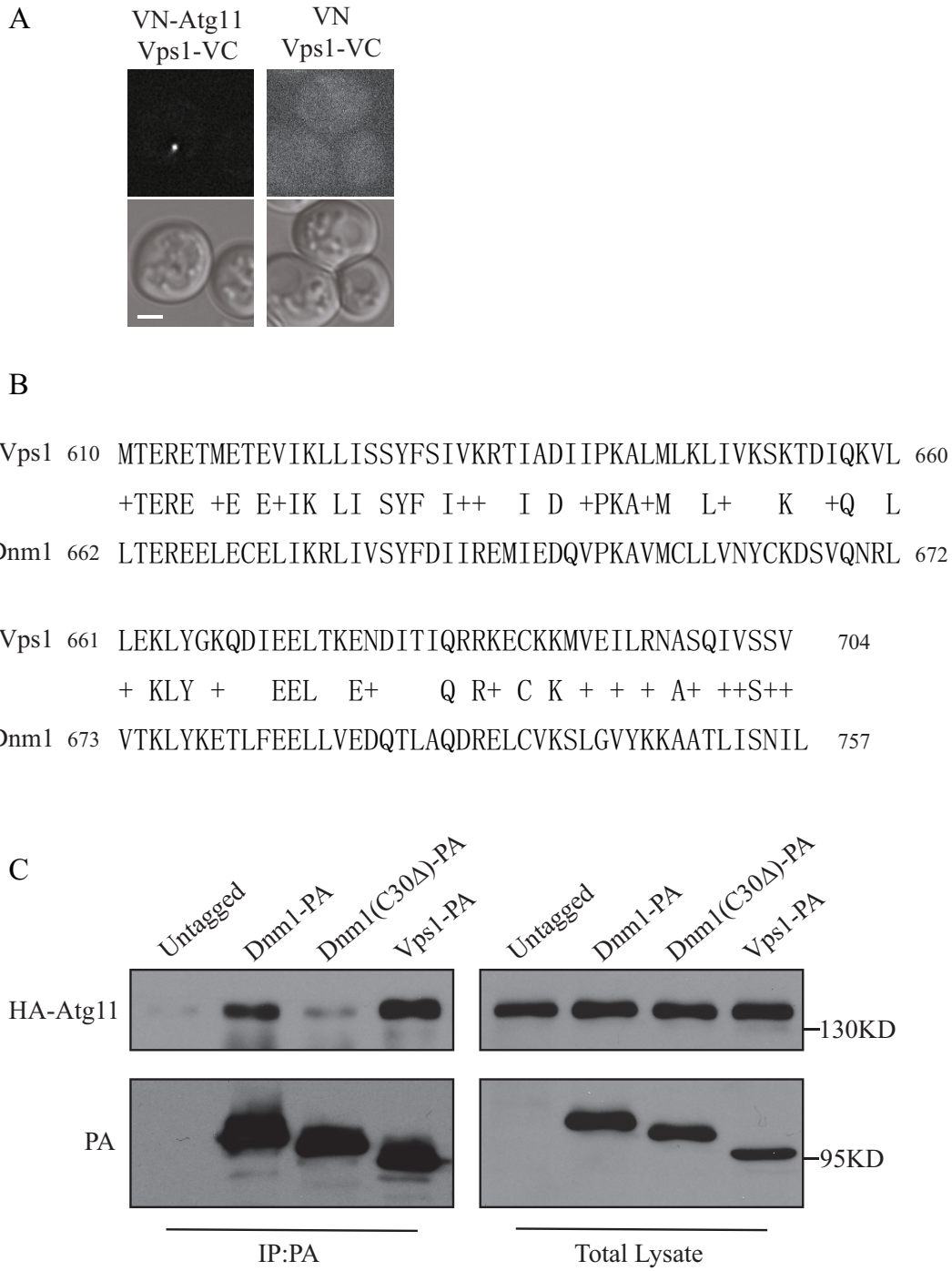

Figure 2.S3. Atg11 recruits Vps1 to peroxisomes that are targeted for degradation. (A) pDnm1-VC was transformed into *VN-ATG11* (KDM1535) and *VN* (XLY085) control cells. These cells were cultured in YTO to induce peroxisome proliferation and subsequently shifted to SD-N for 1 h. All of the images are representative pictures from single Z-sections. DIC, differential interference contrast. Scale bar, 2 μm. (B) Alignment of the C-terminus of Vps1 and Dnm1. (C) The plasmid pCuHA-Atg11 was transformed into *atg11*Δ (YTS147), *atg11*Δ *DNM1-PA* (KDM1247), *atg11*Δ *DNM1(C30*Δ*)*

(KDM1249), and *atg11*Δ *VPS1-PA* (KDM1269) cells. Cells were cultured in YTO to induce peroxisome proliferation and then shifted to SD-N for 2 h. Cell lysates were prepared and incubated with IgG-Sepharose for affinity isolation. The eluted proteins were separated by SDS-PAGE and detected with monoclonal anti-HA antibody and an antibody that binds to PA.

CHAPTER 3. The Atg17-Atg31-Atg29 complex coordinates with Atg11 to recruit the Vam7 SNARE and mediate autophagosome-vacuole fusion[3]

3.1 Abstract

Macroautophagy (hereafter autophagy) is an evolutionarily conserved process in which portions of the cytoplasm are engulfed, degraded and subsequently recycled. The Atg17-Atg31-Atg29 complex translocates to the phagophore assembly site (PAS), where an autophagosome forms, at a very early stage of autophagy, playing a vital role in autophagy induction. Here, we identified a novel role of this complex in a late stage of autophagy where it coordinates with Atg11 to regulate autophagy-specific fusion with the vacuole. Atg17 and Atg11 interact with the vacuolar SNARE (soluble N-ethylmaleimide-sensitive factor attachment protein receptor) Vam7 independent of each other. Several hydrophobic residues in helix 1 and helix 4 of Atg17 and the SNARE domain of Vam7 mediate the Atg17-Vam7 interaction. An F317D mutation of Atg17, which diminished its interaction with Vam7 without affecting its interaction with Atg13 or Atg31, leads to a defect in the fusion of autophagosomes with the vacuole and

[3] This chapter is reprinted from Liu X*, Mao K*, Yu AY, Omairi-Nasser A, Austin J II, Glick BS, Yip CK and Klionsky DJ. (2016) The Atg17-Atg31-Atg29 Complex Coordinates with Atg11 to Recruit the Vam7 SNARE and Mediate Autophagosome-Vacuole Fusion. *Current Biology* 26(2):150-160 (doi.org/10.1016/j.cub.2015.11.054).

decreased autophagy activity. These results provide the first demonstration that the Atg17-Atg31-Atg29 complex functions in both early and late stages of autophagy, and provides a mechanistic explanation for the coordination of autophagosome completion and fusion with the vacuole.

3.2 Introduction

Macroautophagy (hereafter autophagy) is a highly controlled cellular pathway where numerous cargoes including protein aggregates, superfluous or damaged organelles and invading pathogens are targeted to the vacuole, or the analogous organelle in higher eukaryotes, the lysosome, for degradation [1-4]. In yeast, during autophagy an initial double-membrane structure named the phagophore is formed at the PAS. The phagophore engulfs its cargoes sequentially, while expanding through lipid addition. Following closure of the phagophore, the de novo formed autophagosome fuses with the vacuole. The cargoes together with the inner membrane of the autophagosome are degraded in the lumen before they are eventually recycled. Autophagy has many physiological roles, whereas autophagic dysfunction is associated with many pathologies, including cancer, diabetes, and certain types of neurodegenerative disease [5-7].

Following the induction of autophagy, Atg17 is among the very first Atg proteins that translocate to the PAS [8, 9]. Atg17 forms a stable ternary complex with Atg31 and Atg29, with Atg31 positioned as the bridge between the other two proteins [10]. The Atg17-Atg31-Atg29 complex is indispensible for autophagy induction. First, this

complex recruits other Atg proteins, including Atg1and Atg13, to the PAS [11, 12]. Second, structural data indicate that this complex forms a dimer with two crescents [12, 13]; this curved structure might enable the complex together with Atg1 and Atg13 to tether Atg9-containing vesicles, which may be membrane sources for autophagosome formation, positioning them for fusion into the expanding phagophore.

After formation of a complete autophagosome, the double-membrane vesicle fuses with the vacuole. In yeast, previous studies have indicated that the fusion machinery for other targeting pathways that terminate at the vacuole is also required for autophagosome-vacuole fusion, including the Rab GTPase Ypt7, its guanine nucleotide exchange factor Mon1-Ccz1, and SNARE (soluble N-ethylmaleimide-sensitive factor attachment protein receptor) proteins [14-20]. Similarly, the homotypic fusion and protein sorting (HOPS) tethering complex, RAB7 and SNARE proteins also have a role in mammalian autophagy [21-27]. However, those studies in yeast were carried out in strains where the corresponding genes were deleted. As a result, all fusion events at the vacuole, not only autophagosome-vacuole fusion, were affected. Accordingly, those data have not provided specific information on the regulation of autophagosome-vacuole fusion. Here we found that the Atg17-Atg29-Atg31complex coordinates with Atg11 to recruit the SNARE protein Vam7 to the PAS when autophagy is induced. Impaired recruitment of Vam7 resulted in a defect in autophagosome-vacuole fusion and diminished autophagy flux. The results demonstrate that distinct molecular machinery is employed for regulating autophagy-vacuole fusion. Moreover, these data reveal a role of

the Atg17-Atg29-Atg31complex at a late stage of autophagy.

3.3 Results

3.3.1 The Atg17-Atg31-Atg29 Complex Interacts with the Vam7 SNARE Protein at the PAS

The Atg17-Atg31-Atg29 complex is a scaffold that is vital for PAS organization during autophagy induction. In a genome-wide study of protein-protein interaction via the yeast two-hybrid (Y2H) assay, Atg17 was found to bind Vam7, a vacuolar SNARE protein [28]. This interaction appears counterintuitive because the Atg17-Atg31-Atg29 complex was thought to only act at a very early stage of autophagy, whereas Vam7 is required for autophagosome fusion with the vacuole, a relatively late stage of the process. Therefore, we wanted to determine whether this interaction was valid and might reveal a novel role of the Atg17-Atg31-Atg29 complex in regulating autophagy.

First, we confirmed the previous result, interaction between Atg17 and Vam7, using the Y2H assay with the wild-type Y2H strain PJ69-4A (data not shown). Although it is a useful system, in the Y2H assay proteins are typically overexpressed and artificially directed to the nucleus. Therefore, to further validate the Atg17-Vam7 interaction, we utilized another assay, bimolecular fluorescence complementation (BiFC) [29]. In this assay, the Venus yellow fluorescent protein (vYFP) is split into two fragments, VN (N terminus of vYFP) and VC (C terminus of vYFP), and these are separately tagged to two proteins of interest. If the two proteins are able to interact, VN and VC will be brought

into proximity with each other and are essentially able to reform the native three-dimensional structure of vYFP and emit a fluorescent signal.

We tested the interactions between VC-Vam7 and the respective Atg(17, 29, or 31)-VN fusion proteins. None of the three pairs produced a detectable signal under growing conditions (YPD medium, "+"). In contrast, a substantial percentage of Atg17-VN VC-Vam7 and Atg29-VN VC-Vam7, but not Atg31-VN VC-Vam7, cells displayed a vYFP signal under starvation conditions (SD-N medium, "-N") (Figure 3.1A). As controls, we examined *Atg17-VN VC*, *Atg29-VN VC* and *Atg31-VN VC* cells, where only the VC peptide was expressed. None of the cells expressing these combinations showed a vYFP signal even under starvation conditions (Figure 3.S1A). In addition, similar to Vam7, the Vam3 protein is a vacuolar SNARE that is needed for the fusion of autophagosomes with the vacuole. As an additional control for the specificity of the Atg17-Vam7 interaction we examined whether any of the components of the Atg17-Atg31-Atg29 complex showed an interaction with Vam3 via the BiFC assay, however, in all cases the results were negative (Figure 3.S1B and data not shown).

Next, we wanted to determine where the interaction between the ternary complex and Vam7 occurs. Under starvation conditions, approximately 60% of the Atg17-Vam7 puncta (i.e., a vYFP signal) colocalized with CFP-Atg8, a PAS marker (Figure 3.1B). These colocalized puncta were located next to the vacuole, suggesting that the Atg17-Atg31-Atg29 complex recruits Vam7 to the PAS in autophagy-inducing conditions.

3.3.2 The Atg17-Atg31-Atg29 Complex Recruits Cytosolic Vam7 to the PAS at an Early Stage of Autophagy

The next question we addressed was to examine when the Atg17-Atg31-Atg29 complex recruits Vam7 to the PAS. In particular, we wanted to determine whether this recruitment occurs at an early stage of autophagy when the ternary complex itself translocates to the PAS or only after autophagosome completion, as is the case with the mammalian protein STX17 that is recruited to completed autophagosomes to allow fusion with the lysosome [26]. To answer this question, we deleted *ATG1* or *ATG9* in the *ATG17-VN VC-VAM7* strain. In *atg1*Δ or *atg9*Δ strains, autophagy can be initiated, but complete autophagosomes cannot be formed. A vYFP signal was still observed in the null strains after nitrogen starvation, indicating that the Atg17-Atg31-Atg29 complex is able to recruit Vam7 to the PAS at an early stage of autophagy (Figure 3.2A). Noticeably, the percentage of cells showing vYFP puncta was significantly higher in the *atg1*Δ and *atg9*Δ strains compared to the wild-type (WT) strain (Figure 3.2B). This higher level of Atg17-VN-VC-Vam7 puncta likely reflects the block in autophagy and the accumulation of autophagy-related proteins at the PAS.

There are two pools of cellular Vam7; one of these pools is cytosolic, and the other is associated with the vacuolar membrane through its phox homology (PX) domain, which binds phosphatidylinositol-3-phosphate (PtdIns3P) [30]. We constructed a strain with

VC- Vam7$^{\Delta PX}$ and Atg17-VN to determine whether membrane binding was required for the Atg17-Vam7 interaction. The truncated VC- Vam7$^{\Delta PX}$ protein was as stable as the WT protein (Figure 3.2C), but a previous study demonstrated that Vam7$^{\Delta PX}$ localizes only in the cytosol [30]. To verify the localization of the Vam7 construct lacking the PX domain we compared the phenotype of Vam7-GFP to Vam7$^{\Delta PX}$-GFP. In contrast to the punctate and vacuolar membrane distribution seen with Vam7-GFP, the Vam7$^{\Delta PX}$-GFP chimera was distributed diffusely in the cytosol (Figure 3.S2A). In addition, we examined the subcellular distribution of the proteins by fractionation. VC-Vam7 was located primarily in the vacuole membrane-enriched P13 fraction, in addition to a cytosolic pool, whereas VC-Vam7$^{\Delta PX}$ was recovered entirely in the cytosolic supernatant fraction (Figure 3.S2B). Despite its strictly cytosolic localization, under starvation conditions, we were still able to observe a vYFP signal corresponding to Atg17-VN-VC-Vam7$^{\Delta PX}$ (Figure 3.2D and 3.2E). Moreover, these BiFC dots showed good colocalization with CFP-Atg8, implying that the Atg17-Atg31-Atg29 complex recruits cytosolic Vam7 to the PAS (Figure 3.2D). Nonetheless, we cannot rule out the possibility that this complex is also able to recruit membrane-associated Vam7 to the PAS.

Even though the PX domain of Vam7 was not required for the interaction with Atg17, we wondered whether it was necessary for normal autophagy activity. Based on a well established quantitative autophagy assay, the Pho8Δ60 assay [31-33], cells expressing VC-Vam7$^{\Delta PX}$ showed almost a complete block in autophagy, while the activity of VC-Vam7 cells was comparable to wild-type cells (Figure 3.S2C). This

finding suggests that the PX domain of Vam7 plays some other indispensible role(s) in autophagy.

3.3.3 Atg17 Directly Interacts with the SNARE Domain of Vam7

In order to examine the functional consequences of disrupting the interaction between the Atg17-Atg31-Atg29 complex and Vam7, we first asked which component(s) in the ternary complex mediates the interaction. In the BiFC assay, both Atg17-VN-VC-Vam7 and Atg29-VN-VC-Vam7 cells showed a vYFP signal (Figure 3.1A). To determine if one or both of these interactions was direct, we deleted *ATG31* in both strains because this protein connects Atg17 with Atg29 in the complex. We found that the Atg17-VN-VC-Vam7 cells still produced BiFC dots in the absence of Atg31, and these dots colocalized with CFP-Atg8 under starvation conditions (Figure 3.3A and 3.3B). In contrast, an Atg29-VN-VC-Vam7 signal was no longer detected after deletion of *ATG31* (Figure 3.3C and 3.3D).

We have previously constructed a multiple-knockout (MKO) Y2H strain, in which most of the known *ATG* genes are deleted, including *ATG29* and *ATG31* [10]. In this MKO Y2H strain we found that cells with AD-Atg17 and BD-Vam7 still showed robust growth on selection plates, suggesting that the interaction between Atg17 and Vam7 was independent of most other Atg proteins (Figure 3.3E). As expected, Atg29 was not able to bind Vam7 in the MKO Y2H strain, in agreement with our results using the wild-type Y2H strain (data not shown).

Next, we decided to map the Vam7 domain that is required for binding Atg17. Vam7 consists of the N-terminal PX domain, an intermediate region and a C-terminal SNARE domain [30, 34]. We constructed a set of BD-Vam7 constructs that contain various domains of the Vam7 protein (Figure 3.3F). Only cells with AD-Atg17 and BD-Vam7$^{241\text{-}316}$, which contains only the SNARE domain, showed stronger growth on selective plates than the control. In agreement with this result, BD-Vam7$^{\Delta 245\text{-}303}$, in which only the SNARE domain was deleted, was not able to interact with AD-Atg17 (Figure 3.3F). These results suggest that the SNARE domain of Vam7 is necessary and sufficient for interaction with Atg17.

To further validate our findings that Vam7 binds Atg17 and that the SNARE domain mediates this interaction, we carried out an *in vitro* affinity isolation analysis. *Escherichia coli* cells were transformed with plasmids expressing Atg17-hexahistidine (6xHis) and glutathione S-transferase (GST) alone or as a GST-Vam7 SNARE domain chimera (GST-SNARE). Cell lysates were loaded onto glutathione resin and after extensive washing the proteins were eluted and analyzed by western blot. GST-SNARE, but not GST alone, was able to affinity isolate Atg17-6xHis (Figure 3.3G). Based on these results, we conclude that Atg17 directly interacts with the SNARE domain of Vam7.

3.3.4 Hydrophobic Residues in Helix 1 and Helix 4 of Atg17 Mediate its Interaction with Vam7

We could not block the interaction between Atg17 and Vam7 by deleting the SNARE

domain without affecting all fusion events at the vacuole. Thus, in order to determine the function of the recruitment of Vam7 by Atg17 we needed to turn instead to Atg17. Deletion of *ATG17* blocks autophagy at a very early stage, which would obscure a potential role for Atg17 in regulating autophagosome-vacuole fusion. Accordingly, we needed to identify an Atg17 mutant that specifically affects the Atg17-Vam7 interaction without disrupting its interaction with Atg31-Atg29 or Atg13-Atg1. The crystal structure of a partial Atg17-Atg31-Atg29 complex has been resolved, indicating the presence of four highly organized α-helices in Atg17 [13]. To map the domains required for interaction with Vam7, a set of AD-Atg17 deletion mutants were constructed (Figure 3.4A and 3.S3A). Atg17 deletion mutants that lack part of helix 1 (92-106) or helix 4 (296-312, or 313-334) showed diminished interaction with Vam7 by the Y2H assay (Figure 3.4A and 3.S3A).

Because we had shown that the SNARE domain of Vam7, which is also in a helix structure, mediates its interaction with Atg17, we hypothesized that the binding between Atg17 and Vam7 is due to a "helix-helix" interaction, which is usually mediated by hydrophobic residues from both sides of the interacting helices. Based on an alignment of yeast Atg17 homologs, we chose the conserved hydrophobic residues from 92-106 and 296-334, namely I98, L105, I310, L313, I314, F317, I325 and L331, for further analysis (Figure 3.S3B).

We mutated these residues to charged hydrophilic residues by site directed mutagenesis and tested their interaction with Vam7 by the Y2H assay. Among the

mutants that we tested, Atg17^{L105D}, Atg17^{F317D} and Atg17^{I325D} showed diminished interaction with Vam7 (Figure 3.4B). As a control, we tested the stability of these mutants compared to the WT protein. The GFP-Atg17^{L313K,I314D}, GFP-Atg17^{L105D} and GFP-Atg17^{F317D} mutants were somewhat less stable than the GFP-Atg17^{WT} protein (Figure 3.S3C). However, because the AD-Atg17^{L313K,I314D} mutant still showed a strong interaction with BD-Vam7 (Figure 3.4B), the impaired interaction with Vam7 seen with the Atg17^{L105D}, Atg17^{F317D} and Atg17^{I325D} mutants was unlikely to be due to a lower level of the mutant proteins.

To confirm the results seen with the Y2H assay, we analyzed the three mutants by the BiFC assay. The percentage of cells showing a vYFP signal after nitrogen starvation in the Atg17-VN strains with L105D, F317D or I325D mutated was substantially decreased (Figure 3.4C, D).

Next, we determined whether these mutations affected other known interactions of Atg17. Because Atg1 and Atg29 interact with Atg17 through Atg13 and Atg31, respectively, we tested the Atg17 point mutants for interaction with Atg13 and Atg31 by the Y2H assay. The Atg17^{F317D} mutant showed an essentially normal interaction with both Atg13 and Atg31, while Atg17^{L105D} and Atg17^{I325D} were particularly defective in interactions with Atg13 and Atg31, respectively (Figure 3.4E).

Because the Atg17^{F317D} mutant was the only one that showed diminished interaction with Vam7 without substantially affecting its binding affinity to Atg13 and Atg31, we decided to focus our analysis on this mutant. First, the defective interaction of the mutant

with Vam7 was further demonstrated by an *in vitro* affinity isolation assay. Although the GST-Vam7 SNARE domain chimera was able to affinity isolate Atg17-6xHis (Figure 3.3G), it was not able to efficiently pull down Atg17^{F317D}-6xHis (Figure 3.4F,G). We also examined whether the F317D mutation affects the efficiency of Atg17 movement to the PAS. During nitrogen starvation GFP- Atg17^{F317D} displayed significant colocalization with RFP-Ape1 (a PAS marker), at a frequency similar to the wild-type protein (Figure 3.S3D).

As the next part of the analysis we asked whether the Atg17^{F317D} mutant was competent for autophagy based on the Pho8Δ60 assay. Contrary to our expectations, the mutant Atg17^{F317D} did not affect the autophagy activity compared to the wild-type protein. The Atg17^{L105D} mutant showed almost a complete block of autophagy, while the Atg17^{I325D} mutant displayed an approximately 50% decrease in activity (Figure 3.4H). With either of the latter two mutants, however, we were not able to exclude the possibility that the defects in interaction with Atg13 or Atg31, rather than Vam7, led to the autophagy defects.

One possible explanation for the lack of an autophagy phenotype with the Atg17^{F317D} mutant is that the defect in the interaction with Vam7 is not severe enough to cause a detectable block in autophagy activity. We found that cells expressing AD-Atg17^{F317D} and BD-Vam7 still grew quite well on plates lacking histidine (a less stringent selection condition), although they were not able to grow on plates without adenine (a harsher selection condition) (Figure 3.4B). In this case, the residual binding affinity may be

adequate for autophagy to occur at a nearly wild-type level. A second possibility is that another protein might play a partially redundant role in recruiting Vam7 to the PAS, so that the autophagy activity defect from the Atg17^{F317D} mutant was complemented.

We tested the first possibility by isolating mutants that display more severe defects in the interaction between Vam7 than Atg17^{F317D}. Substitutions of glycine, histidine, lysine or glutamine for Phe317, however, did not show a stronger block in binding (Figure 3.S3E). Next, we made some double mutants including Atg17^{F317D,I325A}, Atg17^{F317D,I325G}, and Atg17^{F317G,I325G}. Unfortunately, although these double mutants displayed a stronger defect in binding Vam7, they also had blocks in their interaction with either Atg13 or Atg31 (Figure 3.S3F and 3.S3G, and data not shown), preventing us from excluding the possibility that the F317D mutation caused only a weak phenotype.

3.3.5 Atg11 Recruits Vam7 to the PAS Independent of the Atg17-Atg31-Atg29 Complex

Next, we tested the second possibility by looking at an Atg protein that may have a similar role in recruiting Vam7 as that proposed for Atg17. In this regard, Atg11 stands out for three reasons. First, Atg11 is predicted to have four major α-helical coiled-coil (CC) domains, similar to Atg17, which would allow it to engage in "helix-helix" interactions with Vam7. Second, like Atg17, Atg11 plays a role in formation and organization of the PAS [12, 35]. Third, the *atg17*Δ strain is able to generate a small number of autophagic bodies under starvation conditions, whereas an *atg11*Δ *atg17*Δ

double mutant displays an essentially complete block in autophagy [35].

To assess this possibility, a Y2H assay was conducted in the MKO strain background to examine whether Atg11 could bind directly to Vam7. Cells with AD-Atg11 and BD-Vam7, but not control cells, grew on plates lacking histidine, suggesting a potential direct Atg11-Vam7 interaction (Figure 3.5A). However, the observation that they cannot grow on plates without adenine (data not shown) indicates that the Atg11-Vam7 interaction is weaker than that of Atg17-Vam7. Next, we tested Atg11 mutants that lack each of the four predicted coiled-coil domains to determine which region of Atg11 is involved in mediating the interaction. AD-Vam7 was still able to show binding affinity to AD-Atg11$^{\Delta 272\text{-}321}$ (ΔCC1) and AD-Atg11$^{\Delta 627\text{-}858}$ (ΔCC3), but not toward AD-Atg11$^{\Delta 536\text{-}576}$ (ΔCC2) or AD-Atg11$^{\Delta 859\text{-}1178}$ (ΔCC4), suggesting that the latter two α-helical domains of the protein are required for the interaction (Figure 3.5A).

To further verify the interaction between Atg11 and Vam7, a BiFC assay was performed. In *ATG11-VN VC-VAM7* cells, where Atg11-VN was expressed at its endogenous level, we were not able to detect a vYFP signal (Figure 3.5B). In contrast, the vYFP signal was observed in more than 90% of *VN-ATG11 VC-VAM7* cells, in which Atg11 was tagged at its N terminus, and the VN-Atg11 chimera was overexpressed (Figure 3.5B). Although Atg11 can self-interact, the vYFP signal observed in these cells was not due to overexpression of VN-Atg11; cells expressing *VN-ATG11* and *VC* alone, where both VN-Atg11 and the VC peptide were overexpressed, did not display a vYFP signal (Figure 3.5B).

We next examined whether this interaction occurs at the PAS. Indeed, more than 70% of VN-Atg11-VC-Vam7 vYFP dots colocalized with CFP-Atg8 under starvation conditions (Figure 3.5C and 3.5D). Previous studies have shown that Atg11 interacts with the Atg17-Atg31-Atg29 complex through Atg29 [12]. Therefore, we decided to examine whether Atg11-dependent recruitment of Vam7 to the PAS requires the ternary complex. We deleted either *ATG17* or *ATG29* in the *VN-ATG11 VC-VAM7* strain and carried out a BiFC assay. Similar to the WT strain, significant colocalization of vYFP and CFP-Atg8 (~70%) was still observed in both strains (Figure 3.5C and 3.5D). These data suggest that Atg11 can recruit Vam7 to the PAS independent of the Atg17-Atg31-Atg29 complex.

3.3.6 Impaired Recruitment of Vam7 to the PAS Results in a Defect in Autophagosome-Vacuole Fusion

We next tested whether the Atg17^{F317D} mutant would display a defect in autophagy activity in the *atg11*Δ background. In the *atg11*Δ *atg17*Δ background, compared to wild-type Atg17, the Atg17^{F317D} mutant showed an approximate 30% decrease in autophagy acitivity (Figure 3.6A), in contrast to the essentially wild-type activity seen in the *atg17*Δ background (Figure 3.4H). Moreover, the Atg17^{I325D} mutant, which had approximately 50% of the wild-type activity in the *atg17*Δ strain background, displayed almost a complete block of autophagy in the *atg11*Δ *atg17*Δ background.

To determine whether the autophagy defect we observed with the Atg17^{F317D} mutant in the *atg11*Δ *atg17*Δ background was due to impaired autophagosome-vacuole fusion,

we performed a protease protection assay [36]. In brief, the propeptide of the cytosolic precursor form of the vacuolar hydrolase aminopeptidase I (prApe1) is sensitive to cleavage by exogenous proteases added to lysed yeast spheroplasts; once enclosed in an autophagosome, however, the propeptide is protected from digestion (Figure 3.6B). In the *vam7*Δ cells, as a result of a block in autophagosome-vacuole fusion, approximately half of the prApe1 was protected from exogenously added proteinase K (Figure 3.6C). In contrast, the prApe1 was completely sensitive to proteinase K treatment in the *atg11*Δ *atg17*Δ cells, where autophagosome formation is defective. Compared to cells with wild-type Atg17, in the *atg11*Δ *atg17*Δ cells expressing the $Atg17^{F317D}$ mutant, a small but consistent portion of the prApe1 pool was protected from proteinase K (Figure 3.6C and 3.6D).

Next, to validate our protease protection assay data, we investigated the autophaogosome structure of the $Atg17^{F317D}$ mutant by correlative light and electron microscopy, combining fluorescence microscopy and tomography. GFP-Atg8 was utilized as a PAS/autophagosome marker to correlate the fluorescence with autophagosomal structures observed by EM. In both the *atg17*Δ *vam7*Δ cells expressing the $Atg17^{WT}$ protein, and the *atg11*Δ *atg17*Δ cells expressing the $Atg17^{F317D}$ mutant, we were able to observe circular double-membrane structures correlated with the GFP fluorescence signal in the sections examined by transmission electron microscopy (TEM) tomography (Figure 3.6E), suggesting that the autophagosomes in the $Atg17^{F317D}$ mutant might be sealed. However, by TEM tomography the sections are 0.3 μm, which are not

of sufficient thickness to cover a complete autophaogosome. Accordingly, we further investigated the autophagosomes in the Atg17^{F317D} mutant, using scanning transmission electron microscopy (STEM) tomography, which covers thicker sections (up to 2 μm) [37]. By this method, we observed fully closed autophagosomes in the Atg17^{F317D} mutant (Figure 3.6E).

To further support the observation that autophagosome formation in the Atg17^{F317D} mutant was not defective, we transformed either the empty vector, or a plasmid expressing wild-type *ATG17* or the *ATG17 (F317D)* mutant into *atg11*Δ *atg17*Δ *vam7*Δ cells, where the *VAM7* deletion enhances the accumulation of completed autophagosomes. As expected, in those cells with the empty vector in which autophagosome formation was blocked, the prApe1 was completely sensitive to proteinase K treatment (Figure 3.S4). In contrast, in cells expressing the Atg17^{F317D} mutant, a substantial pool of the prApe1 was insensitive to proteinase K treatment, similar to that seen in cells with wild-type Atg17. Based on these results, we conclude that the autophagy defect seen with the Atg17^{F317D} mutant was due to defective autophagosome-vacoule fusion, but not autophagosome formation.

3.4 Discussion

The Atg17-Atg31-Atg29 complex was identified as a scaffold indispensible for PAS organization and vesicle tethering at a very early stage of autophagy [12, 13]. In this study we characterized a role of this complex in regulating autophagosome-vacuole

fusion, a relatively late stage of the process. We found that the Atg17-Atg31-Atg29 complex recruits the vacuolar SNARE protein Vam7 to the PAS at an early stage of autophagy. *In vitro* and *in vivo* analyses indicate that Atg17 directly interacts with the SNARE core domain of Vam7. This interaction might block SNARE complex formation between Vam7 and other SNARE proteins, such as Vti1 and Vam3, inhibiting premature fusion of incomplete autophagosomes/phagophores with the vacuole. However, if this model is correct, it is not clear how Vam7 is released from Atg17 upon autophagosome maturation. Similar to many other Atg proteins, Atg17 will dissociate from the completed autophagosome and be recycled for the next round of autophagosome formation. A previous study has shown that the clearance of PtdIns3P by the phosphatase Ymr1 is required for disassembly of the Atg machinery from completed autophagosomes, which is a requisite for subsequent fusion with the vacuole [38]. We think it is possible that clearance of PtdIns3P promotes dissociation of Atg17 from autophagosomes, releasing Vam7 to mediate fusion between autophagosomes and the vacuole. In addition, we found that the PX domain of Vam7, which is able to bind PtdIns3P, is required for normal autophagy activity, even though it is not directly involved in mediating the Atg17-Vam7 interaction (Figure 3.2D and 3.S2C). We think it is likely that the removal of PtdIns3P from the membrane normally releases the PX domain of Vam7, promoting the disassociation of the protein from Atg17.

Atg11, which also functions as a scaffold protein in autophagy, interacts with Vam7 at the PAS independent of the Atg17-Atg31-Atg29 complex. Previous data suggest that

Atg11 and Atg17 are partially redundant, with Atg11 functioning in selective types of autophagy, but also in PAS organization primarily under growing conditions [12, 35, 39]. Along these lines, we observed interaction between Atg11 and Vam7 under nutrient-rich conditions by the BiFC assay (data not shown). In contrast, Atg17 did not interact with Vam7 in this condition (Figure 3.1A). Also, a previous study has shown that Atg17 is not required for the cytoplasm-to-vacuole targeting (Cvt) pathway that delivers resident hydrolases to the vacuole under growing conditions [8]. These lines of evidence suggest that Atg11 recruits Vam7 to Cvt vesicles as part of the Cvt pathway. This pool of Vam7 is enough for mediating the fusion of Cvt vesicles with the vacuole considering that the Cvt pathway essentially operates at a basal level relative to induced autophagy. Upon nitrogen starvation autophagy is highly stimulated, and the Atg17-Atg31-Atg29 complex is now needed to recruit an adequate amount of Vam7 to the PAS.

Our analysis of the interaction between Atg17 and Vam7 reveals that certain hydrophobic residues in helix 1 and helix 4 of Atg17 mediate its interaction with Vam7. Point mutants Atg17^{L105D}, Atg17^{F317D} and Atg17^{I325D} are defective in interaction with Vam7, with the Atg17^{F317D} mutant showing only a partial defect. But only the Atg17^{F317D} mutant is still able to interact with Atg13 and Atg31, as does the wild-type protein. In addition, the Atg17^{F317D} mutant is able to suppress the autophagy defect in the *atg17*Δ strain to a level similar to that of the wild-type protein. In contrast, the Atg17^{F317D} mutant can only rescue the autophagy activity to approximately 70% in an *atg11*Δ *atg17*Δ double deletion strain compared to the wild-type protein. This implies that the binding affinity of

wild-type Atg17 for Vam7 is relatively saturated for starvation-induced autophagy so that a partial defect in recruiting Vam7 does not lead to an obvious functional defect.

Previous studies on the topic of autophagosome-vacuole/lysosome fusion demonstrated a requirement for the general fusion machinery that operates at this organelle [14-22, 24-27]. A major question, however, concerned the specific regulation of autophagosome-vacuole/lysosome fusion. Autophagy presents a unique situation in this regard compared to other vesicular transport pathways. For example, in the secretory pathway vesicles do not bud off from the originating organelle until they are essentially complete. Thus, fusion with the target/acceptor organelle cannot occur prematurely. In contrast, the phagophore expands sequentially and thus must be prevented from fusing with the vacuole/lysosome prior to completion. In mammals, the functional counterpart of Atg17 is RB1CC1/FIP200 [40-43]. RB1CC1 is predicted to be largely helical. The similarity in secondary structure might imply a conserved role of RB1CC1 to recruit a SNARE protein(s) to the phagophore or autophagosomes. Recent studies in higher eukaryotes identified the autophagosomal SNARE protein STX17 that specifically mediates fusion of autophagosomes with lysosomes, together with SNAP29 and VAMP8 [26, 27]. It is not known whether RB1CC1 interacts with these SNARE proteins. During the preparation of our manuscript, it was reported that ATG14 interacts with STX17 and SNAP29 on mature autophagosomes to promote membrane tethering and the fusion of autophagosomes with lysosomes [44]. It is possible that RB1CC1 coordinates with ATG14 to recruit these SNAREs to autophagosomes in mammalian cells. Our study

provides evidence that a similar specific mechanism is employed to regulate autophagosome-vacuole fusion in yeast. Overall, conserved molecular machinery might be employed to regulate autophagosome-vacuole/lysosome fusion.

3.5 Experimental Procedures

3.5.1 Yeast Strains, Media and Growth Conditions

Yeast strains used in this study are listed in Table 3.1. Under growing conditions, yeast cells were grown in rich (YPD; 1% yeast extract, 2% peptone, and 2% glucose) or synthetic minimal (SMD; 0.67% yeast nitrogen base, 2% glucose, and auxotrophic amino acids and vitamins as needed) media. To induce autophagy, cells were cultured in nitrogen starvation media (SD-N; 0.17% yeast nitrogen base without ammonium sulfate or amino acids, containing 2% glucose).

3.5.2 Plasmids

For the Y2H assay, pGAD-Atg17 was constructed by ligation of the polymerase chain reaction-amplified *ATG17* open reading frame (ORF) fragment into the pGAD-C1 vector between the ClaI and SalI sites. Plasmids pGAD-Atg11, pGAD-Atg11$^{\Delta 272\text{-}321}$, pGAD-Atg11$^{\Delta 627\text{-}858}$, pGAD-Atg11$^{\Delta 536\text{-}576}$, pGAD-Atg11$^{\Delta 859\text{-}1178}$, pGAD-Atg13, pGAD-Atg31 and pGBDU-Atg17 have been described previously [8, 10]. The truncation and point mutants of Atg17 were made by site-directed deletion or mutagenesis from either pGAD-Atg17 or pGBDU-Atg17. Plasmids pGBDU-Vam7, pGBDU-Vam7(1-125),

pGBDU-Vam7(119-254) and pGBDU-Vam7(241-317) were constructed by ligation of the corresponding polymerase chain reaction-amplified DNA fragments from the *VAM7* ORF into the pGBDU-C1 vector between the EcoRI and BamHI sites. The deletion mutants of Vam7 were made by site-directed mutagenesis based on pGBDU-Vam7.

The *ATG17* ORF fragment was ligated into the ClaI and SalI sites of pCu(416) [45] and pCu-GFP(416) vectors to construct pCu-Atg17(416) and pCu-GFP-Atg17(416). Atg17 point mutants were then made by site-directed mutagenesis.

3.5.3 Bimolecular Fluorescence Complementation assay

The strains for the BiFC assay were made by altering the corresponding genes on the yeast genome through homologous recombination [29]. Using plasmids pFA6a-VC-His3MX6 (KanMX6 or TRP1), pFA6a-VN-His3MX6 (KanMX6 or TRP1), pFA6a-His3MX6 (KanMX6 or TRP1)-RPL7Bp-VC or pFA6a-His3MX6 (KanMX6 or TRP1)-RPL7Bp-VN as templates, DNA fragments with the VN or VC peptide-coding sequence and homologous regions from the genes of interest were amplified by PCR [29]. Subsequent transformation of DNA fragments into the appropriate yeast strains was subsequently conducted and strains were examined by fluorescence microscopy.

3.5.4 Fluorescence Microscopy

For fluorescence microscopy, cells were cultured in YPD medium to mid-log phase and then shifted to SD-N medium for 1 h to induce autophagy. Images were then captured on

a DeltaVision microscope with a 100x objective and a CCD camera (CoolSnap HQ; Photometrics). Twelve Z-sections with 0.3-µm spacing between two neighboring sections were taken for each picture.

3.5.5 In Vitro GST Affinity Isolation

ATG17 (WT) or ATG17 (F317D) was cloned into pQLINK-H using the BamHI and NotI sites N-terminal to the sequence encoding the 6xHis tag, while the SNARE domain of Vam7 was cloned into the pQLINK-G2 vector using the BamHI and NotI sites. The ligase independent cloning method was used to generate two expression constructs by linking the His-tagged Atg17 sequence to the pQLINK-G2-Vam7 SNARE or pQLINK-G2 (negative control). Binary interactions were examined by transforming the two-gene construct into the T7 express strain (NEB, C2566I) and induced with 0.5 mM IPTG at an OD600 of ~0.6. Cells were suspended in lysis buffer (50 mM Tris-HCl, pH 8.0, 150 mM NaCl, 2 mM PMSF, 0.1% Triton X-100, 5% glycerol, 0.5 mM DTT) and lysed by sonication. The lysate was pre-cleared by centrifugation at ~30,000 x g for 30 min. The supernatant fraction was next incubated with glutathione resin (Genscript, L00206) at 4°C for 1 h followed by washes in lysis buffer. SDS-loading buffer was added to the glutathione resin and the samples were boiled and subsequently analyzed by western blotting using anti-His antibody (ABM, G020).

3.5.6 Correlative Fluorescence Microscopy and Electron Tomography

A 100 ml, mid-log phase culture of yeast cells was starved in SD-N for 4 h at 30°C with shaking. Cells were then concentrated by vacuum filtration using a 0.22-µm bottle-top filter (EMD Millipore). The cell paste was transferred to planchettes (Ted Pella), cryo-fixed using a Bal-Tec HPM 010 high-pressure freezing machine (RMC), and placed into cryotubes containing 0.1% uranyl acetate in anhydrous acetone. Samples were freeze-substituted at -80°C for 70 h in an EM AFS2 freeze substitution device (Leica). The temperature was then raised to -50°C and the samples were washed three times with acetone, followed by successive increasing overnight infiltrations with Lowicryl K4M resin (5, 10, 25, 50, 75, and 100%), followed by three 100% resin incubations for 1 h each. Samples were then placed in molds and polymerized at -50°C under UV for 30 h. Sections of 300-2000 nm were cut with an EM UC6 ultramicrotome (Leica) and placed on 200-mesh carbon-formvar coated London-Finder copper grids (EMS).

For fluorescence microscopy, the grid was placed on a glass slide with the resin side up, and a 22x22 mm No. 1.5 glass coverslip with a 10-µl droplet of 500 mM Na^+-HEPES, pH 7.5 was inverted onto the grid. The coverslip was immediately sealed with wax. Imaging was performed with an SP5 confocal microscope (Leica), with 63x oil Plan Apochromat objective and using a pinhole of 1 Airy unit. The grid was then retrieved for analysis by electron microscopy.

For transmission electron microscopy (TEM), TEM tomography and scanning

transmission electron microscopy (STEM) tomography, images were collected on a Tecnai G2 F30 electron microscope (FEI) operating at 300 kV. Grids were prepared for either TEM or STEM tomography by applying for 10 min on each side of the grid a 10-µl solution of 15-nm colloidal gold beads serving as fiduciary markers (BBI solutions, obtained from Ted Pella). The samples were then stained for 8-25 min with 2% uranyl acetate, and placed into a Model 2040 dual-axis tomography holder (Fischione Instruments). For TEM tomography, 300- to 400-nm sections were used to collect digital images at 15,000x magnification with a 4K UltraScan camera (Gatan). For STEM tomography, 1- to 2-µm sections were analyzed. Images were collected using a Model 3000 annular dark field detector (Fischione) placed above the viewing screen, and a Model 805 bright- and dark-field detector (Gatan) below the viewing screen. For both TEM and STEM tomography, images were collected as a dual-axis tilt series over a range of -60° to +60° at tilt angle increments of 1° using serial EM tomography software [46]. The IMOD software was used for all tomographic reconstruction and analysis [47].

3.5.7 Other Methods

Western blot, the Pho8Δ60 assay and the prApe1 protease protection assay were performed as described previously [36, 48, 49].

3.6 References

1. Klionsky, D.J., and Codogno, P. (2013). The mechanism and physiological function of macroautophagy. J Innate Immun *5*, 427-433.

2. Levine, B., Mizushima, N., and Virgin, H.W. (2011). Autophagy in immunity and inflammation. Nature *469*, 323-335.
3. Xie, Z., and Klionsky, D.J. (2007). Autophagosome formation: core machinery and adaptations. Nat Cell Biol *9*, 1102-1109.
4. Yang, Z., and Klionsky, D.J. (2010). Mammalian autophagy: core molecular machinery and signaling regulation. Curr Opin Cell Biol *22*, 124-131.
5. Deretic, V., and Levine, B. (2009). Autophagy, immunity, and microbial adaptations. Cell Host Microbe *5*, 527-549.
6. Lynch-Day, M.A., Mao, K., Wang, K., Zhao, M., and Klionsky, D.J. (2012). The role of autophagy in Parkinson's disease. Cold Spring Harb Perspect Med *2*, a009357.
7. Narendra, D., Tanaka, A., Suen, D.F., and Youle, R.J. (2008). Parkin is recruited selectively to impaired mitochondria and promotes their autophagy. J Cell Biol *183*, 795-803.
8. Cheong, H., Yorimitsu, T., Reggiori, F., Legakis, J.E., Wang, C.-W., and Klionsky, D.J. (2005). Atg17 regulates the magnitude of the autophagic response. Mol Biol Cell *16*, 3438-3453.
9. Suzuki, K., Kubota, Y., Sekito, T., and Ohsumi, Y. (2007). Hierarchy of Atg proteins in pre-autophagosomal structure organization. Genes Cells *12*, 209-218.
10. Cao, Y., Nair, U., Yasumura-Yorimitsu, K., and Klionsky, D.J. (2009). A multiple ATG gene knockout strain for yeast two-hybrid analysis. Autophagy *5*, 699-705.
11. Kabeya, Y., Kamada, Y., Baba, M., Takikawa, H., Sasaki, M., and Ohsumi, Y. (2005). Atg17 functions in cooperation with Atg1 and Atg13 in yeast autophagy. Mol Biol Cell *16*, 2544-2553.
12. Mao, K., Chew, L.H., Inoue-Aono, Y., Cheong, H., Nair, U., Popelka, H., Yip, C.K., and Klionsky, D.J. (2013). Atg29 phosphorylation regulates coordination of the Atg17-Atg31-Atg29 complex with the Atg11 scaffold during autophagy initiation. Proc Natl Acad Sci U S A *110*, E2875-2884.
13. Ragusa, M.J., Stanley, R.E., and Hurley, J.H. (2012). Architecture of the Atg17 complex as a scaffold for autophagosome biogenesis. Cell *151*, 1501-1512.
14. Balderhaar, H.J., Arlt, H., Ostrowicz, C., Brocker, C., Sundermann, F., Brandt, R., Babst, M., and Ungermann, C. (2010). The Rab GTPase Ypt7 is linked to retromer-mediated receptor recycling and fusion at the yeast late endosome. J Cell Sci *123*, 4085-4094.
15. Darsow, T., Rieder, S.E., and Emr, S.D. (1997). A multispecificity syntaxin homologue, Vam3p, essential for autophagic and biosynthetic protein transport to the vacuole. J Cell Biol *138*, 517-529.
16. Fischer von Mollard, G., and Stevens, T.H. (1999). The *Saccharomyces cerevisiae* v-SNARE Vti1p is required for multiple membrane transport pathways to the vacuole. Mol Biol Cell *10*, 1719-1732.

17. Harding, T.M., Morano, K.A., Scott, S.V., and Klionsky, D.J. (1995). Isolation and characterization of yeast mutants in the cytoplasm to vacuole protein targeting pathway. J Cell Biol *131*, 591-602.
18. Ishihara, N., Hamasaki, M., Yokota, S., Suzuki, K., Kamada, Y., Kihara, A., Yoshimori, T., Noda, T., and Ohsumi, Y. (2001). Autophagosome requires specific early Sec proteins for its formation and NSF/SNARE for vacuolar fusion. Mol Biol Cell *12*, 3690-3702.
19. Nordmann, M., Cabrera, M., Perz, A., Brocker, C., Ostrowicz, C., Engelbrecht-Vandre, S., and Ungermann, C. (2010). The Mon1-Ccz1 complex is the GEF of the late endosomal Rab7 homolog Ypt7. Curr Biol *20*, 1654-1659.
20. Wang, C.-W., Stromhaug, P.E., Shima, J., and Klionsky, D.J. (2002). The Ccz1-Mon1 protein complex is required for the late step of multiple vacuole delivery pathways. The J Biol Chem *277*, 47917-47927.
21. Fader, C.M., Sanchez, D.G., Mestre, M.B., and Colombo, M.I. (2009). TI-VAMP/VAMP7 and VAMP3/cellubrevin: two v-SNARE proteins involved in specific steps of the autophagy/multivesicular body pathways. Biochim Biophys Acta *1793*, 1901-1916.
22. Furuta, N., Fujita, N., Noda, T., Yoshimori, T., and Amano, A. (2010). Combinational soluble N-ethylmaleimide-sensitive factor attachment protein receptor proteins VAMP8 and Vti1b mediate fusion of antimicrobial and canonical autophagosomes with lysosomes. Mol Biol Cell *21*, 1001-1010.
23. Gutierrez, M.G., Munafo, D.B., Beron, W., and Colombo, M.I. (2004). Rab7 is required for the normal progression of the autophagic pathway in mammalian cells. J Cell Sci *117*, 2687-2697.
24. Manil-Segalen, M., Lefebvre, C., Jenzer, C., Trichet, M., Boulogne, C., Satiat-Jeunemaitre, B., and Legouis, R. (2014). The *C. elegans* LC3 acts downstream of GABARAP to degrade autophagosomes by interacting with the HOPS subunit VPS39. Dev Cell *28*, 43-55.
25. Takats, S., Pircs, K., Nagy, P., Varga, A., Karpati, M., Hegedus, K., Kramer, H., Kovacs, A.L., Sass, M., and Juhasz, G. (2014). Interaction of the HOPS complex with Syntaxin 17 mediates autophagosome clearance in Drosophila. Mol Biol Cell *25*, 1338-1354.
26. Itakura, E., Kishi-Itakura, C., and Mizushima, N. (2012). The hairpin-type tail-anchored SNARE syntaxin 17 targets to autophagosomes for fusion with endosomes/lysosomes. Cell *151*, 1256-1269.
27. Takats, S., Nagy, P., Varga, A., Pircs, K., Karpati, M., Varga, K., Kovacs, A.L., Hegedus, K., and Juhasz, G. (2013). Autophagosomal Syntaxin17-dependent lysosomal degradation maintains neuronal function in Drosophila. J Cell Biol *201*, 531-539.
28. Uetz, P., Giot, L., Cagney, G., Mansfield, T.A., Judson, R.S., Knight, J.R., Lockshon, D., Narayan, V., Srinivasan, M., Pochart, P., et al. (2000). A comprehensive analysis of protein-protein interactions in *Saccharomyces cerevisiae*. Nature *403*, 623-627.

29. Sung, M.K., and Huh, W.K. (2007). Bimolecular fluorescence complementation analysis system for in vivo detection of protein-protein interaction in *Saccharomyces cerevisiae*. Yeast *24*, 767-775.
30. Cheever, M.L., Sato, T.K., de Beer, T., Kutateladze, T.G., Emr, S.D., and Overduin, M. (2001). Phox domain interaction with PtdIns(3)P targets the Vam7 t-SNARE to vacuole membranes. Nat Cell Biol *3*, 613-618.
31. Klionsky, D.J., and Emr, S.D. (1989). Membrane protein sorting: biosynthesis, transport and processing of yeast vacuolar alkaline phosphatase. EMBO J *8*, 2241-2250.
32. Klionsky, D.J., and Emr, S.D. (1990). A new class of lysosomal/vacuolar protein sorting signals. J Biol Chem *265*, 5349-5352.
33. Noda, T., Matsuura, A., Wada, Y., and Ohsumi, Y. (1995). Novel system for monitoring autophagy in the yeast *Saccharomyces cerevisiae*. Biochem Biophys Res Commun *210*, 126-132.
34. Ungermann, C., and Wickner, W. (1998). Vam7p, a vacuolar SNAP-25 homolog, is required for SNARE complex integrity and vacuole docking and fusion. Embo J *17*, 3269-3276.
35. Cheong, H., Nair, U., Geng, J., and Klionsky, D.J. (2008). The Atg1 kinase complex is involved in the regulation of protein recruitment to initiate sequestering vesicle formation for nonspecific autophagy in *Saccharomyces cerevisiae*. Mol Biol Cell *19*, 668-681.
36. Yen, W.-L., and Klionsky, D.J. (2012). Proteinase protection of prApe1 as a tool to monitor Cvt vesicle/autophagosome biogenesis. Autophagy *8*, 1245-1249.
37. Sousa, A.A., Azari, A.A., Zhang, G., and Leapman, R.D. (2011). Dual-axis electron tomography of biological specimens: Extending the limits of specimen thickness with bright-field STEM imaging. J Struct Biol *174*, 107-114.
38. Cebollero, E., van der Vaart, A., Zhao, M., Rieter, E., Klionsky, D.J., Helms, J.B., and Reggiori, F. (2012). Phosphatidylinositol-3-phosphate clearance plays a key role in autophagosome completion. Curr Biol *22*, 1545-1553.
39. Lynch-Day, M.A., and Klionsky, D.J. (2010). The Cvt pathway as a model for selective autophagy. FEBS Lett *584*, 1359-1366.
40. Chan, E.Y. (2009). mTORC1 phosphorylates the ULK1-mAtg13-FIP200 autophagy regulatory complex. Sci Signal *2*, pe51.
41. Ganley, I.G., Lam du, H., Wang, J., Ding, X., Chen, S., and Jiang, X. (2009). ULK1.ATG13.FIP200 complex mediates mTOR signaling and is essential for autophagy. J Biol Chem *284*, 12297-12305.
42. Hosokawa, N., Hara, T., Kaizuka, T., Kishi, C., Takamura, A., Miura, Y., Iemura, S., Natsume, T., Takehana, K., Yamada, N., et al. (2009). Nutrient-dependent mTORC1 association with the ULK1-Atg13-FIP200 complex required for autophagy. Mol Biol Cell *20*, 1981-1991.

43. Jung, C.H., Jun, C.B., Ro, S.H., Kim, Y.M., Otto, N.M., Cao, J., Kundu, M., and Kim, D.H. (2009). ULK-Atg13-FIP200 complexes mediate mTOR signaling to the autophagy machinery. Mol Biol Cell *20*, 1992-2003.
44. Diao, J., Liu, R., Rong, Y., Zhao, M., Zhang, J., Lai, Y., Zhou, Q., Wilz, L.M., Li, J., Vivona, S., et al. (2015). ATG14 promotes membrane tethering and fusion of autophagosomes to endolysosomes. Nature.
45. Labbé, S., and Thiele, D.J. (1999). Copper ion inducible and repressible promoter systems in yeast. Methods Enzymol *306*, 145-153.
46. Mastronarde, D.N. (2005). Automated electron microscope tomography using robust prediction of specimen movements. J Struct Biol *152*, 36-51.
47. Kremer, J.R., Mastronarde, D.N., and McIntosh, J.R. (1996). Computer visualization of three-dimensional image data using IMOD. J Struct Biol *116*, 71-76.
48. Shintani, T., and Klionsky, D.J. (2004). Cargo proteins facilitate the formation of transport vesicles in the cytoplasm to vacuole targeting pathway. J Biol Chem *279*, 29889-29894.
49. Noda, T., Matsuura, A., Wada, Y., and Ohsumi, Y. (1995). Novel system for monitoring autophagy in the yeast *Saccharomyces cerevisiae*. Biochem Biophys Res Commun *210*, 126-132.
50. James, P., Halladay, J., and Craig, E.A. (1996). Genomic libraries and a host strain designed for highly efficient two-hybrid selection in yeast. Genetics *144*, 1425-1436.
51. Robinson, J.S., Klionsky, D.J., Banta, L.M., and Emr, S.D. (1988). Protein sorting in *Saccharomyces cerevisiae*: isolation of mutants defective in the delivery and processing of multiple vacuolar hydrolases. Mol Cell Biol *8*, 4936-4948.
52. Kanki, T., Wang, K., Baba, M., Bartholomew, C.R., Lynch-Day, M.A., Du, Z., Geng, J., Mao, K., Yang, Z., Yen, W.L., et al. (2009). A genomic screen for yeast mutants defective in selective mitochondria autophagy. Mol Biol Cell *20*, 4730-4738.
53. Mao, K., Liu, X., Feng, Y., and Klionsky, D.J. (2014). The progression of peroxisomal degradation through autophagy requires peroxisomal division. Autophagy *10*, 652-661.

Table 3.1. Yeast strains used in this study.

Name	Genotype	Reference
KDM1586	SEY6210*RPL7Bp-VC-Vam7::HIS3 ATG17-VN::TRP1*	This study
KDM1587	SEY6210 *RPL7Bp-VC-Vam7::HIS3 ATG29-VN::TRP1*	This study
KDM1588	SEY6210 *RPL7Bp-VC-Vam7::HIS3 ATG31-VN::TRP1*	This study
KDM1591	SEY6210 *RPL7Bp-VC-Vam7::HIS3 ATG17-VN::TRP1 CFP-ATG8(405)::LEU2*	This study
KDM1701	SEY6210 *VAM7-GFP::HIS3*	This study
PJ69-4A	MATa *trp1-901 leu2-3,112 ura3-52 his3-200 gal4Δ gal80Δ LYS2::GAL1-HIS GAL2-ADE2 met2::GAL7-lacZ*	[50]
SEY6210	MATα *leu2-3,112 ura3-52 his3-Δ200 trp1-Δ901 suc2-Δ9 lys2-801 GAL*	[51]
WLY176	SEY6210 *pho13Δ pho8Δ60*	[52]
XLY087	SEY6210 *RPL7Bp-VN-ATG11::HIS3 RPL7Bp-VC::TRP1*	[53]
XLY100	SEY6210 *RPL7Bp-VC-VAM7::HIS3 ATG17-VN::TRP1 atg31Δ::KAN CFP-ATG8(405)::LEU2*	This study
XLY101	SEY6210 *RPL7Bp-VC-VAM7::HIS3 ATG29-VN::TRP1 atg31Δ::KAN*	This study
XLY107	SEY6120 *RPL7Bp-VC-VAM7 (ΔPX)::HIS3 ATG17-VN::TRP1 CFP-ATG8(405)::LEU2*	This study
XLY108	SEY6210 *RPL7Bp-VC-VAM7::HIS3 ATG17-VN::TRP1 atg1Δ::URA3*	This study
XLY111	SEY6210 *RPL7Bp-VC-VAM7::HIS3 ATG17-VN::TRP1 atg9Δ::URA3*	This study
XLY124	SEY6120 *ATG11-VN::TRP1 RPL7Bp-VC-VAM7::HIS3*	This study
XLY128	SEY6120 *RPL7Bp-VN-ATG11::TRP1 RPL7Bp-VC-VAM7::HIS3*	This study
XLY129	SEY6120 *RPL7Bp-VN-ATG11::TRP1 RPL7Bp-VC-VAM7::HIS3 CFP-ATG8(405)::LEU2*	This study
XLY130	SEY6120 *RPL7Bp-VN-ATG11::TRP1 RPL7Bp-VC-VAM7::HIS3 CFP-ATG8(405)::LEU2 atg17Δ::KAN*	This study
XLY131	SEY6120 *RPL7Bp-VN-ATG11::TRP1 RPL7Bp-VC-VAM7::HIS3 CFP-ATG8(405)::LEU2 atg29Δ::KanMX*	This study
XLY134	WLY176 *atg17Δ::KanMX*	This study
XLY135	WLY176 *atg11Δ::HIS3*	This study
XLY136	WLY176 *atg11Δ::HIS3 atg17Δ::KanMX*	This study
XLY137	WLY176 *vam7Δ::LEU2*	This study

XLY139	WLY176 *atg17Δ::KanMX RFP-APE1(305)::LEU2*	This study
XLY142	WLY176 *atg17Δ::KanMX vam7Δ::HIS3 GFP-ATG8(405)::LEU2*	This study
XLY143	SEY6210 *RPL7Bp-VC-Vam7::HIS3 ATG17(L105D)-VN::TRP1*	This study
XLY144	SEY6210 *RPL7Bp-VC-Vam7::HIS3 ATG17(F317D)-VN::TRP1*	This study
XLY145	SEY6210 *RPL7Bp-VC-Vam7::HIS3 ATG17(I325D)-VN::TRP1*	This study
XLY146	WLY176 *atg11Δ::HIS3 atg17Δ::KanMX vam7Δ::LEU2*	This study
XLY147	WLY176 *atg17Δ::KanMX atg11Δ::HIS3 GFP-ATG8(405)::LEU2*	This study
XLY149	SEY6210 *ATG17-VN::TRP1 RPL7Bp-VC::KAN*	This study
XLY150	SEY6210 *ATG29-VN::TRP1 RPL7Bp-VC::KAN*	This study
XLY151	SEY6210 *ATG31-VN::TRP1 RPL7Bp-VC::KAN*	This study
XLY152	SEY6210 *ATG17-VN::TRP1 RPL7Bp-VC-Vam3::KAN*	This study
XLY153	SEY6120 *Vam7ΔPX-GFP::HIS3*	This study
XLY154	WLY176 *VC-Vam7::HIS3*	This study
XLY155	WLY176 *VC-Vam7ΔPX::HIS3*	This study
YCY149	SEY6210 *atg1Δ, 2Δ, 3Δ, 4Δ, 5Δ, 6Δ, 7Δ, 8Δ, 9Δ, 10Δ, 11Δ, 12Δ, 13Δ, 14Δ, 16Δ, 17Δ, 18Δ, 19Δ, 20Δ, 21Δ, 23Δ, 24Δ, 27Δ, 29Δ, gal4Δ gal80Δ GAL1-HIS3 GAL2-ADE2 met2::GAL7-lacZ atg31Δ::KanMX*	[10]

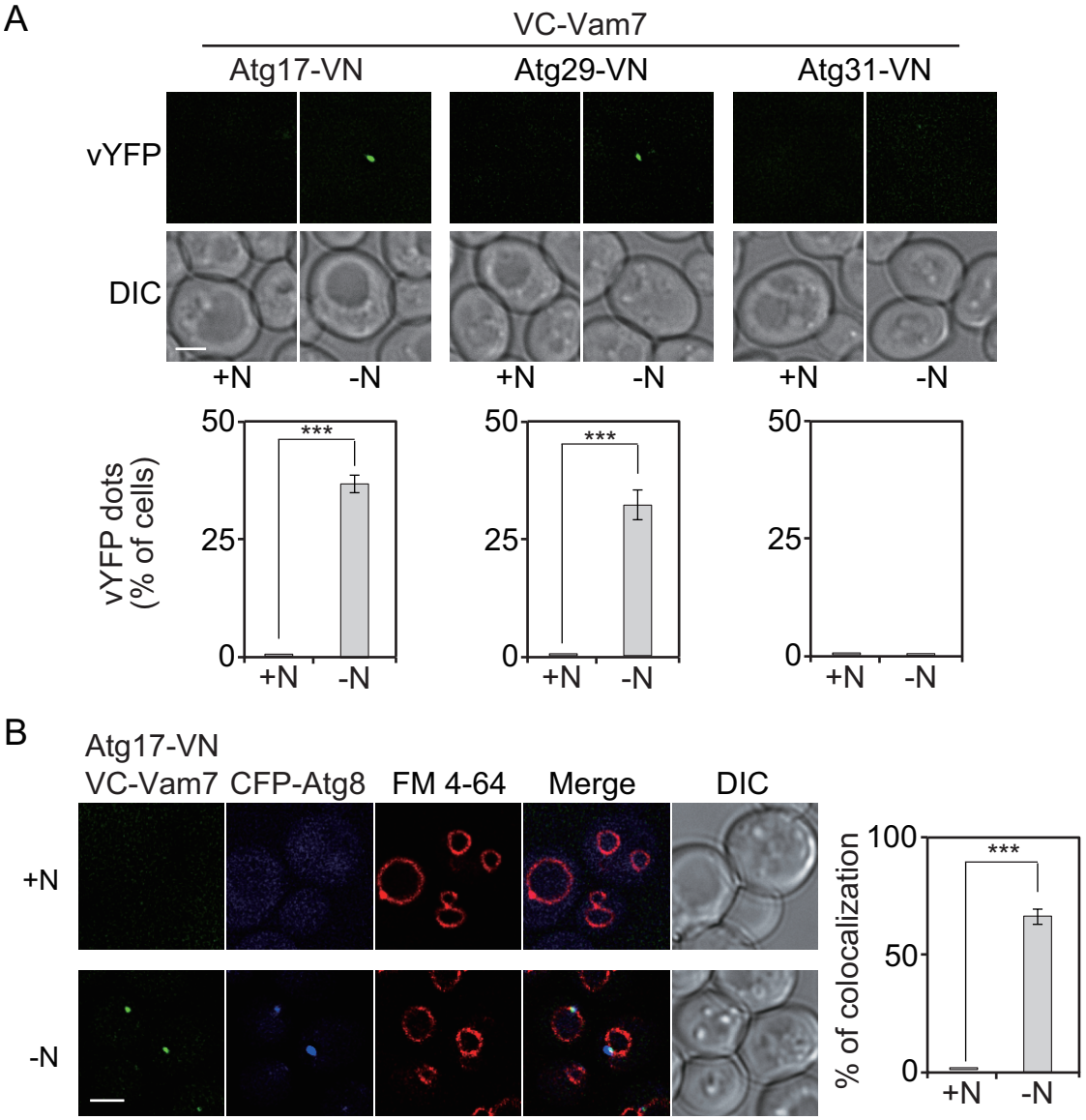

Figure 3.1. The Atg17-Atg31-Atg29 Complex Recruits Vam7 to the PAS upon Autophagy Induction. (A) *VC-VAM7 ATG17-VN* (KDM1586), *VC-VAM7 ATG29-VN* (KDM1587), and *VC-VAM7 ATG31-VN* (KDM1588) cells were grown in YPD to mid-log phase (+N) and then shifted to SD-N medium (-N) for 1 h to induce autophagy. Images were captured by fluorescence microscopy and are representative single Z-sections. Scale bar, 2.5 µm. The quantification of the percentage of cells showing a vYFP signal is indicated below each panel. Error bars represent the standard deviation (SD) of three independent experiments. *** $p<0.001$. DIC, differential interference contrast.

(B) *VC-VAM7/ATG17-VN CFP-ATG8 (405)* (KDM1591) cells were grown as described in (A). FM 4-64 staining was used to visualize the vacuole limiting membrane. Cells were observed under a fluorescence microscope. Images were collected as in (A). The

quantification of colocalization of vYFP and CFP signals is shown on right. The percentage is calculated from the number of cells showing colocalization divided by the total number of cells with both vYFP and CFP signals. Error bars represent the SD of three independent experiments. ***, $p<0.001$. Scale bar, 2.5μm.
(See also Table 3.S1 and Figure 3.S1.)

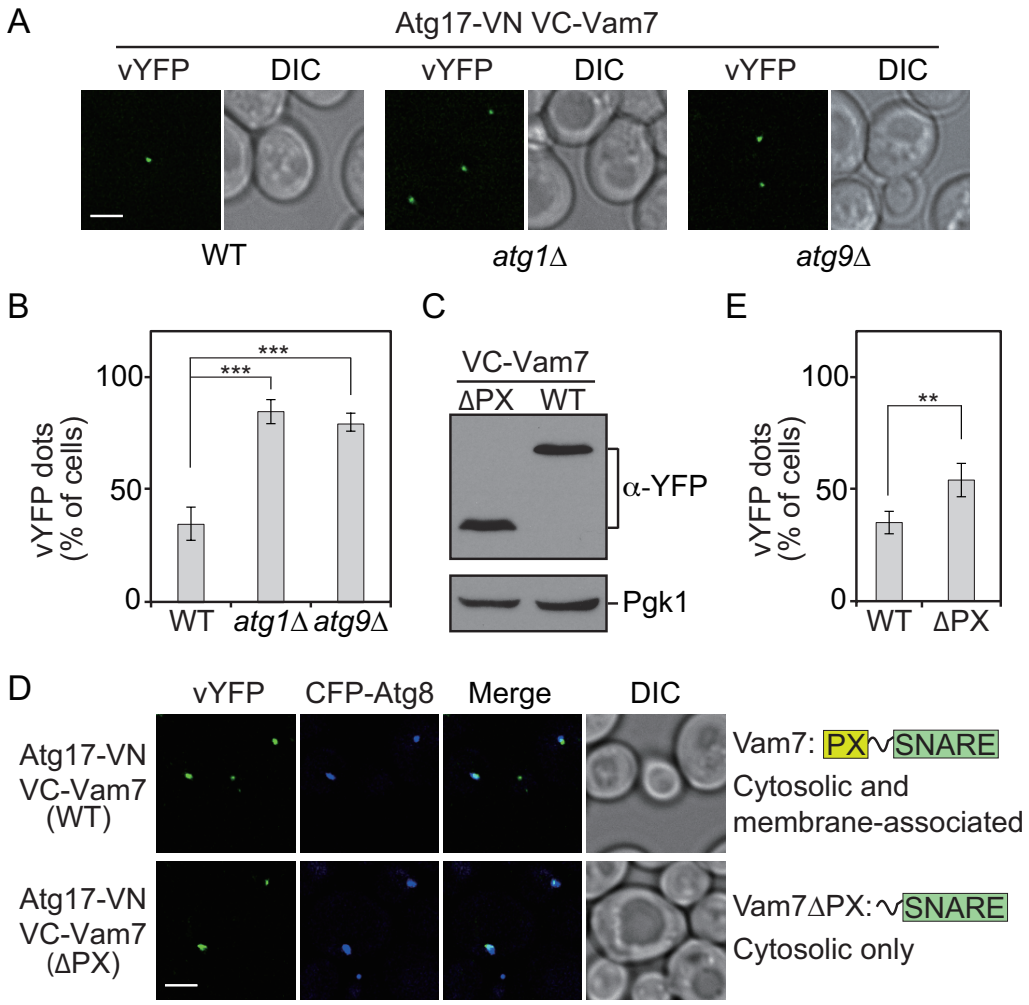

Figure 3.2. Cytosolic Vam7 Is Recruited to the PAS at an Early Stage of Autophagy

(A) *VC-VAM7 ATG17-VN* WT (KDM1586), *atg1*Δ (XLY108), and *atg9*Δ (XLY111) cells were grown as described in Figure 3.1A. Images were captured by fluorescence microscopy and are representative single Z-sections. Scale bar, 2.5 µm.

(B) Quantification of the percentage of cells showing a vYFP signal in (A). Error bars represent the SD of three independent experiments. ***, $p<0.001$.

(C) *VC-VAM7 ATG17-VN CFP-ATG8(405)* (KDM1591) and *VC-VAM7*Δ*PX ATG17-VN CFP-ATG8(405)* (XLY107) cells were grown as described in Figure 3.1A. Cell lysates were prepared, subjected to SDS-PAGE and analyzed by western blot.

(D) *VC-VAM7 ATG17-VN CFP-ATG8(405)* (KDM1591) and *VC-VAM7*Δ*PX ATG17-VN CFP-ATG8(405)* (XLY107) cells were grown as described in Figure 3.1A. Images were captured by fluorescence microscopy and are representative single Z-sections. Scale bar, 2.5 µm.

(E) Quantification of the percentage of cells showing a vYFP signal in (D). Error bars represent the SD of three independent experiments. **, $p<0.01$.

(See also Figure 3.S2.)

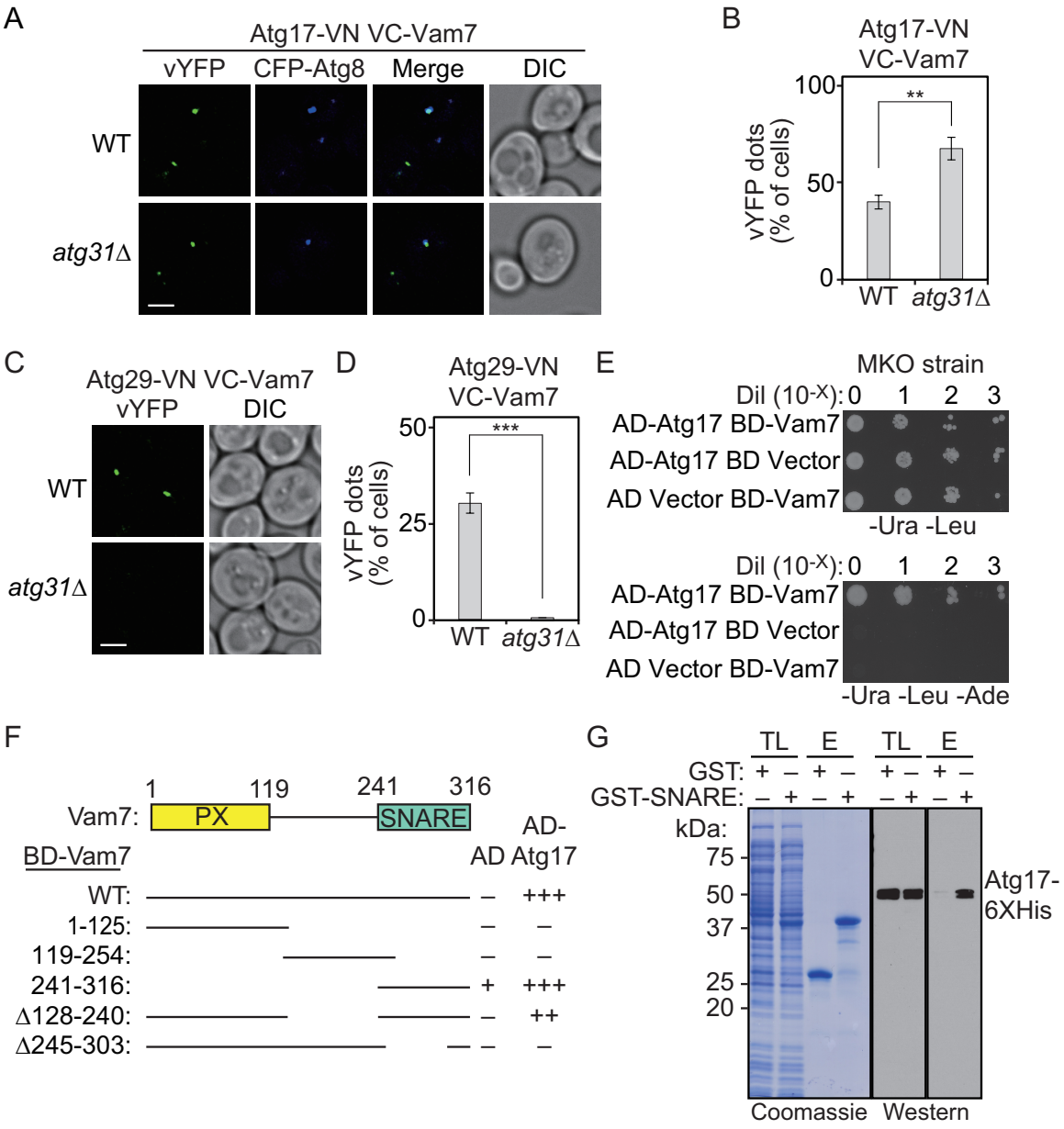

Figure 3.3. Atg17 Directly Interacts with the SNARE Domain of Vam7

(A) *VC-VAM7 ATG17-VN CFP-ATG8(405)* (WT, KDM1591) and *atg31*Δ (XLY100) cells were grown as described in Figure 3.1A. Images were captured by fluorescence microscopy and are representative single Z-sections. Scale bar, 2.5 µm.

(B) Quantification of cells showing a vYFP signal in (A). Error bars represent the SD of three independent experiments. **, $p<0.01$.

(C) *VC-VAM7 ATG29-VN* WT (KDM1587) and *atg31*Δ (XLY101) cells were grown as described in Figure 3.1A. Images were captured by fluorescence microscopy and are representative single Z-sections. Scale bar, 2.5 µm.

(D) Quantification of cells showing a vYFP signal in (C). Error bars represent the SD of three independent experiments. ***, $p<0.001$.

(E) MKO Y2H (YCY149) cells were co-transformed with the indicated plasmids. These cells were grown in SMD -Ura -Leu +Met medium to mid-log phase. Dilutions as indicated were grown on non-selective and selective plates for 3 days and then imaged.
(F) MKO Y2H (YCY149) cells were transformed with the indicated plasmids, and then analyzed for growth as in (E). "–" indicates no significant growth; "+", indicates the relative extent of growth.
(G) Interaction between Atg17 and the Vam7 SNARE domain in vitro. Affinity isolation experiments were performed by co-expressing His-tagged Atg17 with either the GST-tagged Vam7 SNARE domain or the GST tag alone as described in Materials and Methods. The Coomassie-stained gel shows the GST construct inputs. Glutathione resin was used for precipitation and the western blot was probed using anti-His antibody.
TL, total lysate; E, eluate.

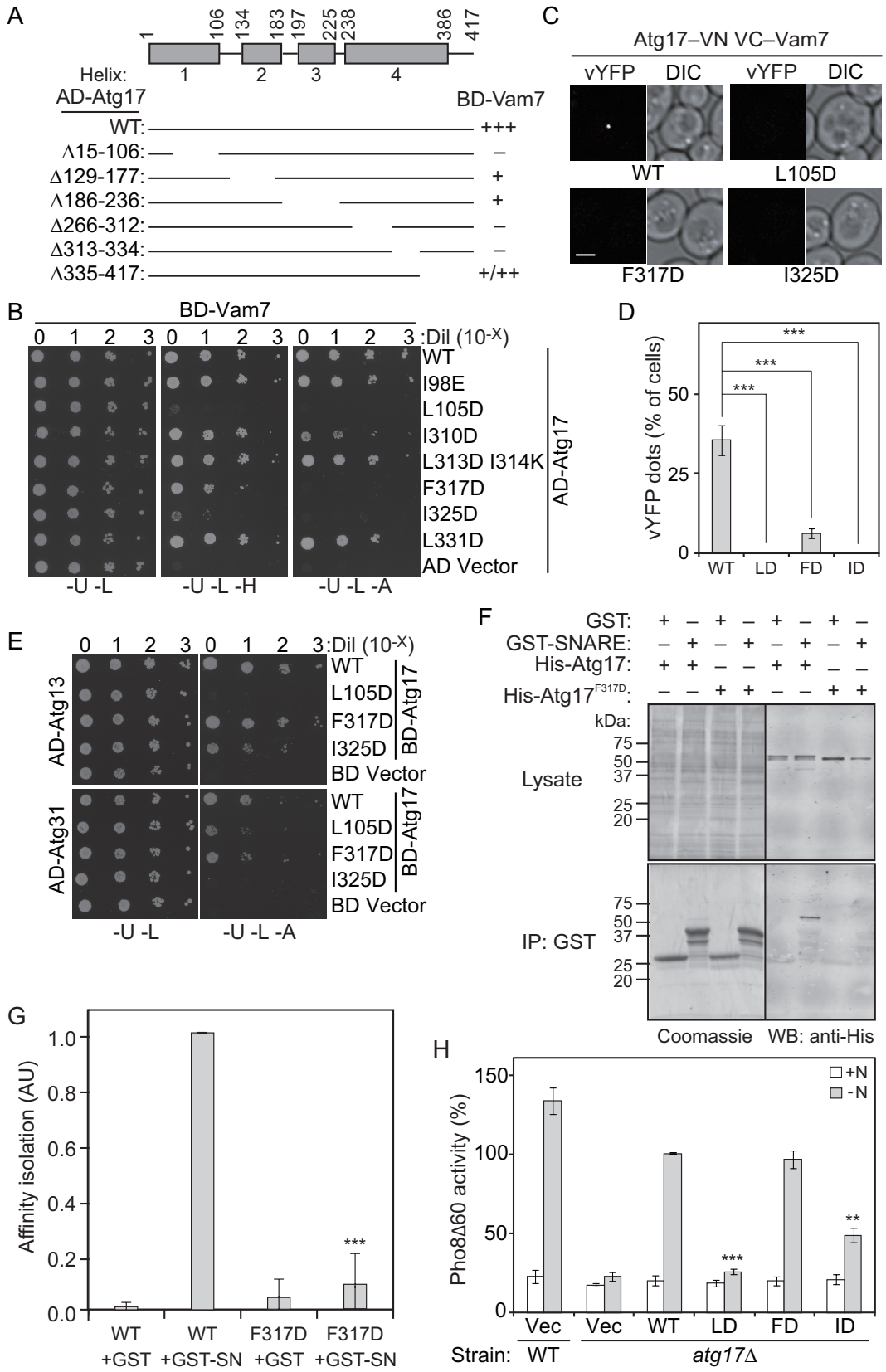

Figure 3.4. Hydrophobic Residues in Helix 1 and Helix 4 of Atg17 Mediate its

Interaction with Vam7

(A) MKO Y2H (YCY149) cells were transformed with the indicated plasmids and analyzed as described in Figure 3.3F. "-" indicates no significant growth; "+", indicates the relative extent of growth.

(B) MKO Y2H (YCY149) cells were co-transformed with the indicated plasmids. Cells were grown as described in Figure 3.3E and imaged. A, H, L and U correspond to adenine, histidine, leucine and uracil, respectively.

(C) *VC-VAM7 ATG17-VN* (KDM1586), *VC-VAM7 ATG17^{L105D}-VN* (XLY143), *VC-VAM7 ATG17^{F317D}-VN* (XLY144) and *VC-VAM7 ATG17^{I325D}-VN* (XLY145) cells were grown as described in Figure 3.1A. Images were captured by fluorescence microscopy and are representative single Z-sections. Scale bar, 2.5 μm.

(D) Quantification of the percentage of cells showing a vYFP signal in (C). Error bars represent the SD of three independent experiments. ***, $p<0.001$. FD, F317D; ID, I325D; LD, L105D.

(E) MKO Y2H (YCY149) cells were co-transformed with the indicated plasmids. These cells were then grown as described in Figure 3.3E and imaged.

(F) Interaction between Atg17^{F317D} and the Vam7 SNARE domain *in vitro*. Affinity isolation experiments were performed by co-expressing His-tagged Atg17 or Atg17^{F317D} with the GST-tagged Vam7 SNARE domain or the GST tag alone. The Coomassie-stained gel shows the GST construct inputs. Glutathione resin was used for precipitation and the western blot was probed using anti-His antibody.

(G) Quantitative infrared western to compare binding affinities between wild-type (WT) Atg17 and Atg17^{F317D} and the Vam7 SNARE domain. Error bars correspond to standard deviation calculated from data obtained from three independent experiments. SN, SNARE. ***, $p<0.001$.

(H) Wild-type (WLY176) cells with empty vector, and *atg17*Δ (XLY134) cells with either empty vector, pCu-Atg17 (WT), pCu-Atg17^{L105D} (LD), pCu-Atg17^{F317D} (FD), or pCu-Atg17^{I325D} (ID) were grown in SMD -Ura medium to mid-log phase. The cells were then shifted to SD-N for 4 h to induce autophagy, and the autophagy activity in these samples was analyzed by the Pho8Δ60 assay. The activity of *atg17*Δ (XLY134) cells with pCu-Atg17 (WT) after starvation was set to 100% and other values were normalized. The graph shows the average activity obtained from three independent experiments. Error bars represent the SD. **, $p<0.01$; ***, $p<0.001$.

(See also 3.S3.)

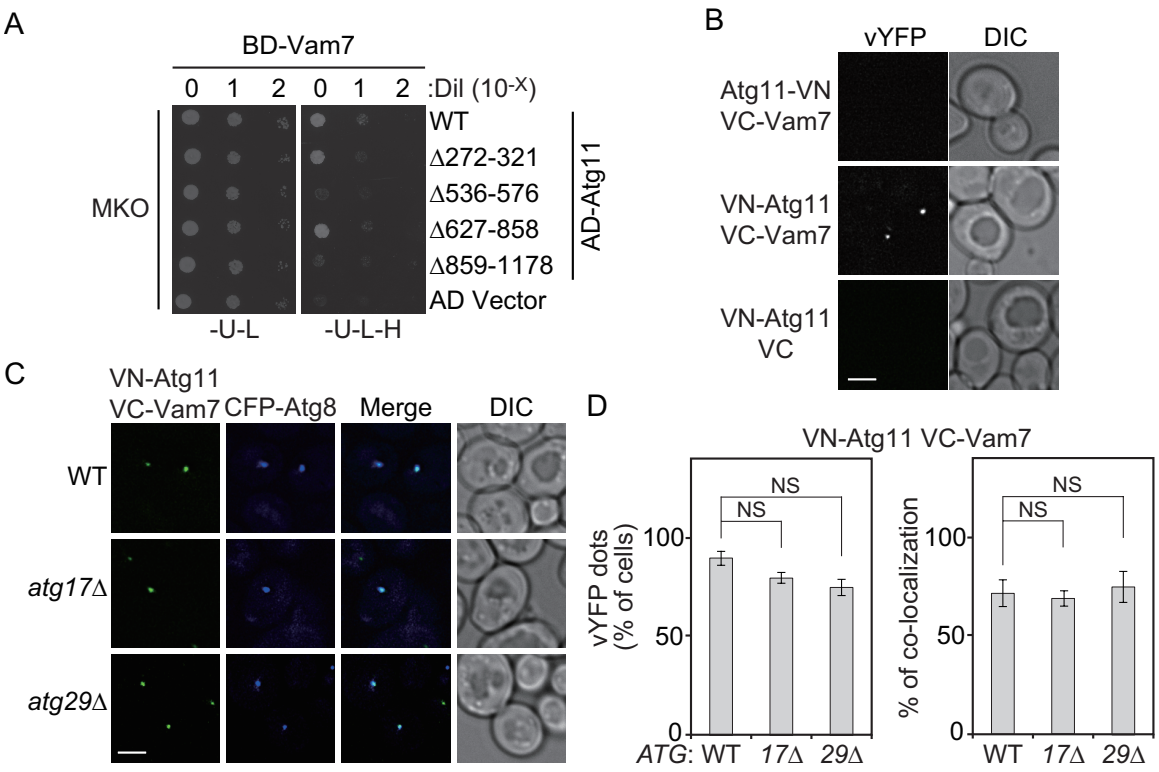

Figure 3.5. Atg11 Recruits Vam7 to the PAS Independent of the Atg17-Atg31-Atg29 Complex

(A) MKO Y2H (YCY149) cells were co-transformed with the indicated plasmids. These cells were grown in SMD -Ura -Leu +Met medium to mid-log phase. Dilutions as indicated were grown on non-selective and selective plates for 4 days and then imaged.

(B) *ATG11-VN VC-VAM7* (XLY124), *VN-ATG11 VC* (XLY087) and *VN-ATG11 VC-VAM7* (XLY128) cells were grown as described in Figure 3.1A. Images were captured by fluorescence microscopy and are representative of single Z-sections. Scale bar, 2.5 μm.

(C) *VN-ATG11 VC-VAM7 CFP-ATG8 (405)* (WT, XLY128), *atg17*Δ (XLY130), *atg29*Δ (XLY131) cells were grown as described in Figure 3.1A. Images were captured by fluorescence microscopy and are representative of single Z-sections. Scale bar, 2.5 μm.

(D) Quantification of cells showing a vYFP signal and colocalization of vYFP and CFP signals in (C). The percentage of colocalization is calculated from number of cells showing co-localization divided by total number of cells with both vYFP and CFP signals. Error bars represent the SD of three independent experiments. NS, not significant.

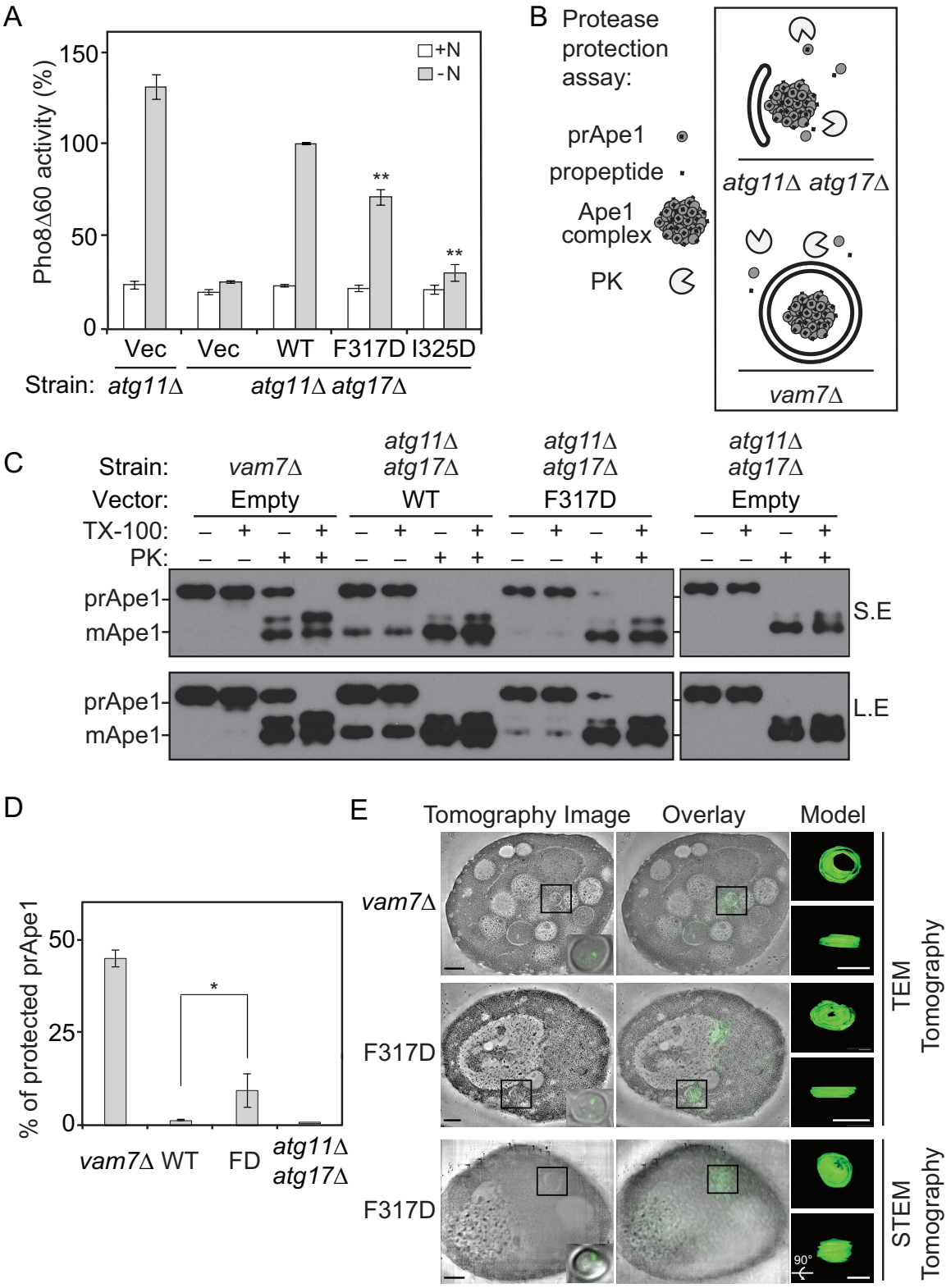

Figure 3.6. Impaired Recruitment of Vam7 to the PAS Leads to Defects in Autophagosome-Vacuole Fusion and Autophagy Activity

(A) *atg11*Δ (XLY135) cells with empty vector, and *atg11*Δ *atg17*Δ (XLY136) cells with

either empty vector, pCu-Atg17 (WT), pCu-Atg17^{F317D}, or pCu-Atg17^{I325D} were grown in SMD -Ura to mid-log phase. The cells were then shifted to SD-N medium for 4 h and autophagy activity was analyzed by the Pho8Δ60 assay. The activity of *atg11*Δ *atg17*Δ (XLY136) cells with pCu-Atg17 (WT) after starvation was set to 100% and other values were normalized. The graph shows the average activity obtained from three independent experiments. Error bars represent the SD. **, $p<0.01$.

(B) A schematic model of the prApe1 protease protection assay. PK, proteinase K.

(C) *vam7*Δ (XLY137) cells with empty vector, and *atg11*Δ *atg17*Δ (XLY136) cells with either empty vector, pCu-Atg17 (WT) or pCu-Atg17 (F317D) were grown in SMD-Ura medium to mid-log phase. The cells were then shifted to SD-N medium for 4 h. Total cell lysates from lysed spheroplasts were centrifuged at 300 x *g* to pellet cell debris. Then the cell lysates were further centrifuged at 5000 x *g* to obtain a prApe1-enriched membrane fraction, which was split into four aliquots and subjected to different treatments: no addition, 0.2% Triton X-100 (TX-100), proteinase K (PK), or proteinase K with 0.2% Trition X-100 on ice for 30 min. After protein precipitation, samples were analyzed by western blot. S.E., short exposure; L.E., long exposure.

(D) The quantification of percentage of protected prApe1 from three independent experiments. The percentage is calculated from amount of prApe1 after PK treatment divided by total level of Ape1 without any treatment. *, $p<0.05$.

(E) The *atg17*Δ *vam7*Δ *GFP-ATG8* (XLY142) cells with pCu-Atg17 (WT), and the *atg11*Δ *atg17*Δ *GFP-ATG8* (XLY147) cells with pCu-Atg17 (F317D) were grown in SMD-Ura to mid-log phase. Cells were then shifted to SD-N medium for 4 h to induce autophagy before samples were frozen and analyzed by correlative light and electron microscopy. The top two panels show samples observed by TEM tomography, while the bottom panel shows results from STEM tomography. The bottom right corner of each electron tomographic image shows the same cell visualized by fluorescence microscopy. An overlay of the fluorescent signal on the tomographic volume of the same cell is also shown. Tomographic models of the outlined autophagic structures are shown to the right; the lower model is the same as the top one, but is rotated 90° around the *x*-axis. Scale bars, 300 nm.

(See also Figure 3.S4.)

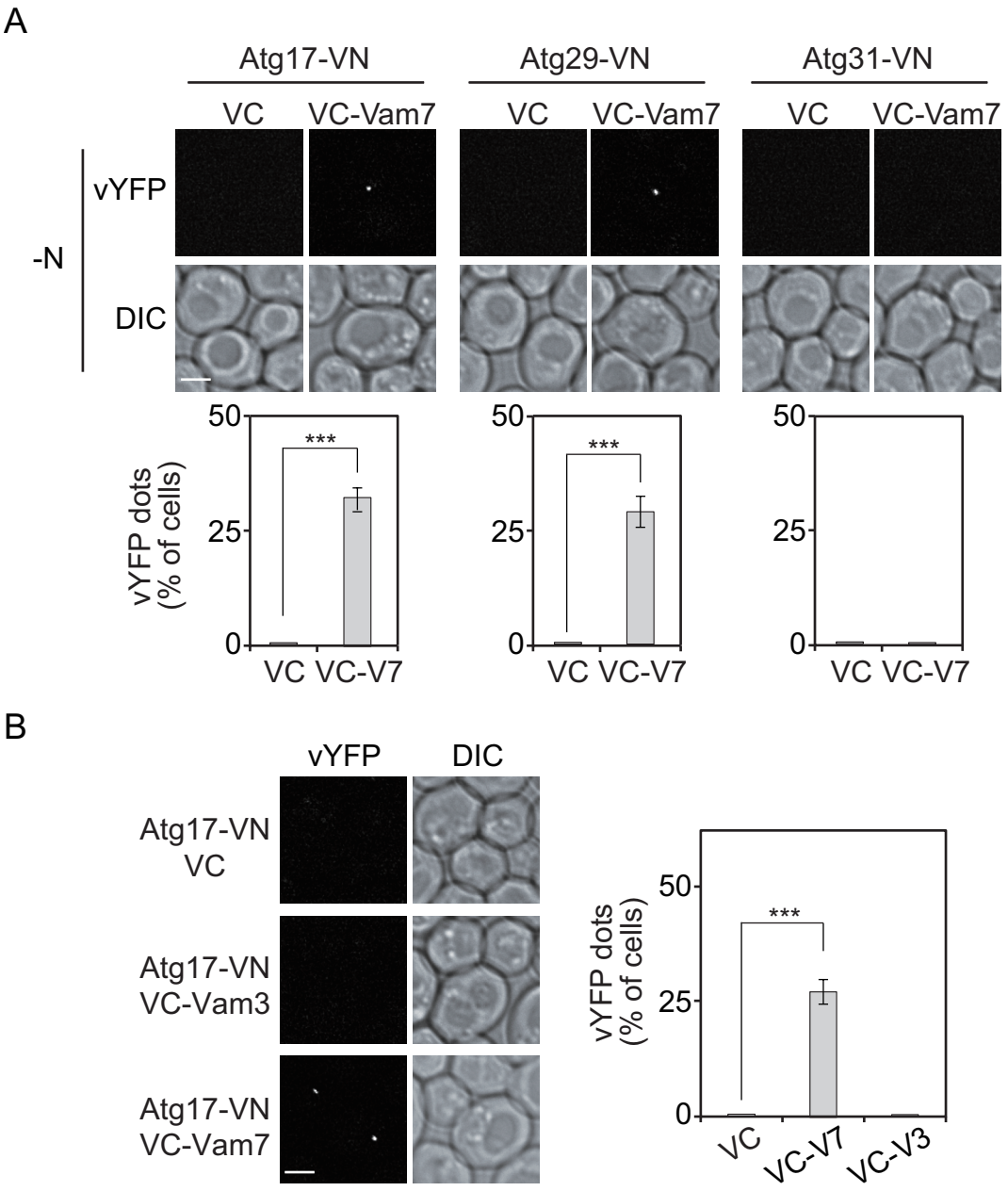

Figure 3.S1 (related to Figure 3.1). The Atg17-Atg31-Atg29 Complex Recruits Vam7 to the PAS upon Autophagy Induction

(A) *VC ATG17-VN* (XLY149), *VC-VAM7 ATG17-VN* (KDM1586), *VC ATG29-VN* (XLY150), *VC-VAM7 ATG29-VN* (KDM1587), *VC ATG31-VN* (XLY151) and *VC-VAM7 ATG31-VN* (KDM1588) cells were grown as described in Figure 3.1A. Images were captured by fluorescence microscopy and are representative single Z-sections. Scale bar, 2.5 μm. The quantification of the percentage of cells showing a vYFP signal is indicated below each panel. Error bars represent the SD of three independent experiments. ***, $p<0.001$.

(B) *VC ATG17-VN* (XLY149), *VC-VAM3 ATG17-VN* (XLY152) and *VC-VAM7*

ATG17-VN (KDM1586) cells were grown as described in Figure 3.1A. Images were captured by fluorescence microscopy and are representative single Z-sections. Scale bar, 2.5 μm. The quantification of the percentage of cells showing a vYFP signal is indicated on the right. Error bars represent the SD of three independent experiments. ***, $p<0.001$.

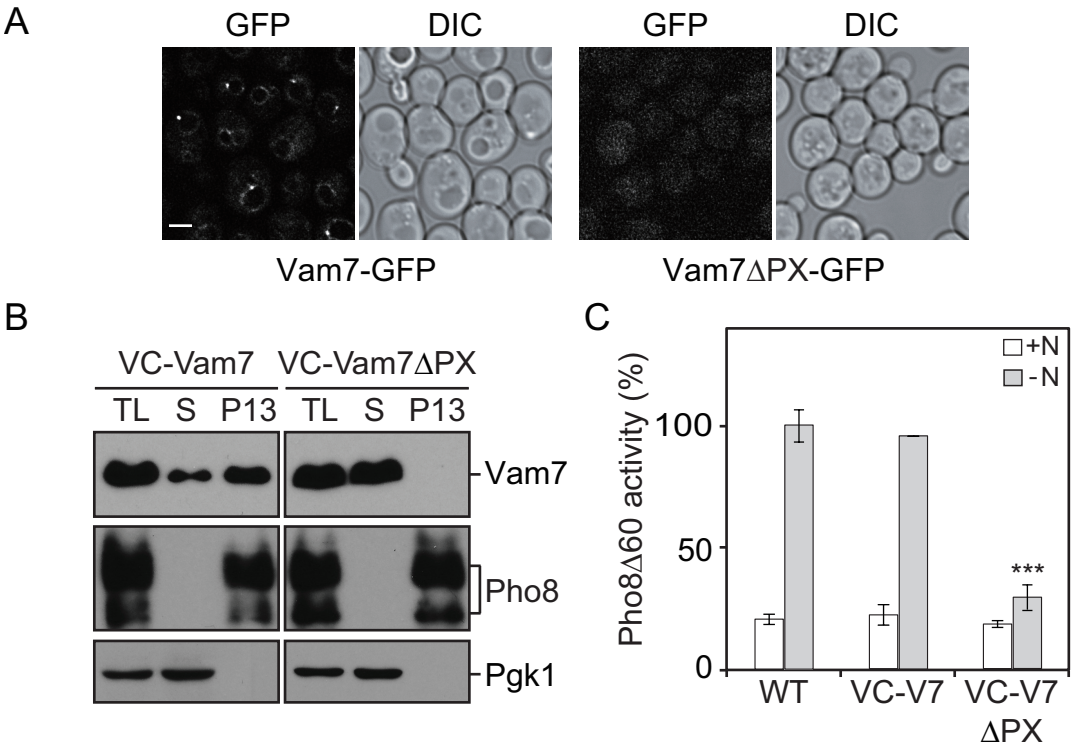

Figure 3.S2 (related to Figure 3.2): Cytosolic Vam7 Is Recruited to the PAS at an Early Stage of Autophagy

(A) *VAM7-GFP* (KDM1701) and *VAM7ΔPX-GFP* (XLY153) cells were grown in YPD to mid-log phase. Then images were captured by fluorescence microscopy and are representative single Z-sections. Scale bar, 2.5 μm.

(B) *VC-VAM7 ATG17-VN CFP-ATG8(405)* (KDM1591) and *VC-VAM7ΔPX ATG17-VN CFP-ATG8(405)* (XLY107) cells were grown in YPD medium to mid-log phase. Total cell lysates from lysed spheroplasts were centrifuged at 300 x *g* to pellet cell debris. The lysates were then evenly divided into two aliquots, with one as the total lysate (TL) sample and the other undergoing centrifugation at 1,3000 x *g* for 10 min to obtain a P13 fraction. The supernatant (S) and P13 pellet fractions and the TL samples were then TCA precipitated and analyzed by western blot.

(C) Wild-type (WLY176), *VC-VAM7* (XLY154) and *VC-VAM7ΔPX* (XLY155) cells were grown in YPD medium to mid-log phase. The cells were then shifted to SD-N for 4 h to induce autophagy, and the autophagy activity in these samples was analyzed by the Pho8Δ60 assay. The activity of wild-type cells after starvation was set to 100% and other values were normalized. The graph shows the average activity obtained from three independent experiments. Error bars represent the SD. ***, $p<0.001$.

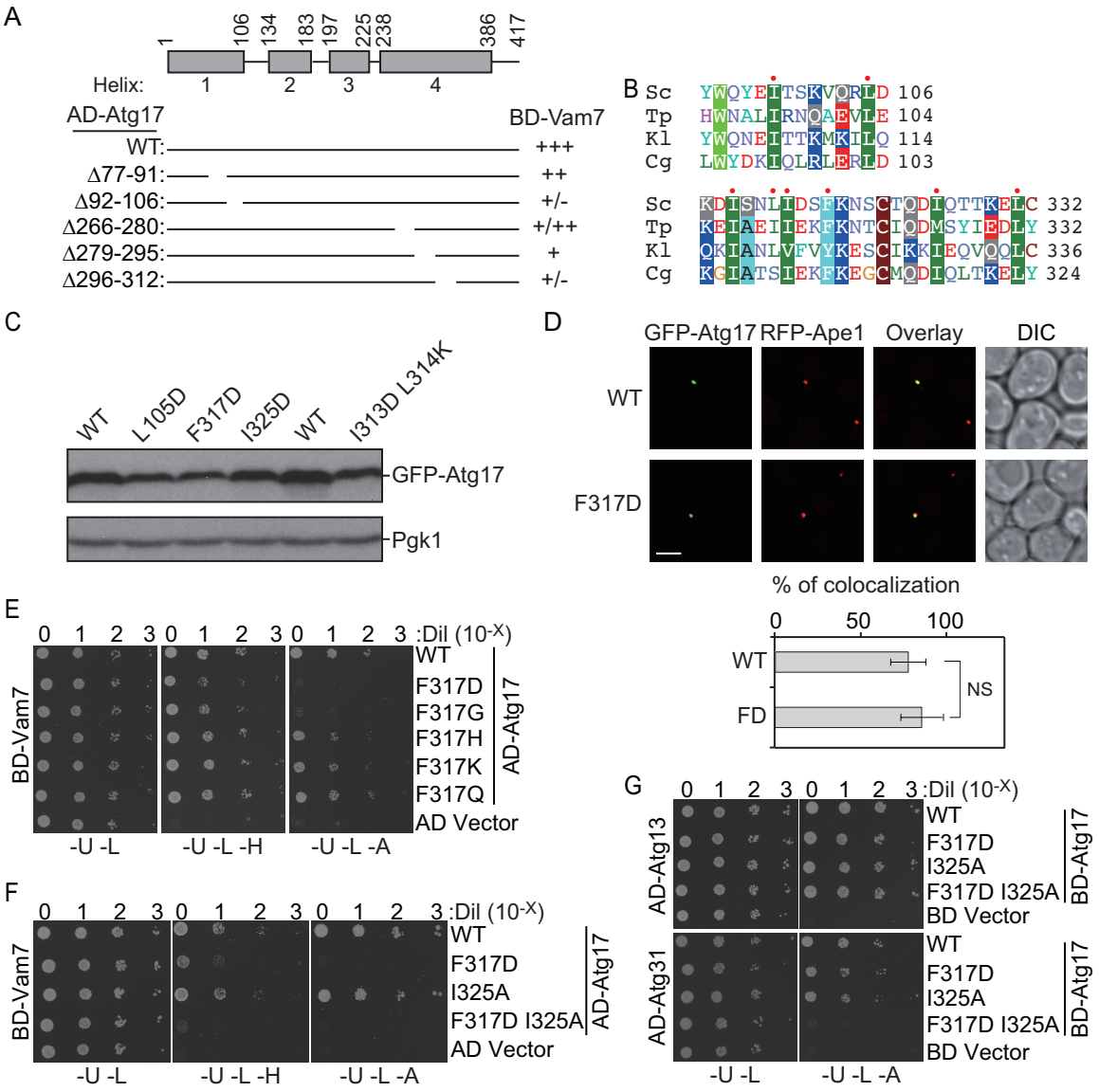

Figure 3.S3 (related to Figure 3.4): Hydrophobic Residues in Helix 1 and Helix 4 of Atg17 Mediate its Interaction with Vam7

(A) MKO (YCY149) cells were transformed with the indicated plasmids. Then they were treated as described in Figure 3.3F. "-" indicates no significant growth; "+", indicates the relative extent of growth.

(B) Alignment of regions of a-helix1 and a-helix4 of yeast Atg17 homologs. Sc, *Saccharomyces cerevisiae*, Tp, *Tetrapisispora phaffii*, Kl, *Kluyveromyces lactis*, and Cg, *Candida glabrata*. The red dots indicate the residues chosen for mutational analysis.

(C) *atg17*Δ (XLY134) cells were transformed with either pCu-GFP-Atg17(WT), pCu-GFP-Atg17(L105D), pCu-GFP-Atg17(I313D L314K), pCu-GFP-Atg17(F317D), or pCu-GFP-Atg17(I325D). They were then grown in SMD-Ura to mid-log phase (+N) and subsequently shifted to SD-N medium (-N) for 1 h to induce autophagy. Cell lysates were prepared, subjected to SDS-PAGE and analyzed by western blot.

(D) *atg17*Δ *RFP-APE1* (XLY139) cells were transformed with either pCu-GFP-Atg17(WT) or pCu-GFP-Atg17(F317D), and were grown as described in (C). Images were captured by fluorescence microscopy and are representative single Z-sections. Scale bar, 2.5 μm. The quantification of the colocalization of GFP and RFP signals are shown below. The percentage colocalization is calculated from the number of cells showing colocalization divided by the total number of cells with both GFP and RFP signals. Error bars represent the SD of three independent experiments. NS, not significant.

(E-G) MKO (YCY149) cells were co-transformed with the indicated plasmids. These cells were then grown as described in Figure 3.3E and imaged. A, H, L and U correspond to adenine, histidine, leucine and uracil, respectively.

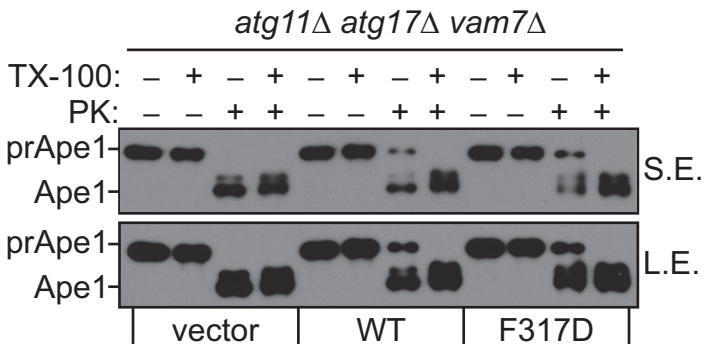

Figure 3.S4 (related to Figure 3.6): Impaired Recruitment of Vam7 to the PAS Leads to Defects in Autophagosome-Vacuole Fusion and Autophagy Activity

*atg11*Δ *atg17*Δ *vam7*Δ (XLY146) cells were transformed with either empty vector, pCu-Atg17(WT) or pCu-Atg17(F317D). The cells were then grown and treated as described in Figure 3.6C. Samples were subsequently analyzed by western blot. S.E., short exposure; L.E., long exposure.

CHAPTER 4. Summary[4]

Autophagy is a highly conserved cellular process among eukaryotes. This process has many physiological roles. Autophagy is associated with development, immunity, longevity, whereas autophagic dysfunction may be a cause of tumor development and neurodegeneration. By studying the molecular machinery and regulation of autophagy, we may be able to identify potential therapeutic targets for autophagy-related diseases. In my thesis, I use the budding yeast *Saccharomyces cerevisiae* as the model organism and explored 1) how peroxisome fission facilitates peroxisomal degradation through autophagy and 2) how autophagosome-vacuole fusion is specifically regulated.

4.1 Atg11 and Atg36 coordinate with peroxisome fission machinery to facilitate degradation of peroxisomes through autophagy

Selective degradation of damaged or surplus organelles is important for maintaining cellular homeostasis. How autophagosomes efficiently sequester organelles is a very interesting question. Compared to cytosolic proteins or RNAs, the organelles are much larger in size; wherease the size and capacity of autophagosomes are limited. Thus specific machinery is necessary to facilitate the capture of organelles. Kai Mao, a

[4] The second part of this chapter is partly reprinted from Liu X, Klionsky DJ. (2016) The Atg17-Atg31-Atg29 complex and Atg11 regulate autophagosome-vacuole fusion. *Autophagy*, 12(5):894-895 (doi.org/10.1080/15548627.2016.1162364).

previous PhD student in the lab, characterized the role of mitochondrial fission machinery in mitophagy. He and colleagues, found that the scaffold Atg11 recruits the dynamin-related GTPase, Dnm1, which is essential for mitochondrial fission, to mitochondria being degraded. The division of mitochondria facilitates the engulfment by autophagosomes.

Since peroxisomes also undergo fission and fusion, we then wondered whether similar mechanism applies to pexophagy. The fission machinery of mitochondria composed of Fis1 and Dnm1 is also involved in mediating peroxisomal fission. In addition, another dynamin-related GTPase, Vps1 is specific for fission of peroxisomes. We found that pexophagy is defective when peroxisomal fission is compromised and that both Atg11 and the pexophagy specific receptor Atg36 interact with Dnm1 and Vps1 on peroxisomes being targeted for degradation, similar to the scenario of mitophagy.

There are some intriguing questions that remain to be answered. First, how the interaction of Atg11 and Atg36 with Dnm1 and Vps1 is regulated under different conditions is unclear. Since Atg11, Atg36, Dnm1 and Vps1 can be phosphorylated, the phosphorylation status of the proteins can regulate the interactions between them. Analysis of serine or tyrosine residues on Atg11, Atg36, Dnm1 and Vps1 important for mediating the interactions may be interesting. The kinases responsible for the phosphorylation events can also be identified. Second, we observed that pexophagy-specific fission mostly occurs close to mitochondria. Is it possible that mitochondria provide membrane or lipid sources for making pexophagy-specific

autophagosomes? In addition, because Dnm1 and Fis1 participate in both mitochondria and peroxisome fission, the peroxisomes in close proximity to mitochondria may recruit Dnm1 and Fis1 more efficiently than others. In other words, the crosstalk between peroxisomes and mitochondria can play indispensible roles in mediating pexophagy.

4.2 The Atg17-Atg31-Atg29 complex and Atg11 regulate autophagosome-vacuole fusion

The autophagy process involves de novo formation of double-membrane autophagosomes; after sequestering cytoplasm these transient organelles fuse with the vacuole/lysosome. Genetic studies in yeasts have characterized over 40 Atg proteins required for autophagy, and the majority of these proteins play roles in autophagosome formation. The fusion of autophagosomes with the vacuole is mediated by the Rab GTPase Ypt7, its guanine nucleotide exchange factor Mon1-Ccz1, and soluble N-ethylmaleimide-sensitive factor attachment protein receptor (SNARE) proteins. However, these factors are not autophagosome-vacuole fusion specific. In chapter 3, we showed that two autophagy scaffold proteins, the Atg17-Atg31-Atg29 complex and Atg11, regulate autophagosome-vacuole fusion by recruiting the vacuolar SNARE Vam7 to the phagophore assembly site, where an autophagosome forms in yeast.

However, some questions still remain to be explored. First, how does Vam7 get released from Atg17 after autophagosome formation is completed? It is possible that other SNARE proteins such as Vam3 and Vti1 are recruited to the PAS after

autophagosome maturation, and that they have stronger binding affinity toward Vam7 than that of Atg17. Thus they may outcompete Atg17 to form a SNARE complex with Vam7, facilitating fusion of autophagosomes with the vacuole. Another possibility is that Atg17 gets dissociated from mature autophagosomes after clearance of PtdIns3P by Ymr1, a PtdIns3P phosphatase, releasing Vam7 as part of the process. Second, it has been shown that Atg11, but not Atg17, is required for the cytoplasm-to-vacuole targeting pathway that delivers resident hydrolases to the vacuole under growing conditions. Along these lines, does Atg11 play the major role in recruiting Vam7 in the Cvt pathway? Further analysis of the Atg11-Vam7 interaction will be needed to answer this question. Third, does the mammalian homolog of Atg17, RB1CC1/FIP200, also regulate autophagosome-lysosome fusion? In mammals, ATG14 interacts with STX17, the autophagosomal SNARE protein, and SNAP29 on mature autophagosomes to promote membrane tethering and the fusion of autophagosomes with lysosomes. Does RB1CC1 coordinate with ATG14 to regulate autophagosome-lysosome fusion? If this is the case, it may suggest that a conserved molecular machinery is employed to regulate the fusion of autophagosomes with the vacuole/lysosome.